Library

NATIONAL AERONAUTICS AND SPACE ADMINISTRATION

Technical Memorandum 33-277

Computation of Torsional Vibration Modes of Ranger and Surveyor Space Vehicles

J. A. Garba
W. H. Gayman
B. Wada

RECEIVED
NASA STI FACILITY
INPUT BRANCH
MAY 1968

N68-22024
(ACCESSION NUMBER) (THRU)
72 1
(PAGES) (CODE)
CR#94293 31
(NASA CR OR TMX OR AD NUMBER) (CATEGORY)
FACILITY FORM 602

JET PROPULSION LABORATORY
CALIFORNIA INSTITUTE OF TECHNOLOGY
PASADENA, CALIFORNIA

April 1, 1968

GPO PRICE $ _____
CFSTI PRICE(S) $ _____
Hard copy (HC) 3.00
Microfiche (MF) _____
ff 653 July 65

NATIONAL AERONAUTICS AND SPACE ADMINISTRATION

Technical Memorandum 33-277

Computation of Torsional Vibration Modes of Ranger and Surveyor Space Vehicles

J. A. Garba
W. H. Gayman
B. Wada

Approved by:

W. H. Gayman

for M. E. Alper, Manager
Applied Mechanics Section

JET PROPULSION LABORATORY
CALIFORNIA INSTITUTE OF TECHNOLOGY
PASADENA, CALIFORNIA

April 1, 1968

TECHNICAL MEMORANDUM 33-277

Copyright © 1968
Jet Propulsion Laboratory
California Institute of Technology

Prepared Under Contract No. NAS 7-100
National Aeronautics & Space Administration

Foreword

The previous work on torsional acceleration transients for *Surveyor* by M. R. Trubert at JPL (Ref. 1), as well as the bulk of the work reported herein, were completed prior to November 1965. Since that time, two independent efforts dealing with the observed torsional transients during *Atlas* engine shutdown have been reported:

(1) Lockheed Missiles and Space Company has reported (Ref. 2) analyses that have included the inertial coupling among longitudinal, bending, and torsion modes to give, essentially, the "free-free" *three-dimensional* normal modes of the *Atlas/Agena/Ranger* space vehicle. By use of these modes and of flight data defining booster-engine chamber-pressure pulsations during thrust decay, reasonably good agreement has been reported between predicted and observed responses in the spacecraft adapter.

(2) M. R. Trubert, in Ref. 3, has extended his analysis of Ref. 1 to use the Fourier transforms of the observed acceleration-time histories in place of the shock spectra, and he shows why a solution in the frequency domain, rather than the time domain, circumvents computational instabilities.

PRECEDING PAGE BLANK NOT FILMED.

Contents

I. Introduction 1

II. *Atlas/Agena/Ranger* Vehicle 2

A. *Ranger* Spacecraft and LMSC Adapter Structure 2

1. Background information 2

2. Modal survey data 8

3. Lumped-parameter representation of spacecraft/adapter first torsion mode 9

4. Conversion of linear acceleration flight data to angular acceleration . . . 12

B. *Atlas* Booster-Engine Representation 13

1. Interim mathematical model 13

2. Final mathematical model 14

C. Composite Model 16

1. Initial model 16

2. Final model 18

III. *Atlas/Centaur/Surveyor* Vehicle 18

A. *Surveyor* Spacecraft and GD/C Adapter Structure 19

1. Hughes modal survey data 19

2. GD/C adapter representation 19

3. Lumped-parameter representation of spacecraft/adapter torsion modes 19

B. *Centaur* Engine Representation 21

C. Composite Model 22

1. Initial model 22

2. Final model 24

IV. Conclusions 24

References 25

Appendix A. Numerical Values for *Atlas/Agena/Ranger* Mathematical Model 26

Appendix B. Torsion Mode Shape Plots for *Atlas/Agena/Ranger* Space Vehicle 29

Contents (contd)

Appendix C. Numerical Values for *Atlas/Centaur/Surveyor* Mathematical Model 39

Appendix D. Torsion Mode Shape Plots for *Atlas/Centaur/Surveyor* Space Vehicle 42

Tables

1. Modal descriptions for *Ranger Block III* structural test model on LMSC adapter structure 3
2. Geometric, inertial, and modal data applying to *Ranger/adapter* first cantilever torsion mode 9
3. Modal displacements of the JPL initial model for *Atlas/Agena/Ranger* 18
4. Modal displacements of the JPL final model for *Atlas/Agena/Ranger* 18
5. Numerical values for *Surveyor/adapter* mathematical model 20
6. Modal displacements of the JPL initial model for *Atlas/Centaur/Surveyor* 24
7. Modal displacements of the JPL final model for *Atlas/Centaur/Surveyor* 24

A-1. Joint coordinates for *Atlas/Agena/Ranger* 27

A-2. Joint inertias for *Atlas/Agena/Ranger* 27

A-3. Spring constants for *Atlas/Agena/Ranger* 28

C-1. Joint coordinates for *Atlas/Centaur/Surveyor* 40

C-2. Joint inertias for *Atlas/Centaur/Surveyor* 40

C-3. Spring constants for *Atlas/Centaur/Surveyor* 41

Figures

1. Test setup for exciting torsion modes of *Ranger Block III* structural test model mounted on LMSC adapter structure 4
2. Modal survey accelerometer at location of "channel 12" flight accelerometer 5
3. Modal survey accelerometer at location of "channel 11" flight accelerometer 6
4. *Ranger Block III* spacecraft feet tangential deflections 7
5. *Ranger Block III*/LMSC adapter-ring distortion in first cantilever torsion mode 8
6. Mode shape and associated inertia torque distribution in first cantilever torsion mode 9

Contents (contd)

Figures (contd)

7. Lumped-parameter mathematical model of spacecraft/adapter combination 10

8. First cantilever mode shape renormalized to give $\mathcal{M}^*_{er} = \mathcal{M}^*_{ee} = 97{,}810$ lb-in.^{2} 11

9. Mathematical model of *Atlas* booster engine 13

10. Normal modes of *Atlas* booster engine 15

11. Gross motion of *Atlas* booster engine in "free-free" torsion mode of space vehicle 15

12. Mathematical model of *Atlas* booster engines relative to joint 41 16

13. *Atlas/Agena/Ranger* mathematical model 17

14. *Surveyor* spacecraft and structural adapter on mockup of *Centaur* upper bulkhead 19

15. GD/C model of adapter/*Centaur* interface 20

16. *Surveyor/adapter* mathematical model 21

17. Mathematical model of *Centaur* engine 21

18. *Atlas/Centaur/Surveyor* torsion model 23

B-1. *Atlas/Agena/Ranger* torsion mode shapes 30

D-1. *Atlas/Centaur/Surveyor* torsion mode shapes 43

Abstract

Mathematical models are synthesized to apply to the calculation of "free-free" torsion modes of two space vehicles: the *Atlas/Agena/Ranger* (*Block III*) and the *Atlas/Centaur/Surveyor*. Input data describing the launch vehicles are obtained as lumped-parameter systems. Spacecraft descriptions are obtained in normal-mode coordinates from modal vibration surveys. A simple technique for deriving compatible coordinate systems is applied. Calculated modal data are presented for both space vehicles.

This work was conducted to provide normal-mode data for use in the synthesis of a torsional acceleration transient for *Surveyor* spacecraft vibration qualification tests.

Computation of Torsional Vibration Modes of *Ranger* and *Surveyor* Space Vehicles

I. Introduction

In flights of *Atlas* vehicles, a torsional pulse at the time of booster engine cutoff (BECO) has been observed in telemetered data from accelerometers in the vicinity of the payload. The existence of this phenomenon was first established from data obtained in the flight of the *Ranger V* space vehicle. Subsequently, requirements for torsional-vibration qualification tests have been imposed on various *Atlas*-boosted spacecraft, including the JPL *Ranger* and *Mariner* spacecraft.

As an initial step in deriving a vibration test specification appropriate to a specific space vehicle, several investigators have undertaken to describe the nature of the *Atlas* BECO forcing function from the observed acceleratory response and the modal vibration characteristics of the instrumented vehicle. The work of P. W. Ullrey, for example, has utilized data from the flight of *Ranger V* in conjunction with the torsional vibration modes associated with a particular mathematical idealization of this space vehicle (Ref. 4).

More recently, JPL has investigated the BECO torsional-transient in the development of qualification test criteria for the *Surveyor* spacecraft. The scope and results of this effort are reported by M. R. Trubert (Ref. 1).

The subject memorandum deals with the computation of the "free-free" torsional vibration modes of the particular space vehicles used by M. R. Trubert in his investigations. While the analyses reported herein were conducted as a part of a total effort having a specific objective, their ramifications in the areas of modal vibration analysis, choice of in-flight sensor locations, and flight data interpretation are substantially broader. As one point, the problems encountered by JPL in effecting the normal-mode computations are characteristic of those confronting any organization that undertakes dynamic loads analyses of a complete space vehicle, the separate stages of which are commonly under development by different industrial contractors, with contractor effort directed, for example, by different segments of NASA. The essential character of these problems is one of technical

communication; the severity of the problems may be great or small, depending on particular circumstances. In the present instance, the problems were minor, but their nature deserves comment to assist future programs.

As another aspect, the work reported herein highlights the importance of a considered choice of flight-accelerometer locations based on prior prediction or measurement of the modal vibration characteristics of the space vehicle. Conversely, a knowledge of these modal vibration characteristics, particularly in the region of flight-accelerometer locations, can be extremely important to the proper interpretation of flight data used for structural loads assessment.

This memorandum gives a purposely detailed accounting of the computation of the torsional vibration modes of two space vehicles. The *Atlas/Agena/Ranger* vehicle analysis is described in Section II. The *Atlas/Centaur/Surveyor* analysis is presented in Section III. A facet common to both analyses is that the mathematical models of the first two stages were obtained either from Lockheed Missiles and Space Company (LMSC) or from General Dynamics/Convair (GD/C) as lumped-parameter models; whereas, the spacecraft mathematical models of both *Ranger* and *Surveyor*, derived experimentally from modal vibration surveys, were expressed in terms of normal vibration modes of the cantilevered spacecraft. Of the several means available for expressing all three stages of a given space vehicle in mutually consistent coordinates, it has been chosen here to convert the normal-mode representations of the spacecraft into equivalent discretized spring-mass systems, which can then be treated as generically compatible "branches" of the launch vehicles in numerical solutions for the eigenmodes. The results of the analyses are presented in terms of normal-mode frequencies, mode shapes, and associated generalized masses.

II. *Atlas/Agena/Ranger* Vehicle

The basic model of the *Atlas/Agena/Ranger* vehicle has been taken from Figs. 5 and 7 of Ref. 4. JPL has modified this model in two respects:

(1) The quasi-rigid-body representation of the *Ranger Block II* (e.g., *Ranger V*) spacecraft has been replaced with a considerably more refined elastic model of the *Ranger Block III* configuration and its LMSC adapter structure as obtained quantitatively from detailed modal vibration surveys.

(2) The representation of the *Atlas* aft of LMSC station 1156 has been upgraded from data requested of and provided by GD/C. These changes include a new concept for modeling the gimbaled booster engines.

The first modification is regarded to be the more important of the two. Studies have confirmed the surmise that mass and stiffness variations of a payload can have an important effect on locations of nodal points in the higher-frequency vibration modes of relevance to the BECO analysis. The placement of "spot-check" accelerometers relative to these payload-sensitive nodal points merits care in data interpretation.

Facets of the JPL reconfiguration of the LMSC mathematical model, and the subsequent analyses leading to descriptions of the "free-free" torsional vibration modes of the composite vehicle are presented in the following discussions.

A. *Ranger* Spacecraft and LMSC Adapter Structure

The mathematical model of the *Ranger Block III* spacecraft has been derived from data obtained in the course of modal vibration surveys of the structural test model (STM). These surveys were conducted with the STM mounted on the LMSC adapter section, which was cantilevered at its base, LMSC station 244.50. This adapter has served as a structural transition between the *Agena* forward midbody, the *Ranger* spacecraft, and the spacecraft nose fairing.

The purpose of this section is to provide relevant background information on these modal surveys, and to show the manner in which the test data were processed to derive a lumped-parameter mathematical model compatible with the models of the *Atlas* and *Agena* stages.

1. Background information. During the early development of the *Ranger Block III* spacecraft, a modal vibration survey of an early configuration of the STM was conducted on a "hard mount." The frequency of the first cantilever torsion mode was observed to be only slightly below the then-recently-recognized dominant frequency (65–70 Hz) in the *Ranger V* (*Block II*) torsional response during the *Atlas* BECO event. Accordingly, and at little weight penalty, bracing in the *Ranger* support-leg structure was added to increase the torsional stiffness. A modal survey made after the addition of the bracing showed that the first-torsion-mode frequency had increased to 96 Hz.

Subsequent to this design change, a decision was made to remove the reinforced-plastic sterilization diaphragm from the LMSC adapter. It was apparent, from the adapter structural configuration, that deletion of this diaphragm would reduce the tangential stiffnesses of the six fittings supporting the *Ranger* spacecraft and, thereby, lower the effective torsional stiffness of the *Ranger* support structure. Accordingly, in September 1963, a program of modal vibration surveys of the *Ranger* STM mounted on a modified LMSC adapter was undertaken.

Three configurations were surveyed in varied detail*:

(1) Configuration 1: *Ranger* spacecraft less solar panels on LMSC adapter (first five modes in quantitative detail).

(2) Configuration 2: *Ranger* spacecraft with solar panels on LMSC adapter ("first torsion mode" only in quantitative detail).

(3) Configuration 3: *Ranger* spacecraft less solar panels on LMSC adapter with LMSC nose fairing installed (qualitative surveys only).

The frequency of the first torsion mode in each of the three configurations was observed to be as follows:

Configuration	*Frequency, Hz*
1	66.2
2	64.5
3	68.0

The reason for the increased frequency in configuration 3 will be discussed in conjunction with data interpretation.

Only the data from the surveys in configuration 1 were processed in detail. This processing led to the computation of a generalized mass matrix from the known mass distribution and the measured mode shapes in the five modes surveyed. Classically, such a mass matrix should be diagonal, since normal modes are, by definition, uncoupled inertially and elastically.

Accordingly, the degree of "non-diagonality" of the generalized mass matrix is a measure of the quality of the testing and of the accuracy of the derived mass distribution. Equation (1) presents the derived mass matrix with modal amplitudes renormalized to produce unit generalized mass in each mode. Table 1 gives modal frequencies, damping coefficients, and a qualitative modal description.

$$[M] = \begin{bmatrix} 1.000 & -0.003 & -0.012 & 0.000 & 0.007 \\ -0.003 & 1.000 & 0.017 & -0.042 & 0.023 \\ -0.012 & 0.017 & 1.000 & -0.040 & 0.013 \\ 0.000 & -0.042 & -0.040 & 1.000 & -0.044 \\ 0.007 & 0.023 & 0.013 & -0.044 & 1.000 \end{bmatrix} \tag{1}$$

Table 1. Modal descriptions for *Ranger Block III* structural test model on LMSC adapter structure

Mode No.	Frequency, Hz	Damping ratio, % critical damping	General description of mode
1	24.8	0.8	First bending, X-Z plane
2	26.7	0.6	First bending, Y-Z plane
3	45.5	1.1	Second bending, X-Z plane
4	50.0	1.1	Second bending, Y-Z plane
5	66.2	1.1	First torsion about Z axis

For reasons beyond the concern of this memorandum, the *Ranger* modal data were not put to use in dynamic loads analysis of the *Atlas/Agena/Ranger* space vehicle until the need arose for the investigation reported in Ref. 1. Then, in the preliminary adaptation of the *Ranger* torsion-mode data to a mathematical model of the complete space vehicle, it was recognized that the modal surveys of September 1963 had not adequately defined the relationships between the modal displacements at the spacecraft feet and the displacements of the adapter at the precise locations of the LMSC flight accelerometers. Accordingly, supplementary tests were conducted in late August 1965, with the identical hardware used in the tests of two years earlier.

Figure 1 gives an overall view of the test setup. Two 25-lb vector-force shakers, pendulously supported, were used to excite the first two torsion modes. A reference accelerometer was left in place at a location of relatively large modal deflection, while a roving accelerometer was moved from point-to-point to define relative amplitude and phase.

*The incorporation of spring-centered, viscous dampers in the solar-panel latching system for the launch configuration dictated this choice of test configurations from theoretical as well as practical considerations.

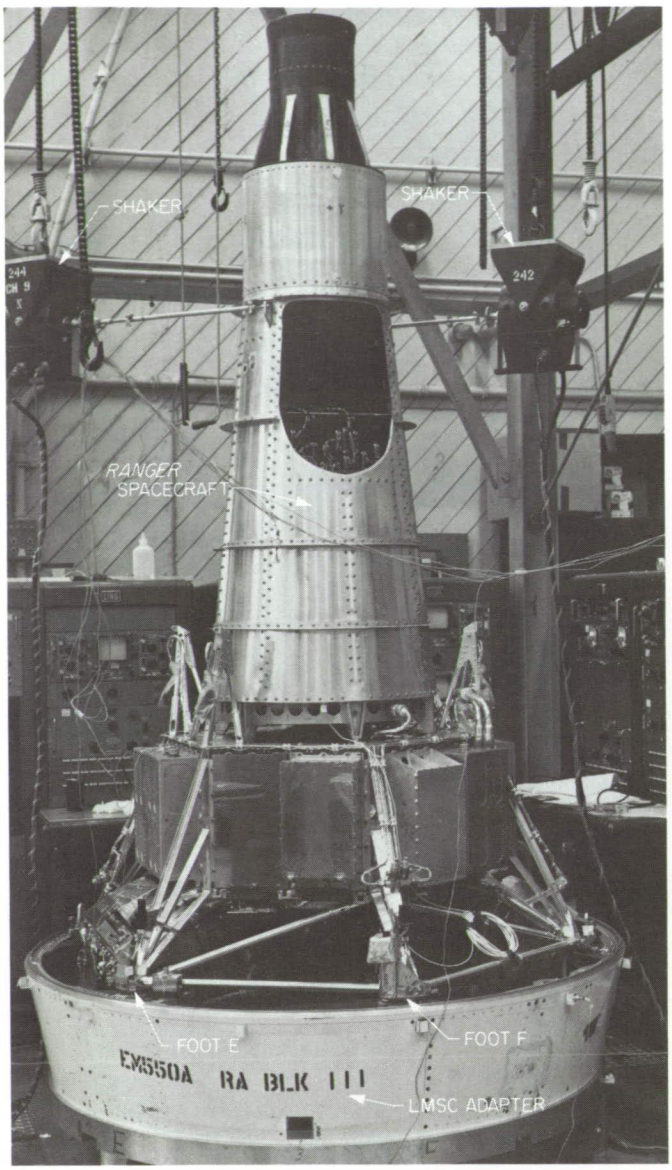

Fig. 1. Test setup for exciting torsion modes of *Ranger Block III* structural test model mounted on LMSC adapter structure

Figure 2 shows the roving accelerometer located at the position of the "channel 12" accelerometers in the flights of *Rangers VI* through *IX*. Figure 3 shows the location for the diametrically opposite "channel 11" accelerometers. It is to be noted that these installations are not symmetric; the channel 11 accelerometer being about 2.5 in. below the separation plane and the channel 12 accelerometer about 5.9 in. below.

A complete modal survey was not performed in the latter series of tests. However, sufficient measurements were made to establish excellent correspondence with the data obtained in 1963, and additional measurements were taken to relate flight-accelerometer modal displacements to the tangential displacements of the adjacent feet of the spacecraft. These relationships for the "first torsion mode" are shown graphically in Fig. 4; numerically, they are as follows:

$$\left.\begin{aligned}\left(\frac{\delta_A}{\delta_{12}}\right)^{(1)} &= 4.4\\ \left(\frac{\delta_D}{\delta_{11}}\right)^{(1)} &= 3.5\end{aligned}\right\}\text{ at 66.4 Hz}$$

These data state, in effect, that the angular acceleration at the base of the spacecraft and at the frequency of the first cantilever torsion mode is nominally four times that "seen" by the flight accelerometers. A reason for this large difference can be inferred from Fig. 5, which shows the in-plane bending of the adapter upper ring associated with the tangential displacements of the six spacecraft-foot/adapter-fitting interconnections. The distortion pattern is not symmetrical because neither the adapter nor the spacecraft is symmetrical, inertially or elastically.

A key to the increase in the first torsion mode frequency with the installation of the LMSC nose fairing is offered in Fig. 5. The nose fairing attachment, circumferentially interdigitated with spacecraft attachments, adds radial stiffness to the adapter upper ring. This stiffness is more significant, in terms of modal frequency, than the added mass of the fairing.

The second cantilever torsion mode was excited at a frequency of 134 Hz. In this mode, the relative tangential displacements of spacecraft feet and adjacent flight accelerometers were established to be as follows:

$$\left.\begin{aligned}\left(\frac{\delta_A}{\delta_{12}}\right)^{(2)} &= -5.5\\ \left(\frac{\delta_D}{\delta_{11}}\right)^{(2)} &= -5.9\end{aligned}\right\}\text{ at 134 Hz}$$

This is to say that nodal points lie between the spacecraft feet and their nearby accelerometers. This situation underscores the need of detailed information on modal behavior in the vicinity of flight accelerometers, if valid interpretations are to be made from telemetered data.

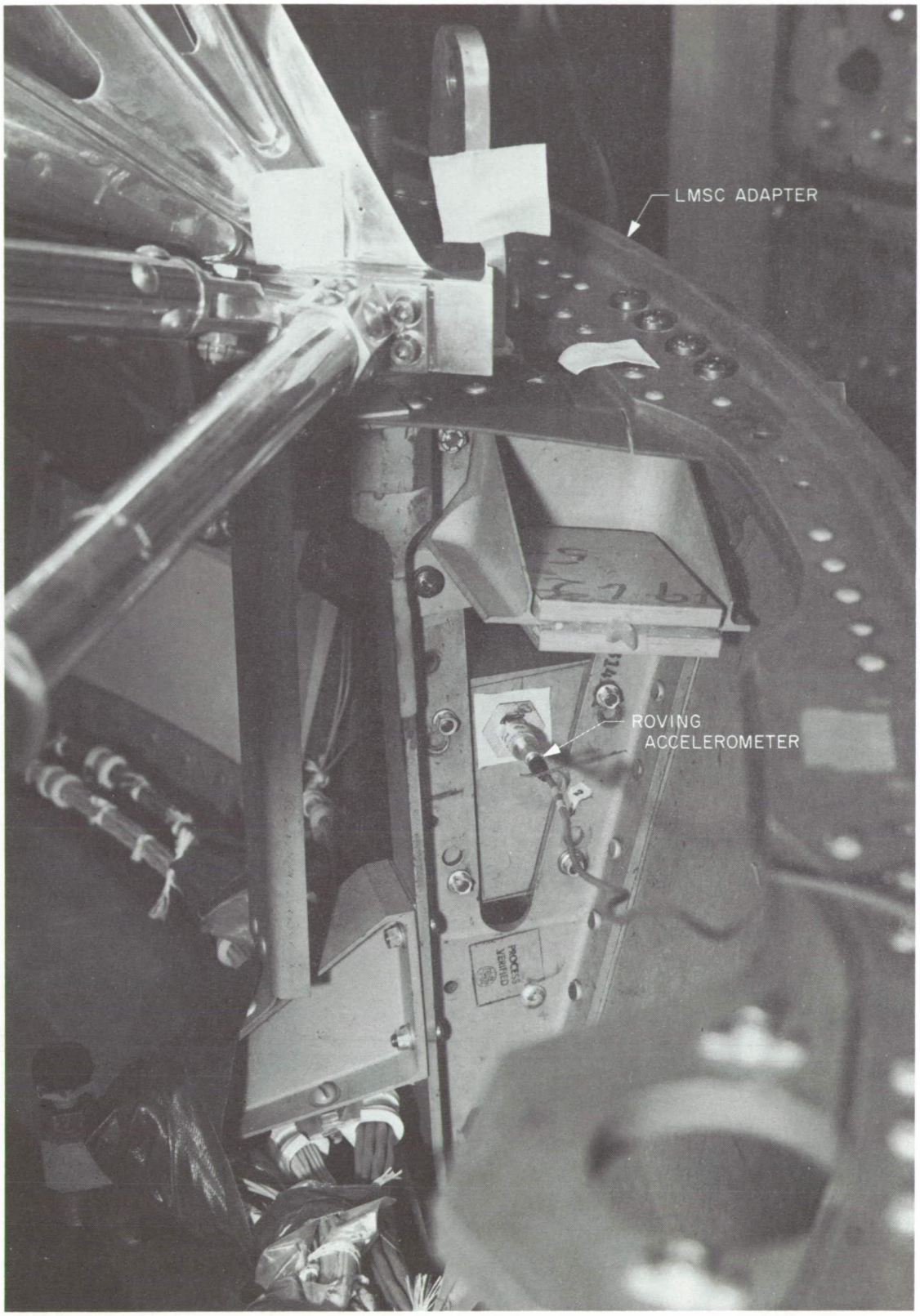

Fig. 2. Modal survey accelerometer at location of "channel 12" flight accelerometer

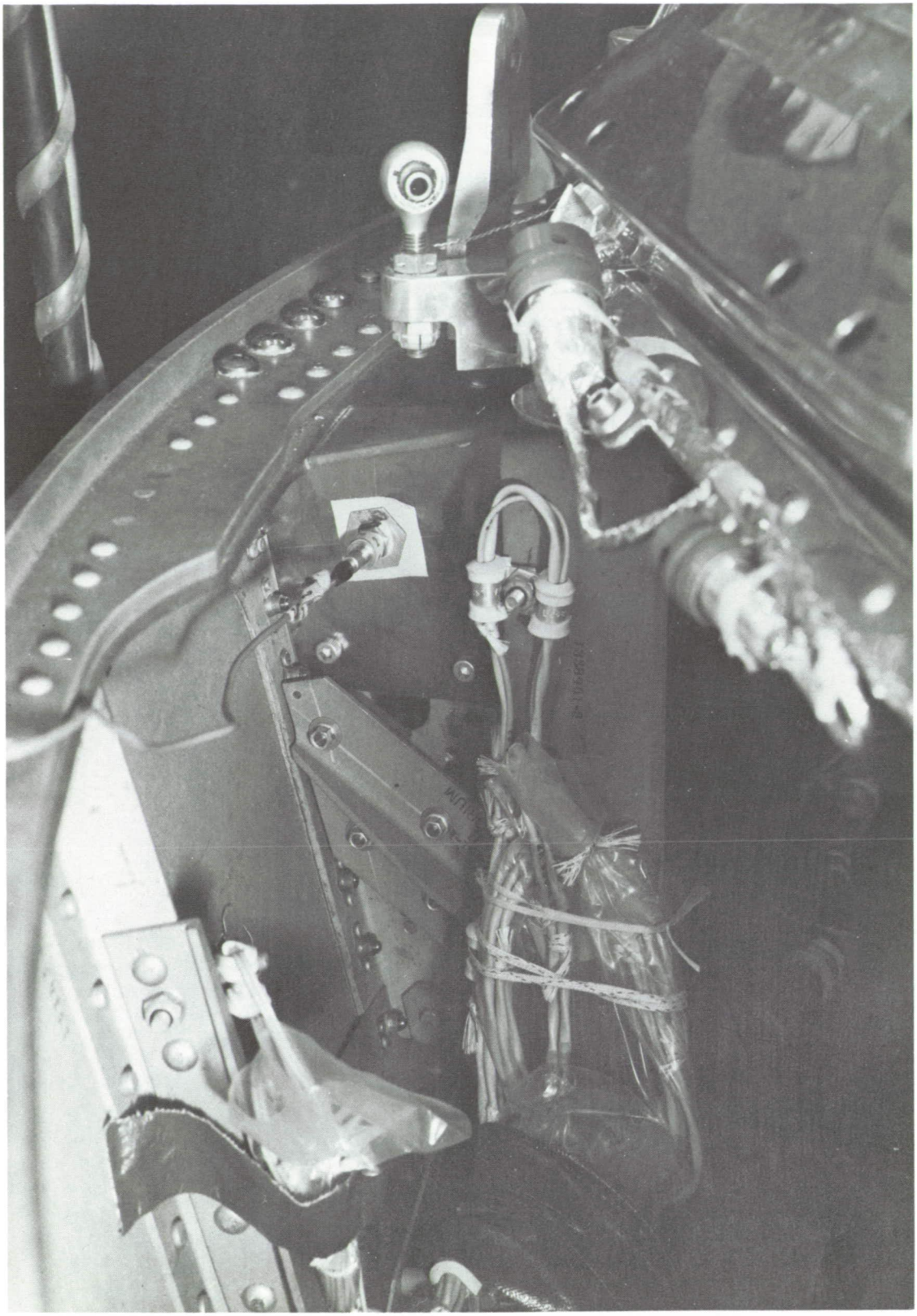

Fig. 3. Modal survey accelerometer at location of "channel 11" flight accelerometer

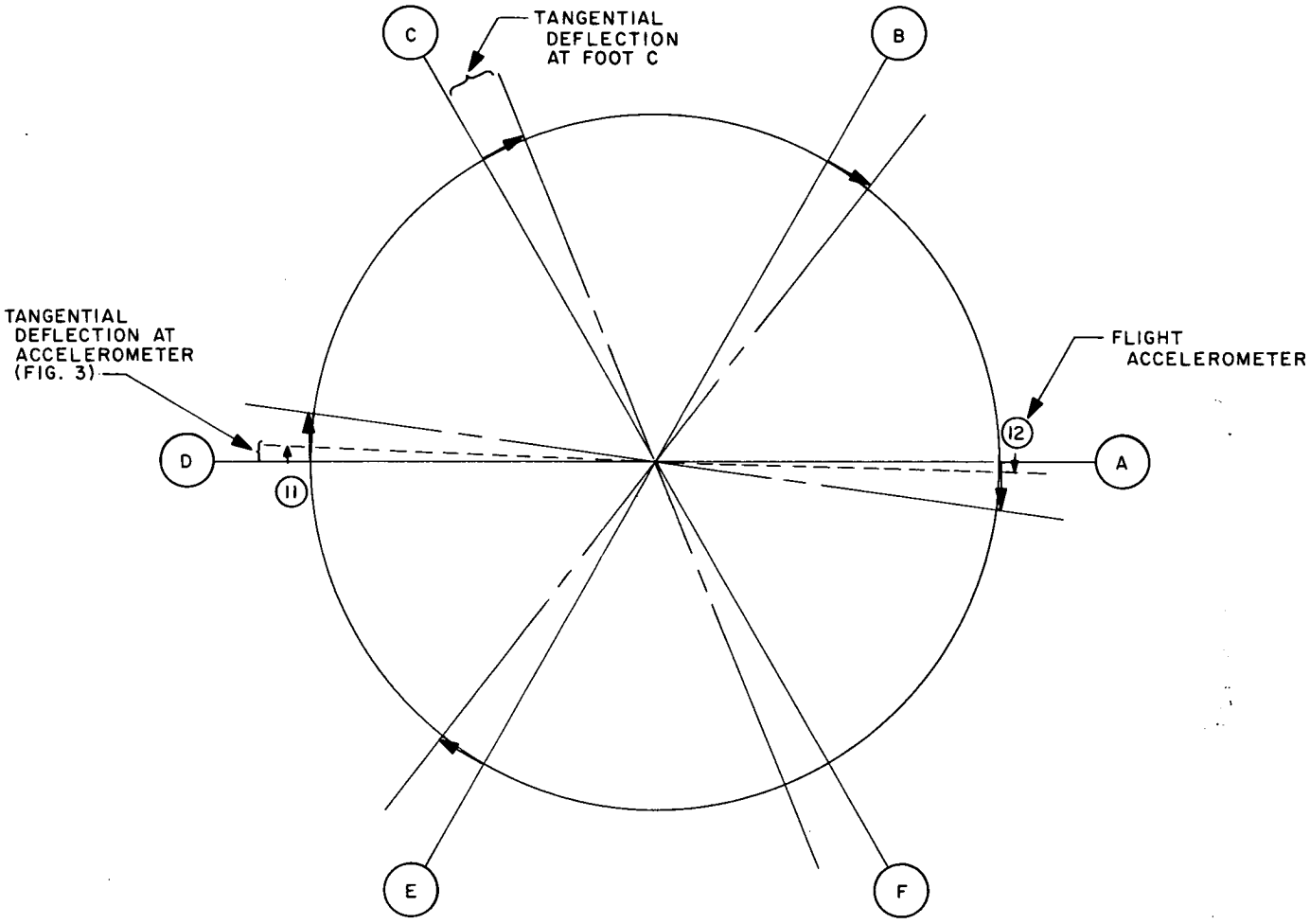

Fig. 4. ***Ranger Block III*** **spacecraft feet tangential deflections**

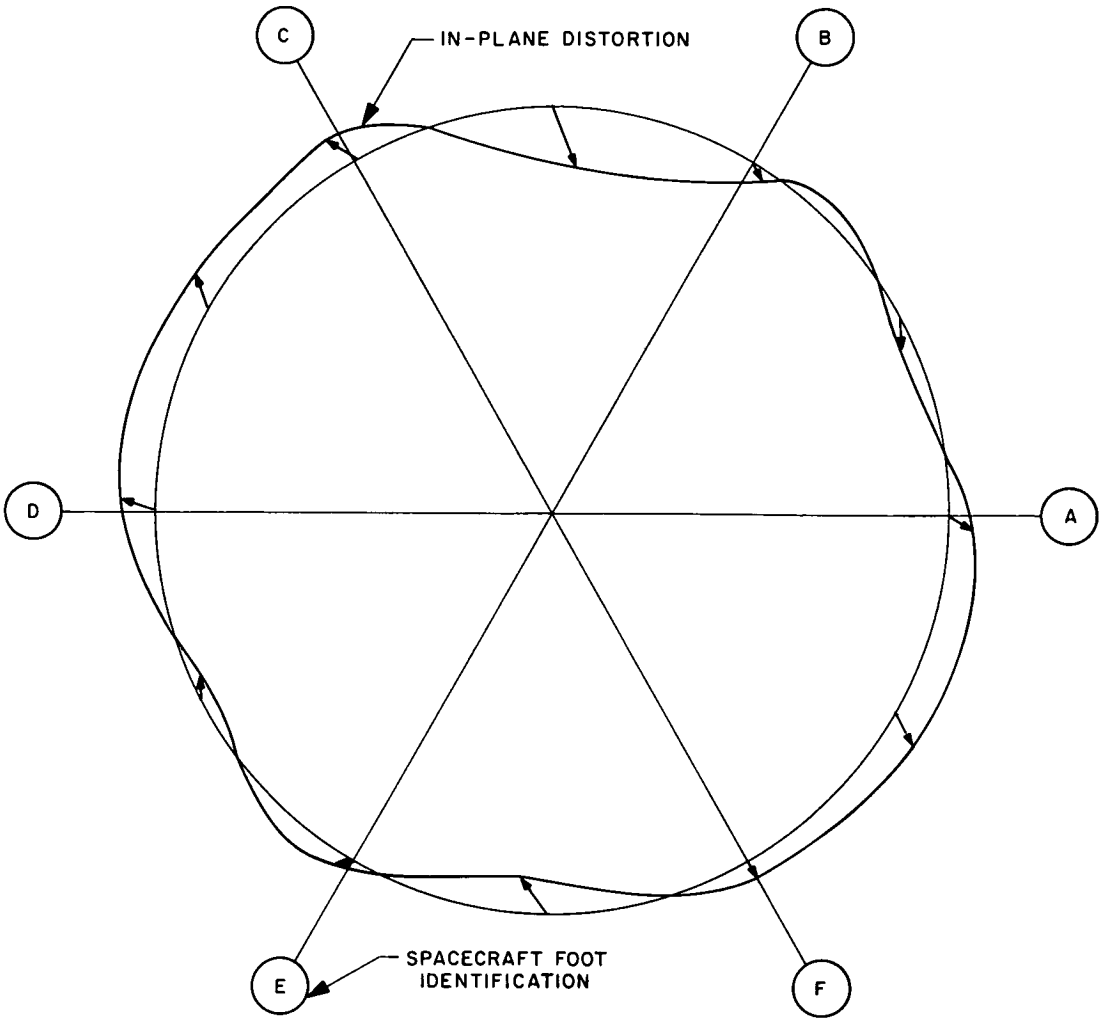

Fig. 5. *Ranger Block III/LMSC adapter-ring distortion in first cantilever torsion mode*

2. ***Modal survey data.*** Table 2 lists data defining the spacecraft mass distribution and the mode shape of the first cantilever torsion mode as measured in the tests of September 1963. This table also summarizes calculations of elements of the generalized mass matrix,

$$[M] \equiv \left[\begin{array}{c|c} M_{rr} & M_{re} \\ \hline M_{er} & M_{ee} \end{array}\right]$$

where

$$M_{rr} = \sum_{i=1}^{i=22} (I_{ZZ})_i$$

$$M_{re} = M_{er} = \sum_{i=1}^{i=22} (I_{ZZ})_i \, \theta_i$$

$$M_{ee} = \sum_{i=1}^{i=22} (I_{ZZ})_i \, \theta_i^2$$

The element M_{rr} is associated with a rigid-body rotation, arbitrarily normalized to 1 rad and, accordingly, is the rigid-body moment of inertia about the roll axis. The element M_{ee} is the generalized mass in the first cantilever torsion mode as normalized. If the frequency of this mode is designated as ω_1 (rad/s), then it can be recognized that the inertia torque T at the base of the adapter is

$$T = \frac{\omega_1^2}{g} M_{re} \text{ (in.-lb)} \tag{2}$$

when M_{re} is expressed in units of lb-in.^{2} and $g = 386$ in./s^2. Figure 6 presents graphs of the mode shape and of the

Table 2. Geometric, inertial, and modal data applying to *Ranger*/adapter first cantilever torsion mode

Station No., i	W, lb	I_{zz}, lb-in.^{2}	θ_i, rad	$I_{zz}\,\theta_i$, lb-in.^{2}	$\Sigma\, I_{zz}\,\theta_i$, lb-in.^{2}	Station (LMSC)
1	4.1	89	0.0812	7	7	144.3
2	79.3	2014	0.0748	151	158	164.8
3	73.5	2670	0.0702	187	345	183.4
4	221.3	13417	0.0694	931	1276	199.6
5–8	3.4	1165	0.0694	81	1357	198.8
9	48.3	620	0.0500	31	1388	214.9
10	40.7	12748	↑	637	⋮	217.9
11	43.8	14339		717	⋮	217.6
12	39.8	11770		589	⋮	217.5
13	45.3	14123		706	⋮	218.6
14	40.5	13570	↓	679	⋮	217.7
15	52.5	17197	0.0500	860	5576	217.7
16	16.6	12961	0.0220	285	⋮	232.5
17	16.8	13117	↑	289	⋮	↑
18	26.3	20530		452	⋮	
19	16.8	13117		289	⋮	
20	16.7	13039	↓	287	⋮	↓
21	12.4	9679	0.0220	213	7391	232.5
22	—	—	0	⋮	7391	244.5
Σ	798.1	186,165		7391		

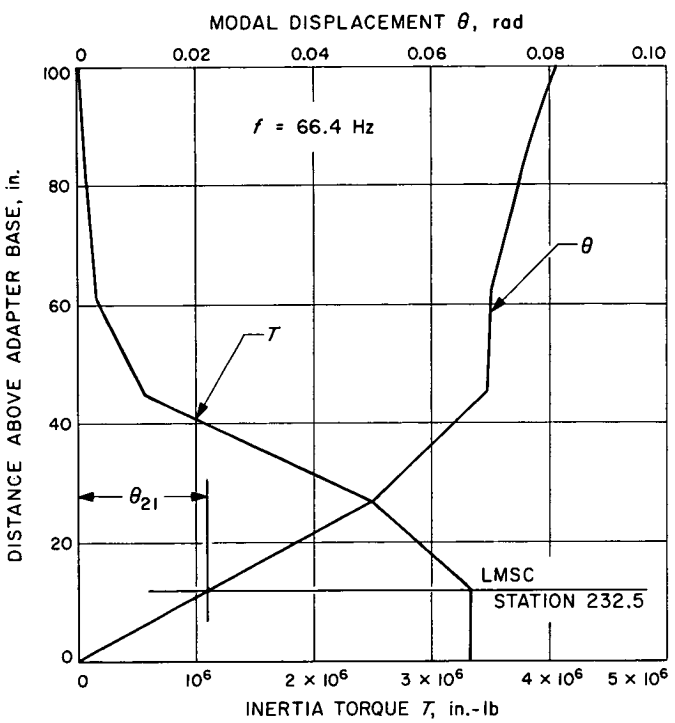

Fig. 6. Mode shape and associated inertia torque distribution in first cantilever torsion mode

inertia torque distribution associated with the modal normalization.

3. Lumped-parameter representation of spacecraft/adapter first torsion mode. The quantitative modal surveys of 1963 present data applying to the spacecraft/adapter combination. To provide for the use of the data from flight accelerometers within the adapter, it is necessary to restructure the modal model of the prior paragraph.

In the mathematical model of the *Agena* vehicle, LMSC has designated station 248 as joint 5 (Fig. 7). The chosen model of the *Ranger* vehicle and its structural connection to the *Agena* through the adapter is represented in Fig. 7, wherein the joints 43, 44, and 45 replace the LMSC joint 17 of Ref. 4.

The relation between this model and the spacecraft/adapter system is derived as follows. The synthesis is made in two stages. First, the adapter is decoupled from the combination to give a spacecraft representation as if it were cantilevered at the separation plane. Next, the adapter is divided to permit introduction of the "accelerometer station," joint 43, using modal survey data from the recent tests.

The initial assumptions made are that the torsional stiffness of the 3.5-in. section of the *Agena* forward midbody between joint 5 and the base of the adapter is essentially infinite in relation to the adapter stiffness, and that this latter stiffness may be computed from the relation:

$$K = \frac{T_o}{\theta_{21}}\ \text{(in.-lb/rad)} \tag{3}$$

JOINT, i	$K_i \times 10^{-8}$, in.-lb/rad	M_i, lb-in.^{2}
45		97,810
	0.952	
44		88,355
	1.97	
43		100
	6.69	
5		SEE TABLE A-2

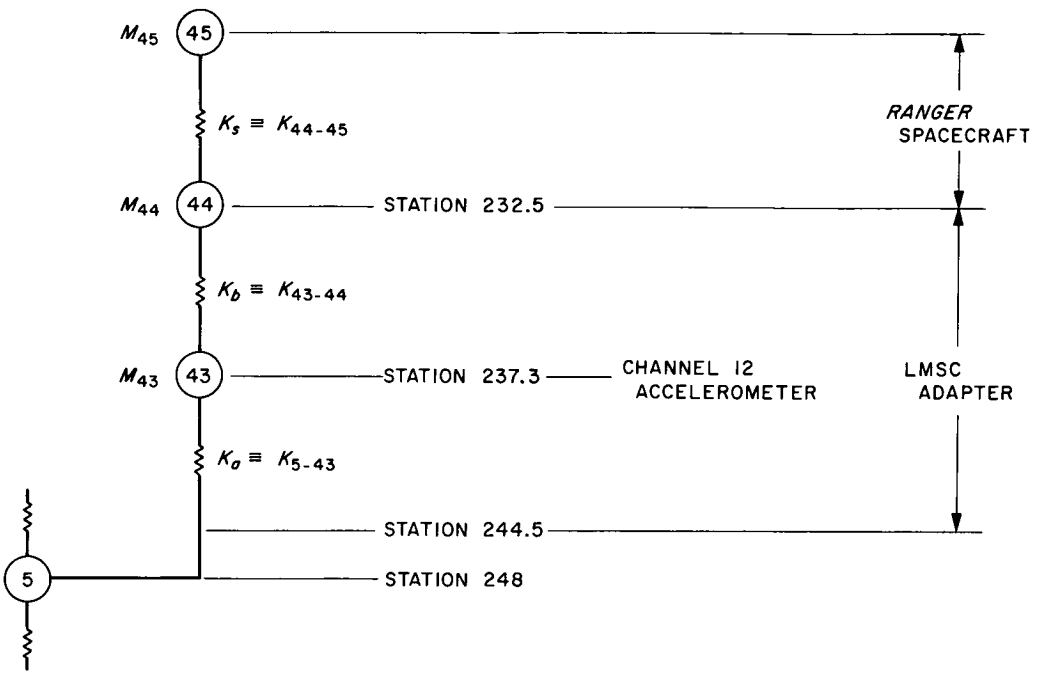

Fig. 7. Lumped-parameter mathematical model of spacecraft/adapter combination

where T_o is the inertia torque at the separation plane and θ_{21} is the apparent angle-of-twist at the separation plane, joint 44. The adequacy of this latter assumption will be tested subsequently.

Using the following values from Table 2,

$$\theta_{21} = 0.0220 \text{ rad}$$

$$M_{re} = 7391 \text{ lb-in.}^2$$

$$f_1 = \frac{\omega_1}{2\pi} = 66.4 \text{ Hz}$$

and using Eqs. (2) and (3),

$$K = \frac{\omega_1^2 M_{re}}{g\theta_{21}}$$

$$= 1.52 \times 10^8 \text{ in.-lb/rad}$$

This treatment, consistent with the processing of the modal survey data, neglects the influence of inertia loads within the adapter structure. Compatible therewith, the spacecraft modal deflection at the ith mass in the first torsion mode, as measured, may be regarded as the sum of a rigid-body rotation θ_{21} and an angle-of-twist $\alpha_i = \theta_i - \theta_{21}$. The associated generalized mass matrix of the *Ranger* spacecraft is

$$[m] \equiv \left[\begin{array}{c|c} m_{rr} & m_{re} \\ \hline m_{er} & m_{ee} \end{array}\right]$$

where

$$m_{rr} = M_{rr}$$

$$m_{re} = \sum_{i=1}^{i=22} (I_{ZZ})_i (\theta_i - \theta_{21})$$

$$= M_{re} - \theta_{21} M_{rr}$$

$$m_{ee} = \sum_{i=1}^{i=22} (I_{ZZ})_i (\theta_i - \theta_{21})^2$$

$$= M_{ee} - 2\theta_{21} M_{re} + \theta_{21}^2 M_{rr}$$

Use of the data in Table 2 gives

$$[m] = \left[\begin{array}{c|c} 186{,}165 & 3{,}295 \\ \hline 3{,}295 & 111.0 \end{array}\right] (\text{lb-in.}^2)$$

This mass matrix is still to be associated with a *Ranger* spacecraft having a single cantilever mode with a generalized mass defined by m_{ee} and a base inertia torque proportional to m_{re}. To convert this "distributed" model to an equivalent, discrete, spring-mass system, it is necessary only to renormalize the amplitude of the elastic mode in a manner that equates the generalized mass to a lumped mass providing the proper root torque. Thus, if μ is the renormalization factor, the new "generalized mass" is

$$\mathcal{M}_{ee} = \mu^2 m_{ee}$$

and the new "rigid-elastic" coupling term, proportional to the root torque, is

$$\mathcal{M}_{re} = \mu m_{re}$$

The requirement is simply that μ be chosen such that

$$\mathcal{M}_{ee} = \mathcal{M}_{re}$$

or that

$$\mu = \frac{m_{re}}{m_{ee}}$$

$$= 29.69$$

The new mass matrix associated with this renormalization is

$$[\mathcal{M}] = \left[\begin{array}{c|c} 186{,}165 & 97{,}810 \\ \hline 97{,}810 & 97{,}810 \end{array}\right] (\text{lb-in.}^2)$$

The mode shape plot of the renormalized first cantilever mode of the *Ranger* spacecraft is presented in Fig. 8.

Application of this criterion* yields a single spring-mass system dynamically equivalent to the *Ranger* spacecraft

*An extension of this normalization concept to the general case of freeing an N-degree-of-freedom cantilevered normal-mode system in all six rigid-body modes will be treated in Ref. 5.

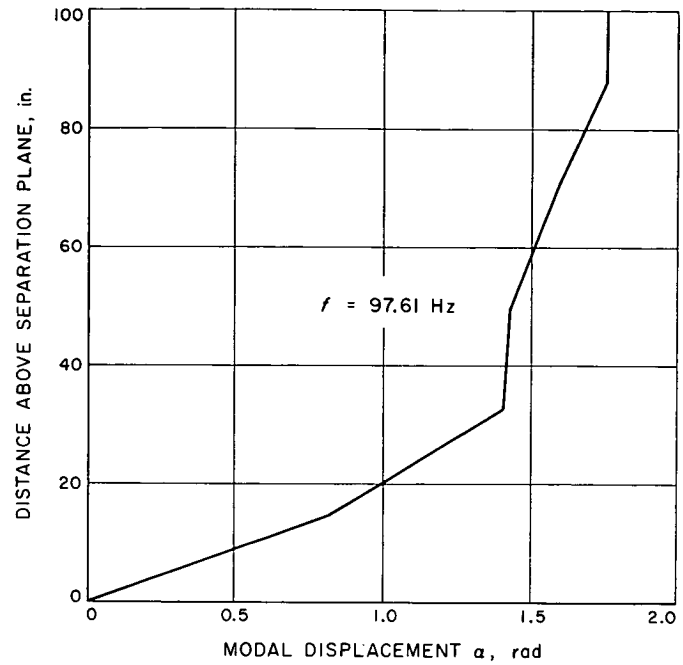

Fig. 8. First cantilever mode shape renormalized to give $\mathcal{M}_{er}^* = \mathcal{M}_{ee}^* = 97{,}810$ lb-in.^{2}

in its first cantilever torsion mode. In terms of the mathematical model under derivation, this is to say that, with joint 44 fixed, the representation is proper. However, since joint 44 is not fixed, the rigid-body mass term must be augmented by an incremental mass:

$$\Delta m = M_{rr} - \mathcal{M}_{ee}$$

Since the LMSC adapter is treated in this analysis as massless, the mathematical model of the spacecraft/adapter combination, as subjected to modal vibration surveys, is now advanced to the representation shown in the adjacent sketch, wherein

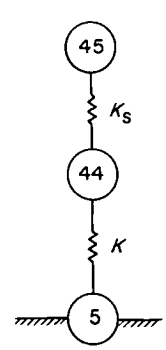

$M_{45} \equiv \mathcal{M}_{ee} = 97{,}810$ lb-in.^{2}

$M_{44} \equiv \Delta W = 88{,}355$ lb-in.^{2}

$K = 1.52 \times 10^8$ in.-lb/rad (from prior assumptions)

For the *Ranger* part of the system, it remains to determine the spring constant K_s from the relevant masses, the derived value of K, and the observed first-torsion-mode frequency of the complete system.

By regarding this system as one in which the generalized coordinates are chosen as independent rotations θ_{44} and θ_{45} of the two masses M_{44} and M_{45}, respectively, the equations of motion for free vibration may be written as

$$-\frac{\omega^2}{g}\begin{bmatrix} M_{45} & 0 \\ 0 & M_{44} \end{bmatrix}\begin{Bmatrix} \theta_{45} \\ \theta_{44} \end{Bmatrix} + \begin{bmatrix} K_s & -K_s \\ -K_s & (K_s + K) \end{bmatrix}\begin{Bmatrix} \theta_{45} \\ \theta_{44} \end{Bmatrix} = \{0\}$$

An "inverse solution" of this equation, making use of the *measured* first root $\omega = \omega_1 = 2\pi(66.4)$, leads to the value:

$$K_s = 95.20 \times 10^6 \text{ in.-lb/rad}$$

From this derived stiffness, the frequency of the first cantilever torsion mode of the *Ranger* spacecraft is computed to be 97.6 Hz, as compared with the measured frequency of 96.0 Hz with the spacecraft "hard-mounted." This agreement is considered to give adequate engineering support to the assumptions made in the derivation of the LMSC adapter torsional stiffness.

Finally, it remains to introduce joint 43, representing an "equivalent station" of flight accelerometer measurements. For this purpose, the station of the channel 12 flight accelerometer is chosen as the reference station. The adapter spring K is replaced with two springs K_1 and K_2 in series. For a torque T applied at joint 44,

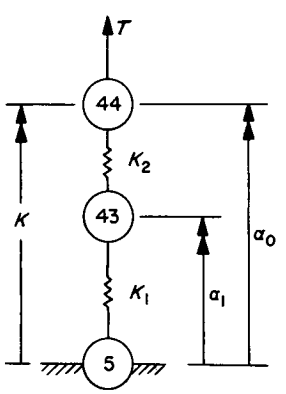

or

$$\frac{\alpha_1}{\alpha_0} = \frac{K}{K_1}$$

$$K_1 = \frac{\alpha_0}{\alpha_1} K$$

From the modal vibration survey of the first torsion mode,

$$\left(\frac{\alpha_0}{\alpha_1}\right)^{(1)} = 4.4$$

Thus,

$$K_1 = 6.69 \times 10^8 \text{ in.-lb/rad}$$

Also,

$$K_2 = \frac{K_1 K}{K_1 - K}$$

$$= 1.97 \times 10^8 \text{ in.-lb/rad}$$

An arbitrarily small moment of inertia is assigned to joint 43, as shown in the tabular inset on Fig. 7, to avoid computational difficulties.

The model of Fig. 7 loses validity for the calculation of space-vehicle "free-free" torsion modes having frequencies much above, say, 100 Hz, because the second cantilever torsion mode at 134 Hz has not been represented in the synthesis.

For the plotting of space-vehicle mode shapes, the lumped-parameter representation of the spacecraft participation factor $\phi_{45}^{(r)}$ is converted back to the mode shape of Fig. 8 as follows. If $\phi_k^{(r)}$ is the total displacement of the kth *Ranger* station in the rth normal mode, then

$$\phi_k^{(r)} = \phi_{44}^{(r)} + \left(\phi_{45}^{(r)} - \phi_{44}^{(r)}\right)\alpha_k$$

4. Conversion of linear acceleration flight data to angular acceleration. The tangentially oriented flight accelerometers of channels 11 and 12 were polarized such that a properly weighted algebraic sum of the instantaneous outputs is proportional to the angular acceleration $\ddot{\theta}_{43}$ at joint 43. If a_{11} and a_{12} are the respective accelerations in g and $d = 60.5$ is the diametral spacing, then

$$\ddot{\theta}_{43} = \frac{a_{12} + \frac{3.5}{4.4} a_{11}}{d}$$

or

$$\ddot{\theta}_{43} = 6.4a_{12} + 5.1a_{11}\,(\text{rad/sec}^2)$$

This relation has been used by M. R. Trubert (Ref. 1) in obtaining a magnetic tape track representing the *Ranger VI–IX* angular acceleration time histories of joint 43 at BECO.

B. *Atlas* Booster-Engine Representation

1. Interim mathematical model. From data provided by GD/C, each *Atlas* booster engine may be represented as shown in Fig. 9, wherein the engine gimbal block has a tangential spring rate $K_{\delta\delta}$ relative to the *Atlas* body structure at GD/C station 1212. The engine is restrained in rotation about the gimbal by a rotational spring of stiffness $K_{\beta\beta}$ provided by the actuating system and the back-up structure. The gimbal block is treated as massless. The engine has a mass m with its CG at a distance r below the gimbal axis, a centroidal pitching moment of inertia I_{o_Y}, and a centroidal rolling moment of inertia I_{o_Z}.

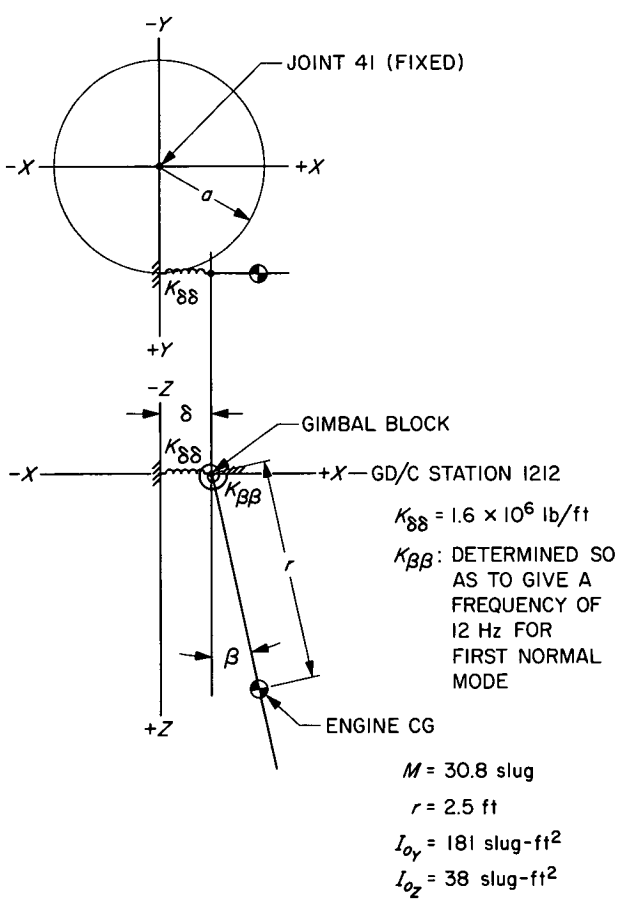

Fig. 9. Mathematical model of *Atlas* booster engine

By defining

$$\delta = \delta_0\, q_1(t)\,(\text{ft})$$

$$\beta = \beta_0\, q_2(t)\,(\text{rad})$$

the equations of motion for free vibration may be derived from application of Lagrange's equations as

$$[M]\,\{\ddot{q}\} + [K]\,\{q\} = \{0\} \tag{4}$$

where

$$[M] = \begin{bmatrix} m\delta_o^2 & mr\delta_o\beta_o \\ mr\delta_o\beta_o & I_Y \end{bmatrix} (\text{slug-ft}^2)$$

$$I_Y = mr^2 + I_{o_Y}$$

$$[K] = \begin{bmatrix} K_{\delta\delta}\delta_o^2 & 0 \\ 0 & K_{\beta\beta}\beta_o^2 \end{bmatrix} (\text{lb-ft})$$

and

$$\{q\} = \begin{Bmatrix} q_1(t) \\ q_2(t) \end{Bmatrix} (\text{non-dimensional})$$

Normalization of the chosen degrees of freedom is optional; thus, if $\delta_o = 1$ ft, and if $\beta_o = 1$ rad,

$$[M] = \begin{bmatrix} m & mr \\ mr & I_Y \end{bmatrix} (\text{slug-ft}^2)$$

$$[K] = \begin{bmatrix} K_{\delta\delta} & 0 \\ 0 & K_{\beta\beta} \end{bmatrix} (\text{lb-ft})$$

By defining

$$\left.\begin{aligned} \omega_\delta^2 &= \frac{K_{\delta\delta}}{m} \\ \omega_\beta^2 &= \frac{K_{\beta\beta}}{I_Y} \end{aligned}\right\} \tag{5}$$

$$A = \left(\frac{\omega_\beta}{\omega_\delta}\right)^2 \tag{6}$$

$$\lambda = \left(\frac{\omega_\delta}{\omega}\right)^2 \tag{7}$$

and by noting that

$$\{\ddot{q}\} = -\omega^2\,\{q\} \tag{8}$$

the frequency equation may be written in determinantal form from Eqs. (4) through (8) as

$$\begin{vmatrix} 1-\lambda & r \\ \dfrac{r}{\rho^2} & 1-A\lambda \end{vmatrix} = 0$$

where $\rho^2 = I_Y/m$.

The natural frequencies ω_1 and ω_2 are obtainable from the roots of the associated quadratic equation in λ. Further, by denoting the (square) modal matrix as

$$[q] \equiv \begin{bmatrix} q_{11} & q_{12} \\ q_{21} & q_{22} \end{bmatrix}$$

the mode shapes are obtainable from

$$\left(\frac{\delta}{\beta}\right)_i = \frac{\delta_o}{\beta_o}\left(\frac{q_{1i}}{q_{2i}}\right)$$

$$= \frac{r}{\lambda_i - 1}, \qquad i = 1, 2$$

The generalized mass matrix in the normal modes is a diagonal matrix,

$$[\mathcal{M}] = [q]^T [M] [q]$$

where the superscript T denotes "transposed."

The inertial data applying to each booster engine are listed in Fig. 9 directly as given by GD/C. The listed translational stiffness $K_{\delta\delta}$ is derived from the stiffnesses given for two springs in series. Further, in accordance with a GD/C recommendation, a value of $K_{\beta\beta}$ is determined by iteration to give a frequency of 12 Hz for the first engine mode, as observed in vibration surveys with an *Atlas* vehicle in a test stand. Thus, in matrix form, the input data to the analysis of the interim mathematical model are as follows:

$$[M] = \begin{bmatrix} 30.8 & 77.0 \\ 77.0 & 373.5 \end{bmatrix} (\text{slug-ft}^2)$$

$$[K] = 10^6 \begin{bmatrix} 1.600 & 0 \\ 0 & 2.242 \end{bmatrix} (\text{lb-ft})$$

Numerical solution yields the modal frequencies,

$$f_1 = 11.96 \text{ Hz} \qquad \omega_1^2 = 5647 \ (\text{rad/s}^2)$$

$$f_2 = 53.73 \text{ Hz} \qquad \omega_2^2 = 11.40 \times 10^4 \ (\text{rad/s}^2)$$

the modal matrix,

$$[q] = \begin{bmatrix} 0.3049 & -4.594 \\ 1.0000 & 1.0000 \end{bmatrix}$$

the generalized mass matrix,

$$[\mathcal{M}] = \begin{bmatrix} 423.3 & 0 \\ 0 & 316.1 \end{bmatrix} (\text{slug-ft}^2)$$

and the generalized stiffness matrix

$$[\mathcal{K}] = \begin{bmatrix} \omega_1^2 \mathcal{M}_{11} & 0 \\ 0 & \omega_2^2 \mathcal{M}_{22} \end{bmatrix}$$

$$= 10^6 \begin{bmatrix} 2.390 & 0 \\ 0 & 36.02 \end{bmatrix} (\text{lb-ft})$$

These modal data are presented in Fig. 10, wherein

$$e_i = \left(\frac{\delta}{\beta}\right)_i$$

2. *Final mathematical model.* The two normal modes computed for the interim mathematical model apply to an *Atlas* vehicle constrained at GD/C station 1212. For the computation of "free-free" torsion modes of the entire space vehicle, consideration must be made that joint 41 at station 1212 can oscillate through an angle α, as shown in Fig. 11. A diametral line B-B', passing through the centers of gravity of the two booster engines, will rotate through an angle α_B. It is, thus, required to account for the rigid-body inertial properties of the booster engines, as well as the inertial coupling between joint 41 rigid-body rotation and the two elastic modes. Thus, the complete mass matrix is

$$[\bar{M}] = \left[\begin{array}{c|c} \mathcal{M}_{rr} & \mathcal{M}_{re} \\ \hline \mathcal{M}_{er} & \mathcal{M}_{ee} \end{array}\right]$$

If $\alpha = \alpha_o q_o(t)$, and the normalization is chosen such that $\alpha_o = 1$ rad, then

$$\mathcal{M}_{rr} = ma^2 + I_{o_Z}$$

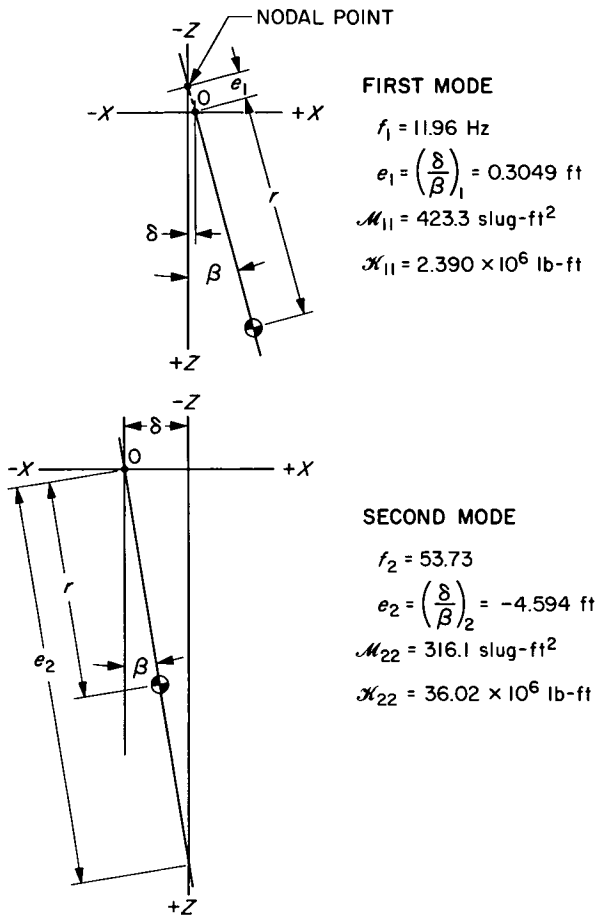

Fig. 10. Normal modes of *Atlas* booster engine

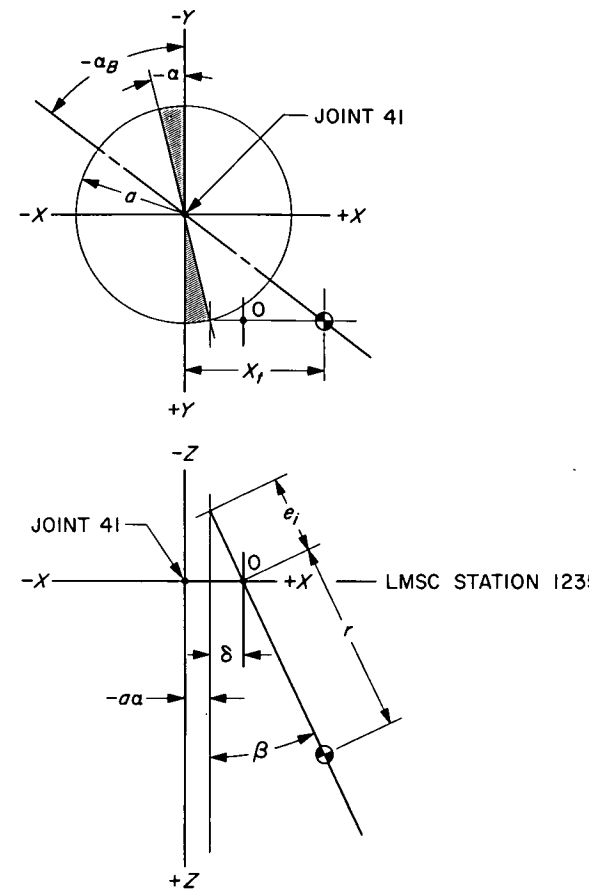

Fig. 11. Gross motion of *Atlas* booster engine in "free-free" torsion mode of space vehicle

The $\mathcal{M}_{ee}$ is the diagonal mass matrix $\mathcal{M}$ of the interim model. For the inertial coupling between the ith elastic mode and rigid-body rotation,

$$(\mathcal{M}_{re})_i = (\mathcal{M}_{er})_i = -ma(r + e_i)$$

where $e_i = (\delta/\beta)_i$ as obtained from the modal matrix $[q]$.

With numerical substitutions,

$$[\bar{M}] = \left[\begin{array}{c|cc} 808.0 & -432.0 & 322.5 \\ \hline -432.0 & 423.3 & 0 \\ 322.5 & 0 & 316.1 \end{array}\right]$$

For synthesis of a simple spring-mass equivalent of each engine normal-mode, the elastic modes are renormalized by a scaling factor μ_i such that

$$(\mathcal{M}^*_{re})_i = \mu_i (\mathcal{M}_{re})_i$$

$$(\mathcal{M}^*_{ee})_i = \mu_i^2 (\mathcal{M}_{ee})_i$$

and

$$(\mathcal{M}^*_{re})_i = (\mathcal{M}^*_{ee})_i$$

It follows that the normalization factor

$$\mu_i = \left(\frac{\mathcal{M}_{re}}{\mathcal{M}_{ee}}\right)_i$$

Thus,

$$\mu_1 = -1.0206$$

$$\mu_2 = 1.0202$$

and the renormalized mass matrix is

$$[\overline{M}^*] = \left[\begin{array}{c|cc} 808.0 & 440.9 & 329.0 \\ \hline 440.9 & 440.9 & 0 \\ 329.0 & 0 & 329.0 \end{array}\right]$$

For both booster engines, with units converted from slug-ft² to lb-in.²,

$$[\overline{W}^*] = 9274\,[\overline{M}^*]$$

$$= 10^6 \left[\begin{array}{c|cc} 7.493 & 4.089 & 3.051 \\ \hline 4.089 & 4.089 & 0 \\ 3.051 & 0 & 3.051 \end{array}\right] \text{(lb-in.}^2\text{)}$$

The associated stiffness matrix is

$$[\overline{K}^*] = \left[\frac{\omega^2}{g}\right][\overline{W}^*]$$

$$= 10^9 \left[\begin{array}{c|cc} 0 & 0 & 0 \\ \hline 0 & 0.05976 & 0 \\ 0 & 0 & 0.8998 \end{array}\right] \text{(in.-lb/rad)}$$

In modifying the given lumped-parameter model of the *Atlas*, the incremental moment of inertia to be added to joint 41 to preserve the proper rigid-body representation is

$$\Delta\overline{W}^* = \overline{W}^*_{rr} - \sum(\overline{W}^*_{ee})_i$$

$$= 0.353 \times 10^6 \text{ lb-in.}^2$$

Thus, the representation is as shown in Fig. 12. As a result of the modal renormalization,

$$\left.\begin{aligned} (\delta^*_o)_i &= \mu_i\,\delta_o \\ (\beta^*_o)_i &= \mu_i\,\beta_o \end{aligned}\right\} i = 1, 2$$

If $\{\phi^{(r)}\}$ is the eigenvector representing the shape of the rth normal mode of the "free-free" composite vehicle, then the net tangential displacement of the CG of the particular booster engine (shown in Figs. 10 and 11) is

$$x_T^{(r)} = -a\phi_{41}^{(r)} + (e_1 + r)\,\mu_1\,\beta_o\,(\phi_{46}^{(r)} - \phi_{41}^{(r)})$$

$$+ (e_2 + r)\,\mu_2\,\beta_o\,(\phi_{47}^{(r)} - \phi_{41}^{(r)})$$

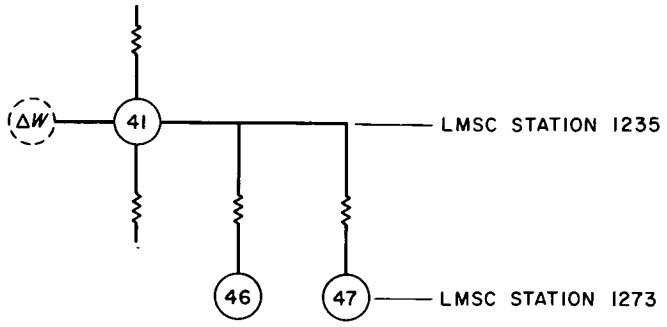

$K_{41\text{-}46}$ = 0.5976 × 10^8 in.-lb/rad
$K_{41\text{-}47}$ = 8.998 × 10^8 in.-lb/rad
W_{46} = 4.089 × 10^6 lb-in.²
W_{47} = 3.051 × 10^6 lb-in.²
ΔW = 0.353 × 10^6 lb-in.²

Fig. 12. Mathematical model of *Atlas* booster engines relative to joint 41

For the plotting of mode shapes, booster engine modal participation is represented by the angle

$$\phi_B^{(r)} = -\frac{x_T}{a}$$

$$= \phi_{41}^{(r)} + 0.5725\,(\phi_{46}^{(r)} - \phi_{41}^{(r)}) + 0.4273\,(\phi_{47}^{(r)} - \phi_{41}^{(r)})$$

C. Composite Model

Eigenvalues and eigenvectors for two different representations of the *Atlas/Agena/Ranger* vehicle were obtained. The normal modes for the composite model used by M. R. Trubert (Ref. 1) were obtained using the JPL initial model of the *Atlas/Agena/Ranger* system. The JPL final model was upgraded in two areas: (1) the *Atlas* booster engine representation, and (2) the LMSC adapter representation.

The final mathematical model of the *Atlas/Agena/Ranger* vehicle is shown in Fig. 13. The numerical values corresponding to this model are listed in Appendix A.

1. Initial model. The initial model consisted of three separate systems:

(1) The *Atlas/Agena/Ranger* torsion model less *Atlas* booster engines.

(2) The +Y *Atlas* booster engine.

(3) The −Y *Atlas* booster engine.

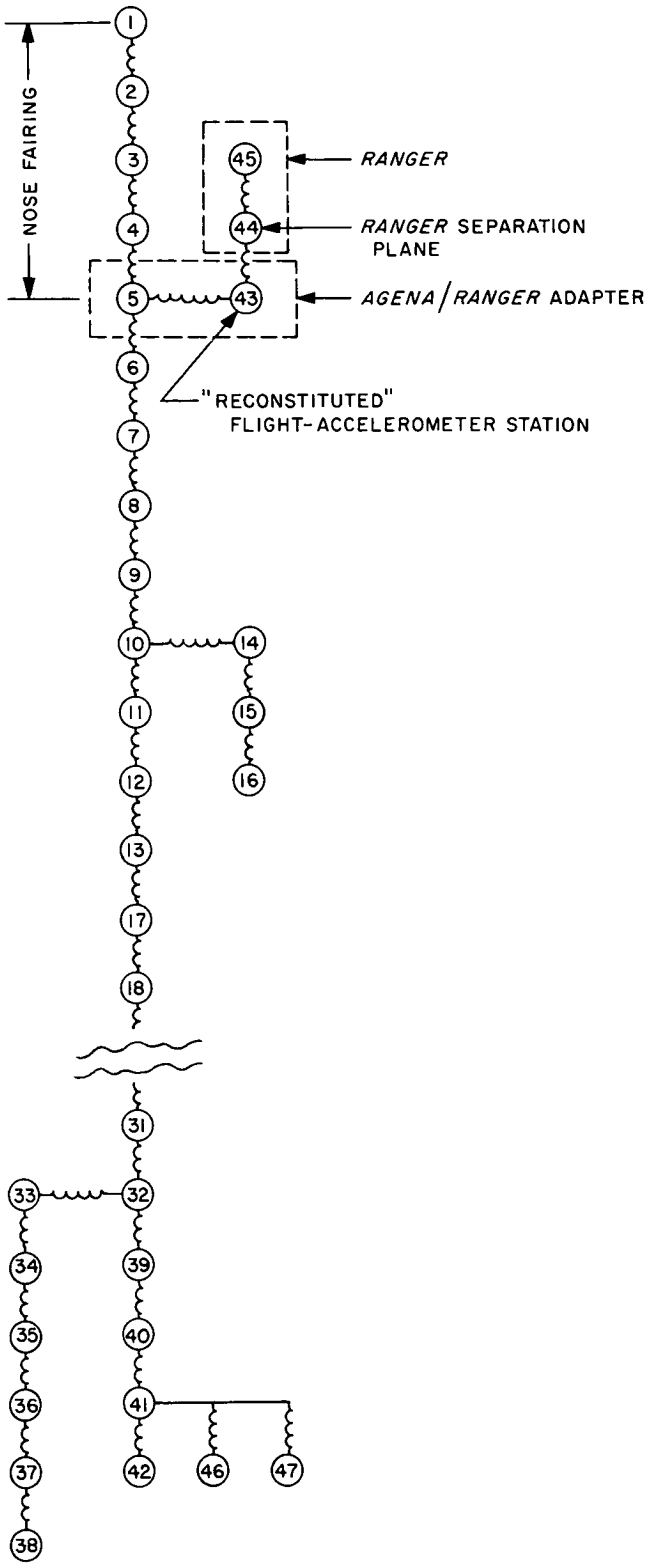

Fig. 13. *Atlas/Agena/Ranger* mathematical model

The *Atlas/Agena/Ranger* model less the *Atlas* booster engines is obtained by deleting joints 46 and 47 and their associated springs from the model given in Fig. 13. Since the *Atlas* booster engines were represented as separate systems in this model, the inertia at joint 41 is reduced by 0.353×10^6 lb-in.^{2} to 0.75662×10^7 lb-in.^{2} The adapter stiffness deviated from the upgraded final model as follows: $K_{5-43} = 0.8216 \times 10^9$ in.-lb/rad, and $K_{43-44} = 0.1865 \times 10^9$ in.-lb/rad.

The interim mathematical model for the *Atlas* booster engine, as described in Section II-B, was used for each of the two engines in the initial composite model.

The eigenvectors and eigenvalues of the unrestrained composite system were obtained by using the JPL Modal Combination Program. This program is based on the component mode synthesis method developed by W. C. Hurty (Ref. 6) and implemented by R. M. Bamford (Ref. 7). It requires the eigenvectors and eigenvalues of the various systems as input.

Twenty eigenvectors and the associated eigenvalues for the composite system, less the booster engines, were obtained using the JPL Stiffness Matrix Structural Analysis Program (Ref. 8). The system was temporarily restrained at joint 31.

For the *Atlas* booster engines, the normal mode representation of the interim mathematical model, as described in Section II-B, was used.

Within the Modal Combination Program, displacement compatibility of both *Atlas* booster engines and joint 41 of the *Atlas/Agena/Ranger* model, less engines, was established. Using appropriate geometric transformations, overall system generalized mass and spring matrices, including rigid-body modes, are computed. These are of the form:

$$[M] = \left[\begin{array}{c|c} M_{rr} & M_{re} \\ \hline M_{er} & M_{ee} \end{array}\right]$$

$$[K] = \left[\begin{array}{c|c} 0 & 0 \\ \hline 0 & K_{ee} \end{array}\right]$$

Here M_{ee} is no longer a diagonal matrix. To obtain the "free-free" eigenvalues of the composite vehicle, the following eigenvalue problem must be solved:

$$[M_{ee} - M_{er} M_{rr}^{-1} M_{re}] \{\ddot{q}\} + [K_{ee}] \{q\} = \{0\}$$

To solve this problem within the existing program, the M_{rr} matrix must be nonsingular. To insure this, rigid body inertial properties for the additional five degrees of freedom were included at the temporarily fixed joint 31.

The frequencies and modal displacements at joints 41 and 43 for the first "free-free" composite system modes, as used by M. R. Trubert, are given in Table 3.

Table 3. Modal displacements of the JPL initial model for *Atlas/Agena/Ranger*

f_r, Hz	Joint 43 adapter accelerometers, $\phi_{43}^{(r)}$	Joint 41 gimbal blocks, $\phi_{41}^{(r)}$
12.02	-0.17260×10^{-6}	-0.13690×10^{-6}
12.58	0.12638×10^{-2}	0.98453×10^{-3}
34.48	0.14064×10^{-1}	-0.12334×10^{-2}
53.90	-0.41446×10^{-7}	0.75397×10^{-8}
55.29	0.34258×10^{-2}	-0.60356×10^{-3}
67.62	0.57771×10^{-2}	0.13865×10^{-2}
79.82	0.15257×10^{-2}	-0.82467×10^{-3}
80.46	-0.46660×10^{-2}	-0.13787×10^{-2}
110.62	-0.41532×10^{-2}	0.13208×10^{-2}
147.18	0.16342×10^{-2}	-0.85519×10^{-3}

The values given in Table 3 are normalized such that the generalized mass is unity.

The "free-free" eigenvectors contain in-phase modes because of the *Atlas* booster engine representation. These "symmetric" modes, occurring at 12.02 and 53.90 Hz, are inertially balanced by a rigid-body displacement of the whole space vehicle and are of no interest for the problem at hand. The modal displacements for the points of interest in these two modes are several orders of magnitude less than in the true torsion modes.

2. Final model. The final *Atlas/Agena/Ranger* torsion model (Fig. 13) has been obtained similarly to the initial model, except that the *Atlas* booster engines were transformed to equivalent lumped spring mass systems, as described in Section II-B. The numerical values corresponding to Fig. 13 are listed in Appendix A.

The frequencies and the modal displacements at joints 41 and 43 for the first eight "free-free" composite system normal modes are given in Table 4.

Table 4. Modal displacements of the JPL final model for *Atlas/Agena/Ranger*

f_r, Hz	Joint 43 adapter accelerometers, $\phi_{43}^{(r)}$	Joint 41 gimbal blocks, $\phi_{41}^{(r)}$
12.58	-0.12516×10^{-2}	-0.97591×10^{-3}
34.58	0.14149×10^{-1}	-0.12236×10^{-2}
55.29	0.35157×10^{-2}	-0.59902×10^{-3}
67.56	0.64876×10^{-2}	0.13797×10^{-2}
79.78	0.93196×10^{-3}	-0.90644×10^{-3}
80.42	-0.38160×10^{-2}	-0.13051×10^{-2}
104.37	-0.41045×10^{-2}	0.11597×10^{-2}
144.82	-0.17270×10^{-2}	0.10388×10^{-2}

The values given in Table 4 are normalized to give a unit generalized mass. Because of the different engine representation in this model as compared to the initial model, the symmetric modes are not present. Plots of the first eight eigenvectors are shown in Appendix B.

The *Ranger* participation has been calculated as described in Section II-A. The effective angle-of-twist for the booster engines has been derived in Section II-B.

III. *Atlas/Centaur/Surveyor* Vehicle

The basic mathematical model of the *Atlas/Centaur/Surveyor* vehicle was provided by GD/C under JPL Contract No. 950994. The JPL program has modified this model in three respects:

(1) The representation of the *Surveyor* spacecraft and the adapter structure supporting the spacecraft has been replaced with one derived from modal vibration surveys conducted by the Hughes Aircraft Company (HAC).

(2) The representation of the *Atlas* stage aft of GD/C station 1133 (LMSC station 1156) has been modified in accordance with the *Atlas* model of Section II.

(3) The *Centaur* main engine representation has transformed the GD/C inertial and elastic data into a coordinate system more adaptable to the chosen method of eigen-mode analysis.

The nature of the JPL reconfiguration of the GD/C mathematical model and the subsequent analyses leading to descriptions of the "free-free" torsional vibration modes of the composite vehicle are presented in the following discussion.

A. *Surveyor* Spacecraft and GD/C Adapter Structure

The mathematical model of the *Surveyor* spacecraft has been derived from data obtained in the course of a modal vibration survey of Structural Test Model S-2. This survey, described in Ref. 9, was conducted by the HAC. The test vehicle consisted of the S-2 mounted on the GD/C adapter section, which was cantilevered at its base, GD/C station 172.45. This adapter serves as a structural transition between the *Centaur* bulkhead and the *Surveyor* spacecraft, as shown in Fig. 14.

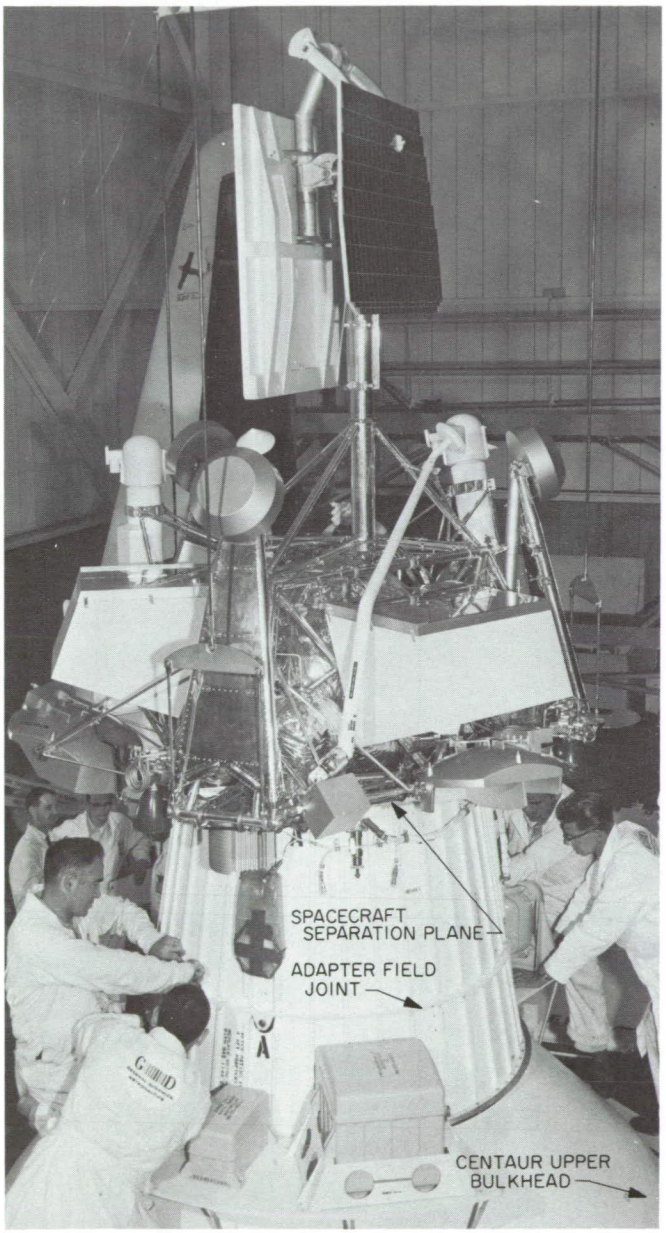

Fig. 14. *Surveyor* spacecraft and structural adapter on mockup of *Centaur* upper bulkhead

The purpose of this section is to describe the manner in which the HAC modal data were used to derive a lumped-parameter mathematical model compatible with the GD/C models of the *Atlas* and *Centaur* stages.

1. Hughes modal survey data. Reference 9 describes the spacecraft mass distribution and the mode shapes for nine elastic modes identified in a frequency range below 60 Hz. In summary, the modal data are described by a generalized mass matrix

$$[M] = \left[\begin{array}{c|c} M_{rr} & M_{re} \\ \hline M_{er} & M_{ee} \end{array}\right]$$

and the modal frequencies.

Here, this M_{rr} matrix, 6 by 6, describes the rigid-body properties of the test vehicle. The modal data are normalized such that the M_{ee} matrix is a 9 by 9 unit matrix; the M_{re} matrix, 6 by 9, indicates the rigid-elastic coupling.

In the modal data, the GD/C adapter has been represented by three mass points. These three masses, at 0.35 slugs each, have been lumped at the three attachment points between the spacecraft and the adapter. Such a presentation of the GD/C adapter results in a contribution of the adapter to the overall test vehicle roll moment of inertia of 3.63 slug-ft^2.

Since the adapter structure is essentially rigid in any of the elastic modes surveyed, this representation is adequate for purposes of the computation of a generalized mass. The inconsistency (i.e., incompleteness of the matrix M_{rr}) is, however, evident.

2. GD/C adapter representation. The adapter/*Centaur* interface area was modeled by GD/C, as shown in Fig. 15. The lumped mass at joint 16, $I_{16} = 15.9$ slug-ft^2, is due to the adapter mass. The mass at joint 26, $I_{26} = 246.6$ slug-ft^2, consists of 241.2 slug-ft^2 *Centaur* bulkhead contribution and 5.4 slug-ft^2 adapter mass.

3. Lumped-parameter representation of spacecraft/adapter torsion modes. The lumped-parameter representation of the spacecraft/adapter, in reflecting the best-available consistent data, had to meet one additional requirement: a mass point had to be introduced at the field joint. This requirement stemmed from the testing method employed by M. R. Trubert (Ref. 1); only the upper part of the adapter was to be used in the shake-table test. The adapter field joint was bolted to the shake fixture.

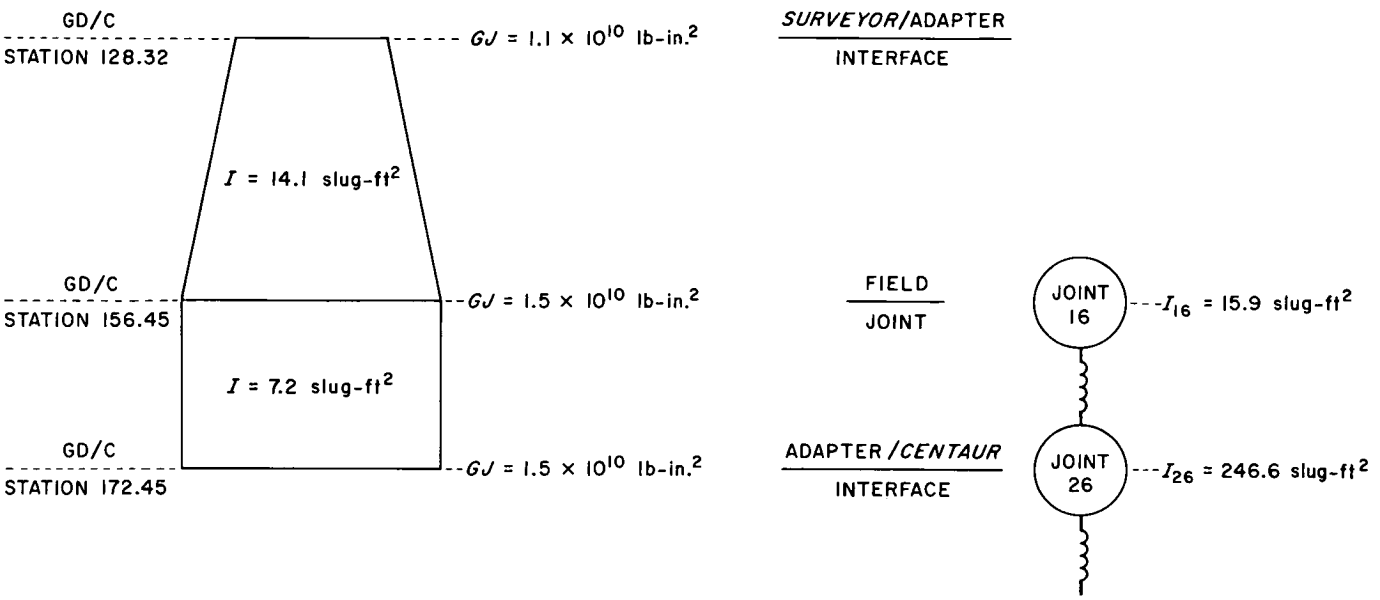

Fig. 15. GD/C model of adapter/*Centaur* interface

By examining the HAC and GD/C model, it is seen that inconsistencies exist. The HAC modal survey data lacks the proper adapter mass representation, as well as the modal deflections at the field joint. It does, however, account for the elasticity in the adapter. Since the normal modes surveyed are truly three-dimensional modes, an approach as used for the *Ranger* spacecraft (in Section II-A) to extract the elasticity of the adapter from the modal data was not practical.

Any mathematical representation derived from the HAC and GD/C representations would have to be based on certain assumptions. The following model was used as a best approximation of the structural system:

(1) The adapter mass, less the mass accounted for by the HAC modal data at the *Surveyor*/adapter interface, was lumped at the field joint (joint 16).

(2) The spring constant for the section between joints 16 and 26 was derived directly from the GD/C model.

Mathematically the *Surveyor*/adapter system was attached at the field joint, rather than at the base of the adapter. This treatment of the adapter is justified as follows:

(1) The lower adapter portion is relatively stiff, hence, the mode shapes for the *Surveyor*/adapter combination cantilevered at the field joint would differ little, if any, from those obtained by HAC. This similarity of mode shapes is substantiated by the fact that, during the survey, HAC found essentially no elastic participation of the adapter.

(2) The adapter mass distribution is nearly the same as that supplied by GD/C with the exception of the mass accounted for by HAC at the *Surveyor*/adapter interface. This incremental mass has been deleted from joint 16.

The mathematical model for the *Surveyor* spacecraft and GD/C adapter structure as used in the composite model is diagramed in Fig. 16 with numerical values given in Table 5.

Table 5. Numerical values for Surveyor/adapter mathematical model

Joint	I, lb-in.^{2}	Connecting joints	K, lb-in./rad
26	0.11424×10^7	26–16	0.9380×10^9
16	0.89240×10^6	16–17	0.8518×10^3
17	0.11689×10^3	16–18	0.1800×10^5
18	0.62322×10^3	16–19	0.1990×10^6
19	0.35008×10^4	16–20	0.1060×10^7
20	0.80699×10^4	16–21	0.5470×10^5
21	0.35611×10^3	16–22	0.1930×10^5
22	0.81760×10^2	16–23	0.1473×10^6
23	0.53802×10^3	16–24	0.4371×10^5
24	0.12998×10^3	16–25	0.1641×10^5
25	0.44670×10^2		

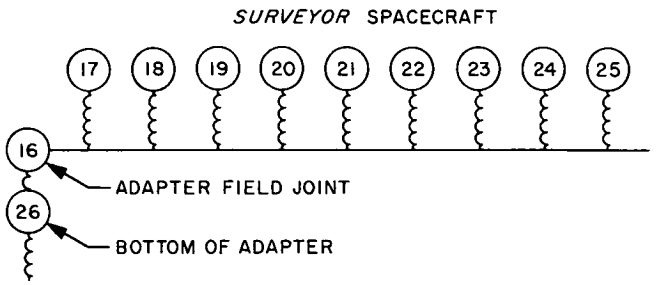

Fig. 16. Surveyor/adapter mathematical model

The method used in reducing the HAC modal data to the lumped-parameter representation, shown in Fig. 14, is identical with that used for the *Ranger* spacecraft described in Section II-A. Only those terms of the M_{re} matrix contributing to torsion have been considered. An approach for the general problem of formulating equivalent spring-mass systems from modal data is described in Ref. 5.

Joint 16 represents, in addition to part of the adapter, the *Surveyor* spacecraft rigid-body mass term augmentation of 836,233 lb-in.[2]

B. *Centaur* Engine Representation

From data provided by GD/C, each *Centaur* main engine may be represented as shown in Fig. 17. The approach in synthesizing an equivalent lumped-parameter model is similar to the treatment given the *Atlas* booster engines. Here, however, the idealization is simplified by virtue of deletion of the δ degree of freedom (Fig. 9).

At the recommendation of GD/C, the gimbal angle spring constant $K_{\beta\beta}$ was determined to give an engine rocking mode frequency of 12 Hz; i.e., since

$$I_Y = mr^2 + I_{o_Y}$$

$$= 64.78 \text{ slug-ft}^2$$

and

$$\omega_\beta = 2\pi f = 75.40 \text{ rad/s}$$

then

$$K_{\beta\beta} = \omega_\beta^2 I_Y = 3.68 \times 10^5 \text{ ft-lb/rad}$$

The generalized coordinates are chosen as

$$\alpha = \alpha_0 q_0(t)$$

$$\beta = \beta_0 q_1(t)$$

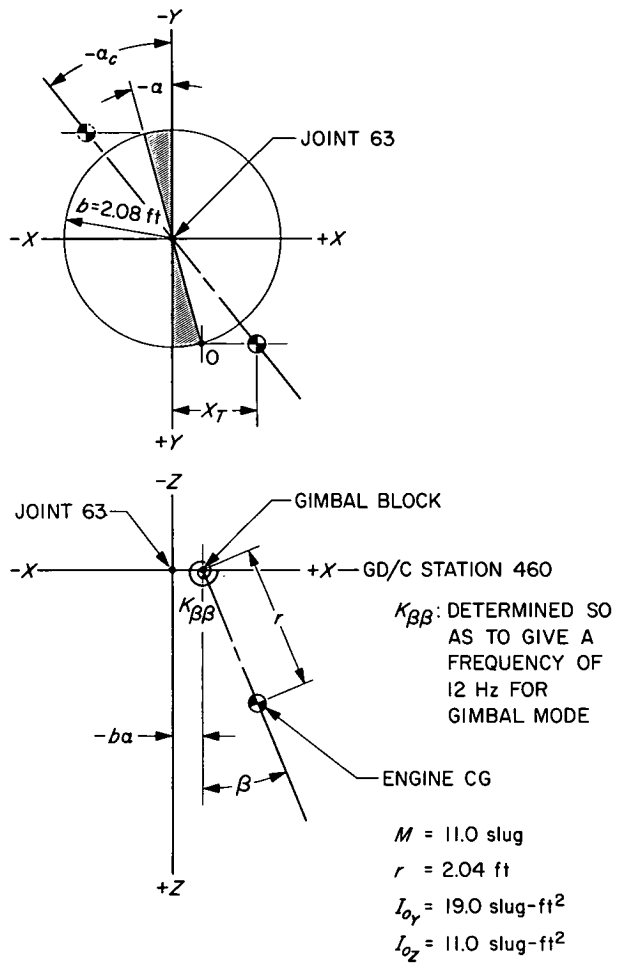

Fig. 17. Mathematical model of *Centaur* engine

and the initial normalization sets $\alpha_0 = \beta_0 = 1$ rad. The associated mass matrix is

$$[M] = \left[\begin{array}{c|c} M_{rr} & M_{re} \\ \hline M_{er} & M_{ee} \end{array}\right]$$

wherein

$$M_{rr} = mb^2 + I_{o_Z}$$

$$M_{ee} = I_Y$$

$$M_{re} = M_{er} = -mbr$$

Thus,

$$[M] = \left[\begin{array}{c|c} 58.59 & -46.68 \\ \hline -46.68 & 64.78 \end{array}\right]$$

The gimbal-angle mode is now renormalized such that

$$\beta_o^* = \mu\beta_o$$

and

$$\mu = \frac{M_{re}}{M_{rr}}$$

$$= -0.7206$$

Now,

$$M_{re}^* = \mu M_{re}$$

$$M_{ee}^* = \mu^2 M_{ee}$$

and, per engine,

$$[M^*] = \left[\begin{array}{c|c} 58.59 & 33.64 \\ \hline 33.64 & 33.64 \end{array}\right] (\text{slug-ft}^2)$$

For both engines,

$$[W^*] = 9274\,[M^*]$$

$$= 10^6 \left[\begin{array}{c|c} 0.5433 & 0.3119 \\ \hline 0.3119 & 0.3119 \end{array}\right] (\text{lb-in.}^2)$$

The associated stiffness matrix is

$$[K^*] = \left[\frac{\omega^2}{g}\right][W^*]$$

$$= 10^6 \left[\begin{array}{c|c} 0 & 0 \\ \hline 0 & 4.594 \end{array}\right] (\text{in.-lb/rad})$$

The lumped-parameter model may now be represented as shown in the adjacent sketch, wherein

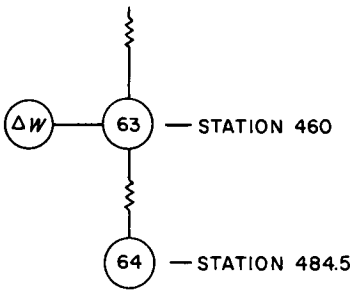

$$W_{64} = 0.3119 \times 10^6 \text{ lb-in.}^2$$

$$\Delta W = W_{rr}^* - W_{ee}^*$$

$$= 0.2314 \times 10^6 \text{ lb-in.}^2$$

$$K_{63-64} = 4.594 \times 10^6 \text{ in.-lb/rad}$$

In the complete model of Fig. 18 and Table C-2, the moment of inertia of joint 63 includes the ΔW.

The tangential deflection of the *Centaur* engine CG (Fig. 17) is, in the rth normal mode,

$$x_T^{(r)} = -b\phi_{63}^{(r)} + r\mu\beta_o(\phi_{64}^{(r)} - \phi_{63}^{(r)})$$

For the plotting of mode shapes, *Centaur*-engine modal participation is represented by the angle

$$\phi_c^{(r)} = -\frac{x_T^{(r)}}{b}$$

$$= \phi_{63}^{(r)} + 0.7067\,(\phi_{64}^{(r)} - \phi_{63}^{(r)})$$

C. Composite Model

Two different representations of the *Atlas/Centaur/Surveyor* vehicle were used to obtain the composite system eigenvalues. Eigenvalues and eigenvectors of the initial model as used by M. R. Trubert were obtained in mid-September 1965. Early in November 1965, after the *Surveyor* qualification tests had been completed, discussion with GD/C revealed that JPL had misinterpreted the *Centaur*-engine representation, accounting for the *Centaur* engines twice in the initial model. Thus, the final model differs from the initial model in two areas: (1) the method of representing the *Atlas* booster engines, and (2) the method of representing the *Centaur* engines correcting for the error in the initial data.

1. Initial model. The initial model consisted of six separate systems:

(1) The forward half of the *Atlas/Centaur/Surveyor* torsion model restrained at joint 13.

(2) The aft half of the *Atlas/Centaur/Surveyor* torsion model (less the *Atlas* booster engines and the *Centaur* engines) restrained at joint 13.

(3) The $+Y$ *Atlas* booster engine.

(4) The $-Y$ *Atlas* booster engine.

(5) The $+Y$ *Centaur* engine.

(6) The $-Y$ *Centaur* engine.

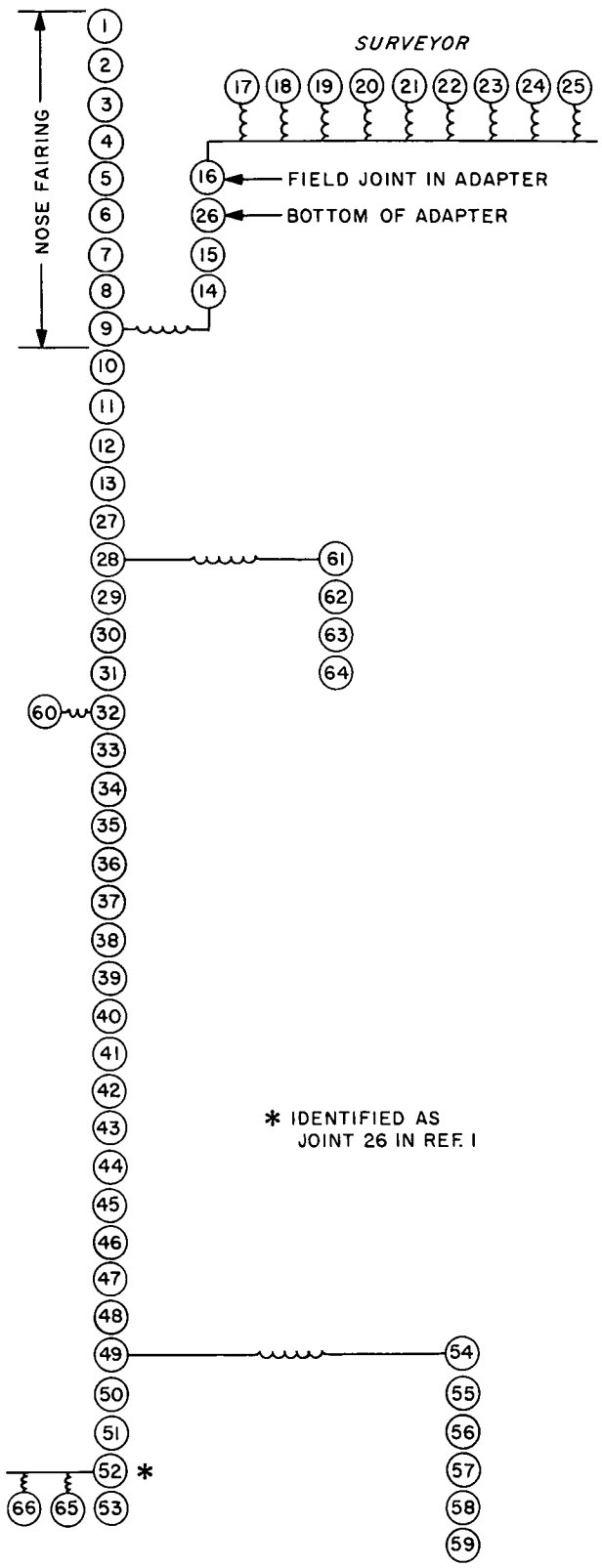

Fig. 18. *Atlas/Centaur/Surveyor* torsion model

The *Atlas/Centaur/Surveyor* model (Fig. 18) has been represented by a series of lumped masses and springs. For the initial model, the *Atlas/Centaur/Surveyor* system less *Atlas* booster engines and *Centaur* engines was used as shown in Appendix C, except as follows:

(1) Joints 64, 65, and 66 and their associated springs were omitted and the inertias at joints 52 and 63 were reduced to 0.75662×10^7 lb-in.^{2} and 0.524×10^6 lb-in.^{2}, respectively. The lower inertias are due to the different method of treating the engines.

(2) Erroneously, joint 67 (not shown in Fig. 18) of the final model was retained. This joint was connected by a single spring to joint 63. The inertia used at this joint was 6.601×10^5 lb-in.^{2}, the spring constant $K_{63-67} = 1.4 \times 10^7$ lb-in./rad.

(3) The interim mathematical model of the *Atlas* booster engine described in Section II-B and the *Centaur* engine representation described in Section III-B were used for the initial composite model.

Twenty eigenvalues and eigenvectors for each of the two systems (the forward model and the aft model) were obtained using the JPL Stiffness Matrix Structural Analysis Program (Ref. 8). Both of these systems were restrained at joint 13.

The eigenvectors and eigenvalues of the unrestrained composite system were obtained in the JPL Modal Combination Program (Ref. 7), using essentially the same method as described in Section II-C. Within this program, first, displacement compatibility between the forward and aft parts of the model is established at joint 13. Second, the two *Atlas* booster engines are attached at joint 52. Third, the *Centaur* engines are attached at joint 63. Finally, the composite system "free-free" eigenvalues are calculated.

The eigenvalues and the modal displacements at joints 16 and 52 for the first 27 "free-free" composite system modes are given in Table 6. The values given in Table 6 are normalized to give a unit generalized mass.

Because of the engine representations in this model, "free-free" eigenvectors are obtained wherein the *Atlas* booster engines and the *Centaur* engines have in-phase displacements. These "symmetric" modes, occurring at 12.01, 12.54, and 55.54 Hz, are inertially balanced by a rigid-body displacement of the whole space vehicle and are not of interest for the problem at hand. The modal displacement for the points of interest in these three

Table 6. Modal displacements of the JPL initial model for *Atlas/Centaur/Surveyor*

f_r, Hz	Joint 16 field joint, $\phi_{16}^{(r)}$	Joint 52 gimbal block, $\phi_{52}^{(r)}$
8.45	0.32393×10^{-5}	-0.43615×10^{-5}
11.74	0.10840×10^{-2}	-0.23721×10^{-3}
12.01	0.33197×10^{-7}	0.15829×10^{-8}
12.17	0.95338×10^{-3}	0.21914×10^{-3}
12.54	0.30693×10^{-8}	-0.56252×10^{-9}
14.22	0.38167×10^{-3}	-0.75921×10^{-3}
16.80	0.81889×10^{-3}	-0.44056×10^{-3}
16.48	0.35791×10^{-2}	-0.19327×10^{-2}
23.58	0.15257×10^{-4}	0.34364×10^{-4}
35.81	0.47065×10^{-3}	0.46710×10^{-4}
38.78	0.14301×10^{-3}	0.13196×10^{-4}
45.43	0.49796×10^{-2}	0.80271×10^{-3}
48.07	-0.20366×10^{-4}	-0.16443×10^{-4}
51.77	0.19141×10^{-3}	-0.17316×10^{-4}
54.35	-0.16377×10^{-2}	-0.22556×10^{-3}
55.54	-0.17567×10^{-8}	-0.17029×10^{-9}
57.36	0.18347×10^{-3}	-0.10780×10^{-4}
57.98	0.15627×10^{-3}	-0.55802×10^{-5}
67.50	0.51868×10^{-3}	-0.21188×10^{-2}
70.19	0.13474×10^{-1}	-0.20455×10^{-3}
79.97	0.93115×10^{-4}	-0.12717×10^{-2}
96.60	-0.82726×10^{-2}	-0.59479×10^{-3}
110.0	0.50664×10^{-2}	-0.79742×10^{-3}
130.0	-0.15283×10^{-2}	0.73311×10^{-3}
132.6	-0.21674×10^{-2}	-0.76145×10^{-3}
145.0	-0.85950×10^{-2}	-0.26403×10^{-3}
158.1	-0.34112×10^{-2}	0.94587×10^{-3}

modes are several orders of magnitude less than in the true torsion modes.

In comparing the table of modal deflections given by M. R. Trubert in Ref. 1 with Table 6, only an incompatibility in nomenclature will be found. Because the model was divided into the forward and aft part to obtain the restrained eigenvectors, an interim nomenclature had to be adapted within the JPL Stiffness Matrix Structural Analysis Program. The gimbal block reported as joint 26 in Ref. 1 is indeed identical with joint 52 as shown in Table 7 and in the model of Fig. 18.

2. *Final model.* The final *Atlas/Centaur/Surveyor* dynamic torsion model (Fig. 18) has been represented by a series of lumped masses and massless springs. The dynamic models of the *Surveyor* vehicle, *Atlas* booster engines, and *Centaur* engines have been transformed to equivalent spring-mass systems. The springs, inertias, and stations of the model are given in Appendix C. The "free-free" eigenvalues were calculated in two steps. First, twenty eigenvectors and eigenvalues of both the forward and the aft system were computed using the JPL Stiffness Matrix Structural Analysis Program. The "free-free" eigenvalues were obtained in the JPL Modal Combination Program, establishing displacement compatibility between the forward and aft systems at joint 13.

Table 7. Modal displacements of the JPL final model for *Atlas/Centaur/Surveyor*

f_r, Hz	Joint 16 field joint, $\phi_{16}^{(r)}$	Joint 52 gimbal block, $\phi_{52}^{(r)}$
8.45	0.32582×10^{-5}	-0.43529×10^{-5}
11.76	0.10560×10^{-2}	-0.20600×10^{-3}
12.18	0.99224×10^{-3}	0.24445×10^{-3}
16.60	-0.35292×10^{-2}	0.20739×10^{-2}
16.82	-0.64912×10^{-3}	0.38267×10^{-3}
13.58	0.24576×10^{-4}	0.32523×10^{-4}
35.81	0.48706×10^{-3}	0.46370×10^{-4}
38.78	0.14833×10^{-3}	0.13286×10^{-4}
45.25	0.50680×10^{-2}	0.78694×10^{-3}
48.07	-0.16795×10^{-4}	-0.15494×10^{-4}
51.77	0.19247×10^{-3}	-0.17485×10^{-4}
54.23	0.16278×10^{-2}	0.19232×10^{-3}
57.36	0.18407×10^{-3}	-0.10544×10^{-4}
57.98	0.15652×10^{-3}	-0.55073×10^{-5}
67.18	-0.67502×10^{-3}	0.21032×10^{-2}
70.19	0.13470×10^{-1}	-0.18481×10^{-3}
79.93	0.75597×10^{-4}	-0.12411×10^{-2}
95.48	0.79372×10^{-2}	0.60694×10^{-3}
109.75	0.52439×10^{-2}	-0.77004×10^{-3}
128.54	0.31011×10^{-2}	-0.29290×10^{-3}
131.14	0.17761×10^{-2}	0.10104×10^{-2}
144.57	-0.84192×10^{-2}	-0.22175×10^{-3}
157.90	0.32225×10^{-2}	-0.94377×10^{-3}

The eigenvalues and the modal displacements at joints 16 and 52 for the first 23 modes are given in Table 7. The values given in Table 7 are consistent to give a unit mass for the final system generalized mass in every mode. Due to the different engine representation in this model as compared to the initial model, the symmetric modes are not present.

Mode shape plots for these 23 normal modes are shown in Appendix D. The effective angle-of-twist for the *Atlas* booster engine has been calculated as described in Section II-B. The *Centaur*-engine angular deflection has been calculated as described in Section III-B. Because of the complicated, three-dimensional nature of the cantilever modes of the *Surveyor* spacecraft, only the modal participation factors of the spacecraft have been plotted, and these are shown at arbitrarily chosen stations.

IV. Conclusions

The *Ranger* vehicle modes above 100 Hz and the *Surveyor* vehicle modes above 60 Hz have accuracies impaired by the absence of spacecraft modal data in the higher frequency ranges. This situation was recognized

in the application of the "free-free" torsion modes to the analysis of Ref. 1, and in the subsequent formalization of the torsional test specification for the *Surveyor* spacecraft.

The technique for converting a mathematical model expressed in cantilever normal-mode coordinates to an equivalent lumped-parameter model is judged to be effective and convenient. Its initial application in the subject analysis led to the more general treatment presented in Ref. 5.

The results of the *Ranger* modal vibration surveys show the importance of knowing mode shapes when prescribing flight accelerometer locations and when interpreting flight acceleration data. Moreover, there are inherent pitfalls in limiting accelerometer placement to a single plane near or coincident with a contractual interface, because there are certain to be some modes having nodal points nearby. As can be inferred from Fig. 6, the torsional moment is at a maximum at a nodal point and, unlike the acceleration, is not changing rapidly for small distances forward or aft of the nodal point. This situation suggests that, in planning flight test instrumentation, greater consideration should be given to the judicious use of strain gage bridges in place of accelerometers.

References

1. Trubert, M. R., *Use of Ranger Flight Data in the Synthesis of a Torsional Acceleration Transient for Surveyor Vibration Qualification Testing*, Technical Memorandum 33-237. Jet Propulsion Laboratory, Pasadena, Calif., Apr. 19, 1966.
2. *Ranger Vehicle Post Flight Structural Dynamic Evaluation*, Report No. A778337. Lockheed Missiles and Space Company, Sunnyvale, Calif., Jan. 28, 1966.
3. Trubert, M. R., *A Fourier Transform Technique for the Prediction of Torsional Transients for a Spacecraft from Flight Data of Another Spacecraft Using the Same Booster*, Technical Memorandum 33-350. Jet Propulsion Laboratory, Pasadena, Calif., Oct. 15, 1967.
4. Ullrey, P. W., *Torsional Analysis of the EOGO Vehicle*, Structures Report No. SS/905/5522; LMSC Report No. A/729524. Lockheed Missiles and Space Company, Sunnyvale, Calif., Jan. 1965.
5. Bamford, R. M., and Wada, B. K., *Equivalent Spring-Mass System for Normal Modes*, Technical Memorandum 33-380. Jet Propulsion Laboratory, Pasadena, Calif. (under preparation).
6. Hurty, W. C., *Dynamic Analysis of Structural Systems by Component Mode Synthesis*, Technical Report 32-530. Jet Propulsion Laboratory, Pasadena, Calif., Jan. 15, 1964.
7. Bamford, R. M., *A Modal Combination Program for Dynamic Analysis of Structures*, Technical Memorandum 33-290. Jet Propulsion Laboratory, Pasadena, Calif., Aug. 15, 1966.
8. Wada, B. K., *Stiffness Matrix Structural Analysis*, Technical Report 32-774. Jet Propulsion Laboratory, Pasadena, Calif., Oct. 31, 1965.
9. Hendrick, W. R., and Harter, R. J., *Revised Mathematical Model of the Surveyor Mounted on the GD/A Adapter*, Report 2222.4/9. Hughes Aircraft Company, Culver City, Calif., July 23, 1964.

Table A-1. Joint coordinates for *Atlas/Agena/Ranger*[a]

JOINT NO.	LMSC STATION, INCHES
1	0.6580E 02
2	0.1358E 03
3	0.1760E 03
4	0.2240E 03
5	0.2480E 03
6	0.2650E 03
7	0.2950E 03
8	0.3250E 03
9	0.3600E 03
10	0.3830E 03
11	0.4040E 03
12	0.4450E 03
13	0.4960E 03
14	0.3950E 03
15	0.4220E 03
16	0.4570E 03
17	0.5430E 03
18	0.5830E 03
19	0.6230E 03
20	0.6630E 03
21	0.7030E 03
22	0.7430E 03
23	0.7830E 03
24	0.8230E 03
25	0.8630E 03
26	0.9030E 03
27	0.9430E 03
28	0.9930E 03
29	0.1043E 04
30	0.1083E 04
31	0.1123E 04
32	0.1156E 04
33	0.1163E 04
34	0.1183E 04
35	0.1203E 04
36	0.1223E 04
37	0.1243E 04
38	0.1263E 04
39	0.1178E 04
40	0.1213E 04
41	0.1235E 04
42	0.1273E 04
43	0.2150E 03
44	0.2150E 03
45	0.2150E 03
46	0.1273E 04
47	0.1273E 04

[a]Described by Fig. 13.

Table A-2. Joint inertias for *Atlas/Agena/Ranger*

JOINT NO.	INERTIA, POUND INCHES SQUARED
1	0.11955E 06
2	0.10665E 06
3	0.12635E 06
4	0.14026E 06
5	0.23610E 05
6	0.22870E 06
7	0.74580E 05
8	0.61050E 05
9	0.81800E 05
10	0.17740E 05
11	0.75190E 05
12	0.11920E 06
13	0.14308E 06
14	0.38640E 05
15	0.77280E 05
16	0.27820E 05
17	0.23800E 06
18	0.20400E 06
19	0.20200E 06
20	0.26100E 06
21	0.27600E 06
22	0.24500E 06
23	0.26100E 06
24	0.27600E 06
25	0.29100E 06
26	0.38400E 06
27	0.57100E 06
28	0.13920E 07
29	0.76500E 06
30	0.18680E 07
31	0.14680E 07
32	0.57880E 06
33	0.56210E 06
34	0.45210E 06
35	0.55450E 06
36	0.23390E 06
37	0.26870E 06
38	0.44800E 06
39	0.28337E 07
40	0.45125E 07
41	0.79190E 07
42	0.52203E 07
43	0.10000E 03
44	0.88354E 05
45	0.97810E 05
46	0.40890E 07
47	0.30510E 07

Table A-3. Spring constants for *Atlas/Agena/Ranger*

JOINT A	JOINT B	K, IN-LB/RADIAN
1	2	0.7800E 09
2	3	0.1360E 10
3	4	0.1690E 10
4	5	0.4540E 10
5	6	0.5650E 10
6	7	0.2590E 10
7	8	0.2680E 10
8	9	0.2600E 10
9	10	0.4800E 10
10	11	0.5790E 10
11	12	0.3110E 10
12	13	0.2610E 10
10	14	0.2220E 10
14	15	0.1480E 10
15	16	0.1140E 10
13	17	0.1700E 10
17	18	0.4360E 10
18	19	0.3530E 10
19	20	0.5500E 10
20	21	0.6250E 10
21	22	0.5740E 10
22	23	0.5920E 10
23	24	0.6420E 10
24	25	0.7050E 10
25	26	0.7230E 10
26	27	0.7740E 10
27	28	0.6950E 10
28	29	0.7030E 10
29	30	0.1010E 11
30	31	0.1043E 11
31	32	0.1391E 11
32	33	0.6000E 11
33	34	0.1400E 11
34	35	0.7000E 10
35	36	0.1400E 10
36	37	0.1400E 10
37	38	0.1400E 10
32	39	0.3132E 11
39	40	0.2400E 11
40	41	0.4140E 11
41	42	0.2250E 11
5	43	0.6690E 09
43	44	0.1970E 09
44	45	0.9520E 08
41	46	0.5980E 08
41	47	0.9001E 09

Appendix B

Torsion Mode Shape Plots for *Atlas/Agena/Ranger* Space Vehicle

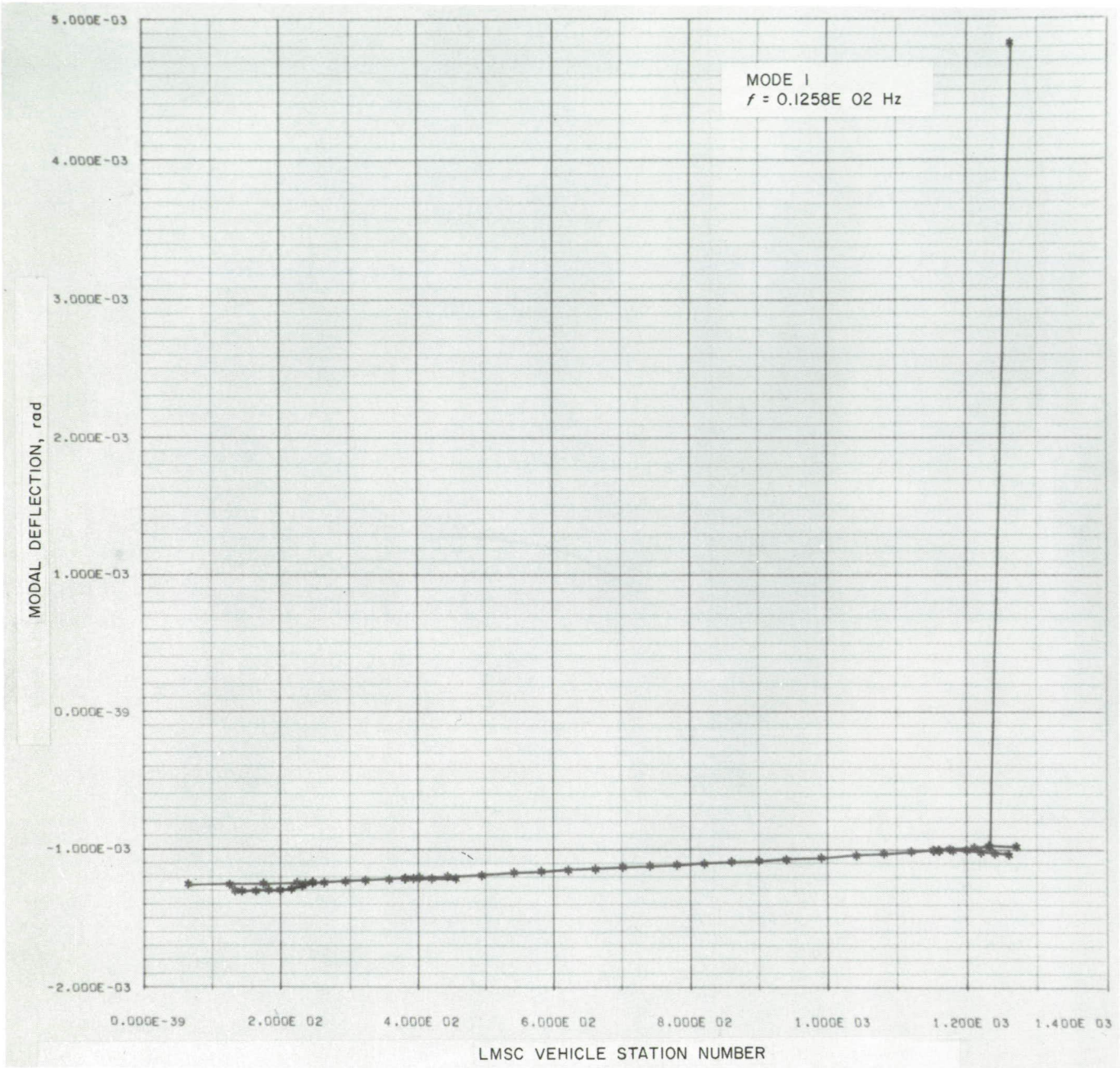

Fig. B-1. ***Atlas/Agena/Ranger*** **torsion mode shapes**

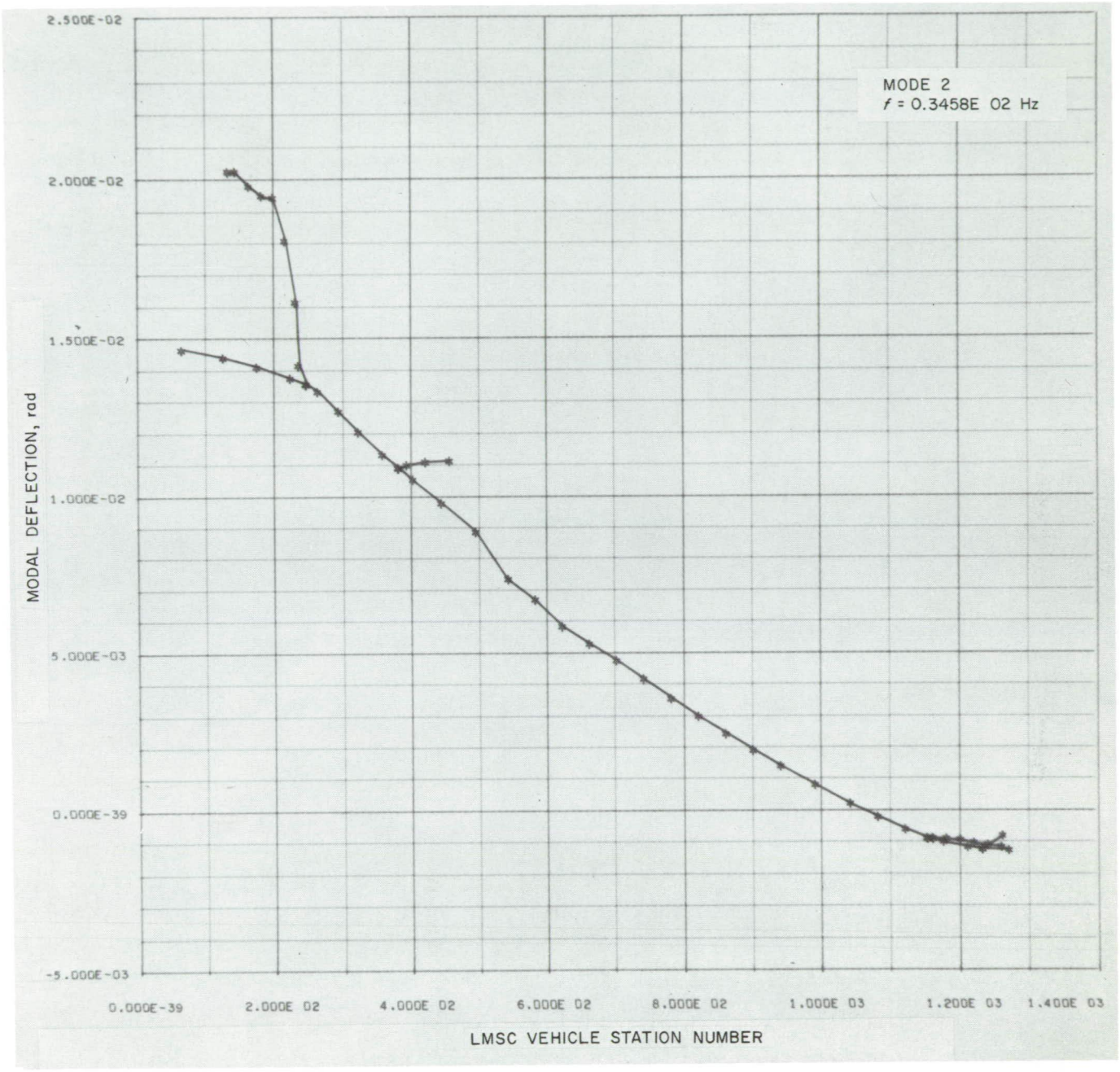
MODE 2
f = 0.3458E 02 Hz
2.500E-02
2.000E-02
1.500E-02
1.000E-02
5.000E-03
0.000E-39
-5.000E-03
MODAL DEFLECTION, rad
0.000E-39
2.000E 02
4.000E 02
6.000E 02
8.000E 02
1.000E 03
1.200E 03
1.400E 03
LMSC VEHICLE STATION NUMBER

Fig. B-1 (contd)

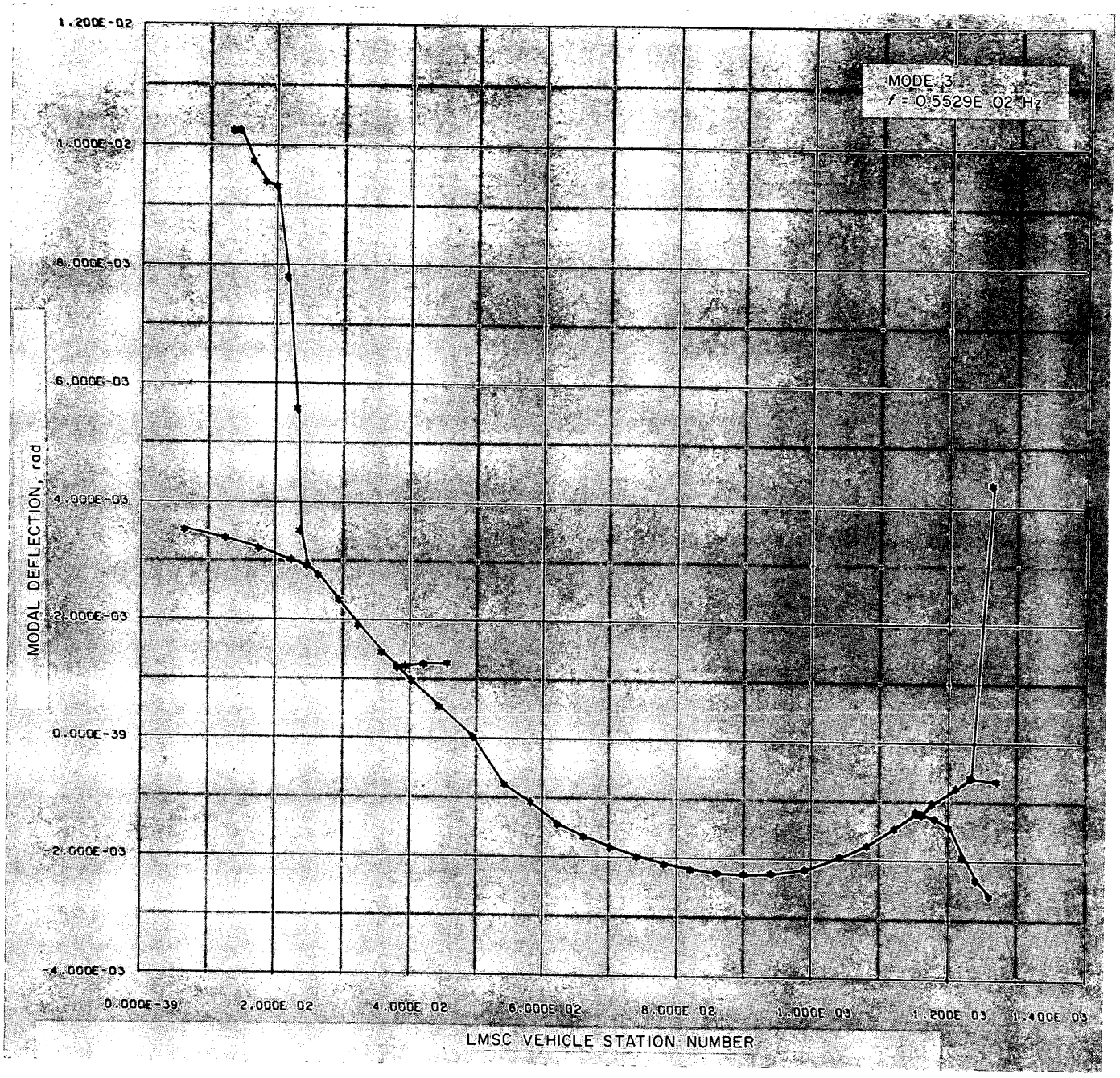
MODE 3
f = 0.5529E 02 Hz
1.200E-02
1.000E-02
8.000E-03
6.000E-03
4.000E-03
2.000E-03
0.000E-39
-2.000E-03
-4.000E-03
MODAL DEFLECTION, rad
0.000E-39
2.000E 02
4.000E 02
6.000E 02
8.000E 02
1.000E 03
1.200E 03
1.400E 03
LMSC VEHICLE STATION NUMBER

Fig. B-1 (contd)

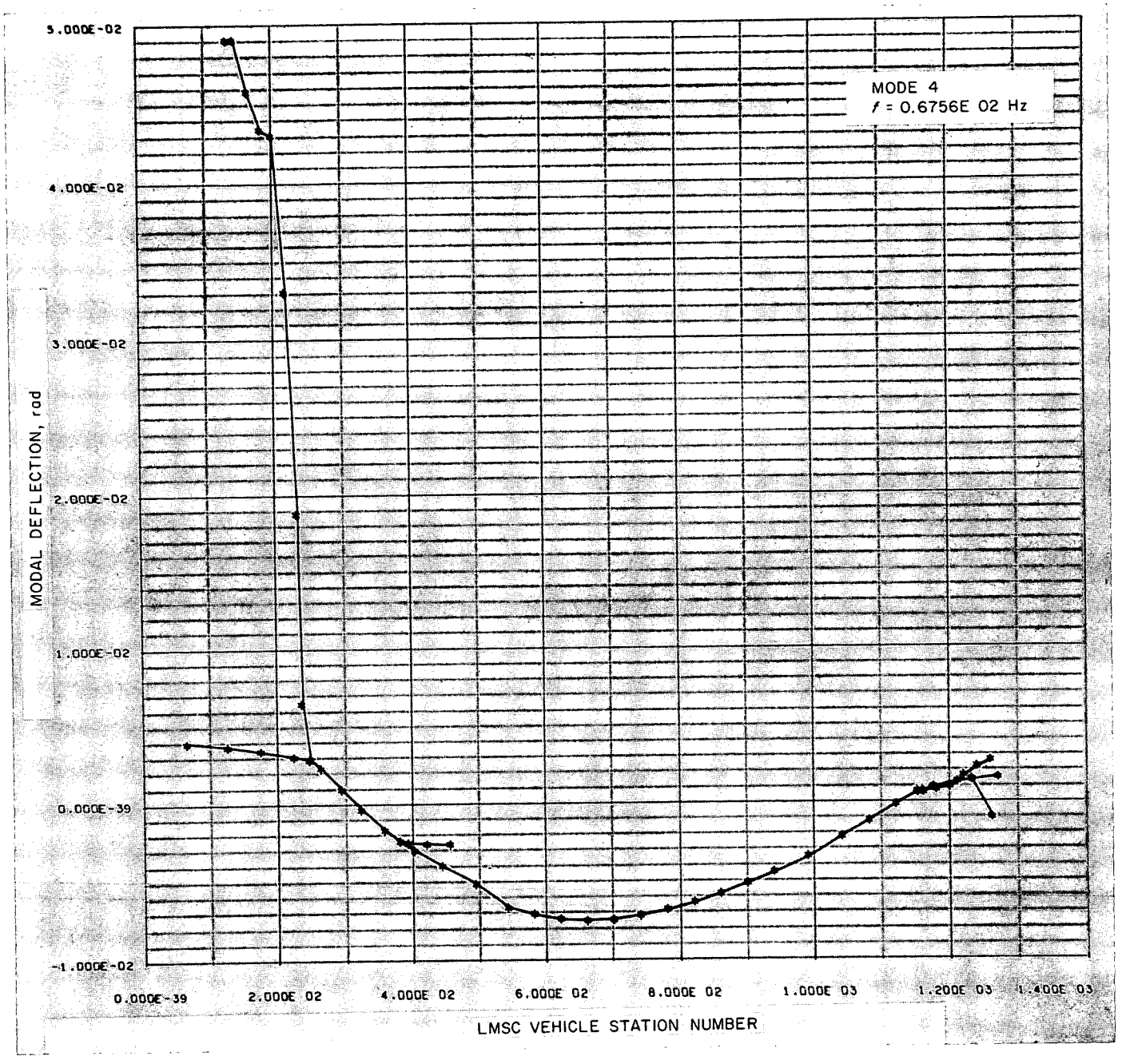
MODE 4
f = 0.6756E 02 Hz
5.000E-02
4.000E-02
3.000E-02
2.000E-02
1.000E-02
0.000E-39
-1.000E-02
MODAL DEFLECTION, rad
0.000E-39
2.000E 02
4.000E 02
6.000E 02
8.000E 02
1.000E 03
1.200E 03
1.400E 03
LMSC VEHICLE STATION NUMBER

Fig. B-1 (contd)

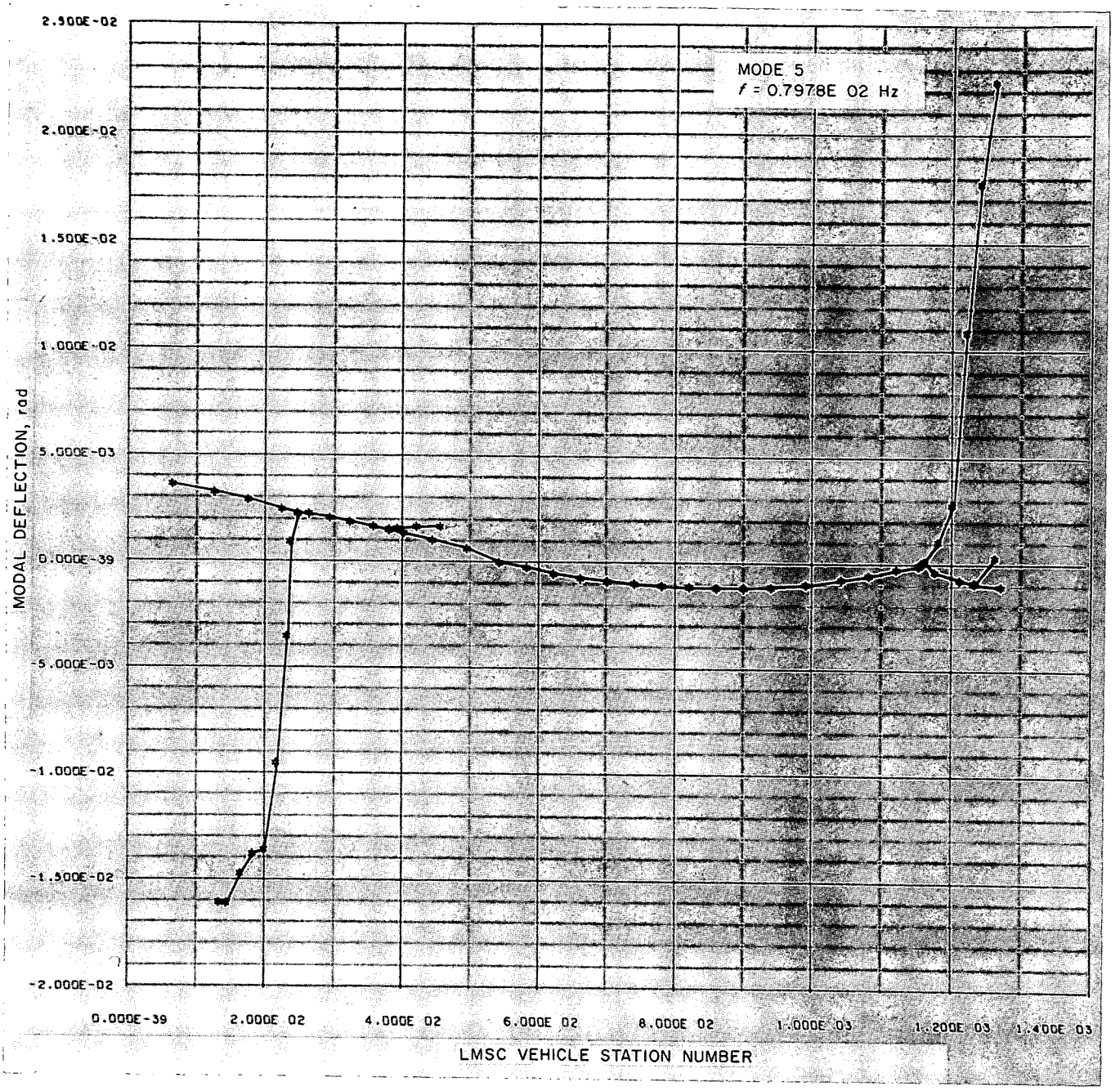
MODE 5
f = 0.7978E 02 Hz
2.500E-02
2.000E-02
1.500E-02
1.000E-02
5.000E-03
0.000E-39
-5.000E-03
-1.000E-02
-1.500E-02
-2.000E-02
MODAL DEFLECTION, rad
0.000E-39
2.000E 02
4.000E 02
6.000E 02
8.000E 02
1.000E 03
1.200E 03
1.400E 03
LMSC VEHICLE STATION NUMBER

Fig. B-1 (contd)

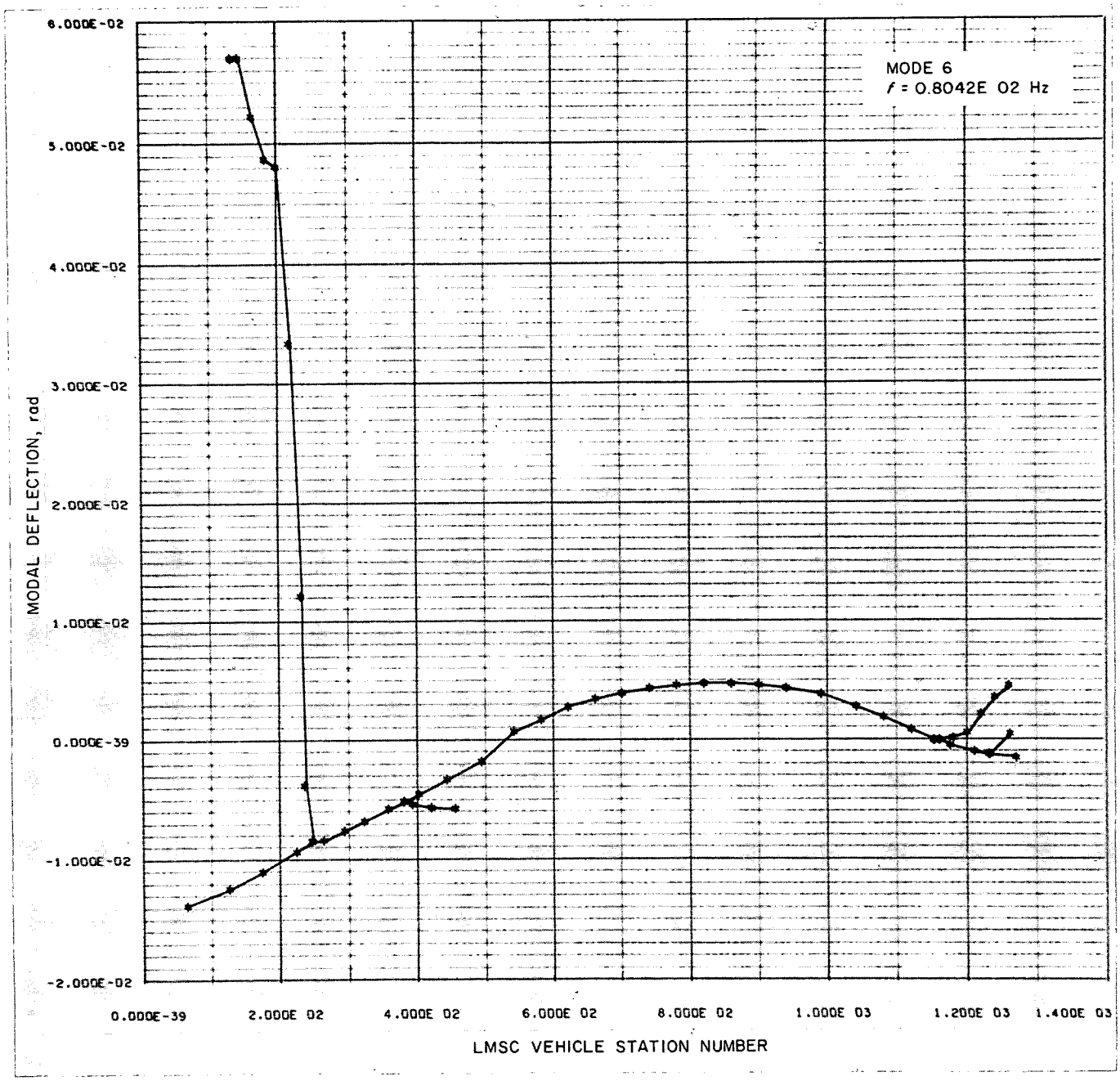
MODE 6
f = 0.8042E 02 Hz
6.000E-02
5.000E-02
4.000E-02
3.000E-02
2.000E-02
1.000E-02
0.000E-39
-1.000E-02
-2.000E-02
MODAL DEFLECTION, rad
0.000E-39
2.000E 02
4.000E 02
6.000E 02
8.000E 02
1.000E 03
1.200E 03
1.400E 03
LMSC VEHICLE STATION NUMBER

Fig. B-1 (contd)

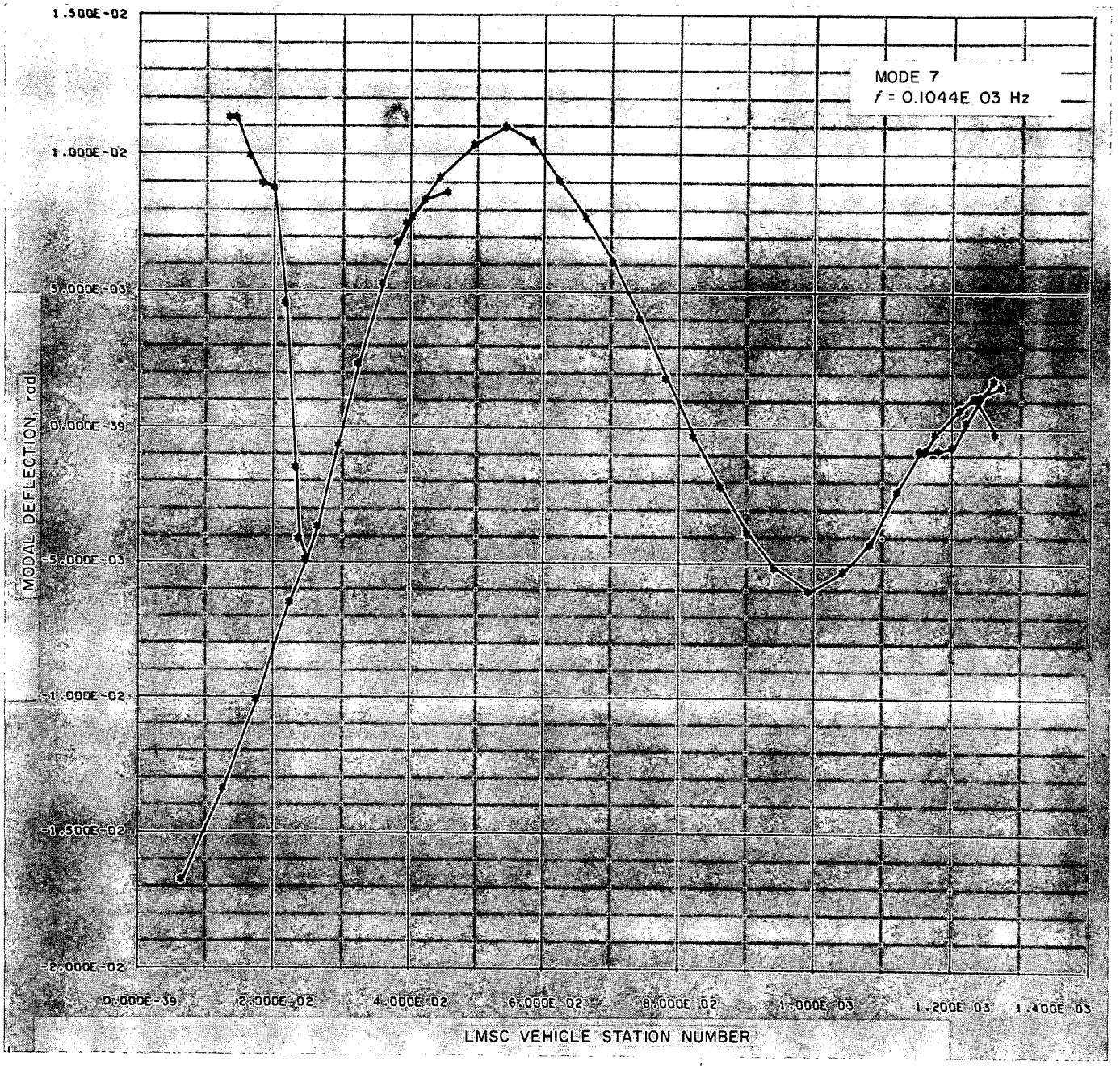
MODE 7
f = 0.1044E 03 Hz
1.500E-02
1.000E-02
5.000E-03
0.000E-39
-5.000E-03
-1.000E-02
-1.500E-02
-2.000E-02
MODAL DEFLECTION, rad
0.000E-39
2.000E 02
4.000E 02
6.000E 02
8.000E 02
1.000E 03
1.200E 03
1.400E 03
LMSC VEHICLE STATION NUMBER

Fig. B-1 (contd)

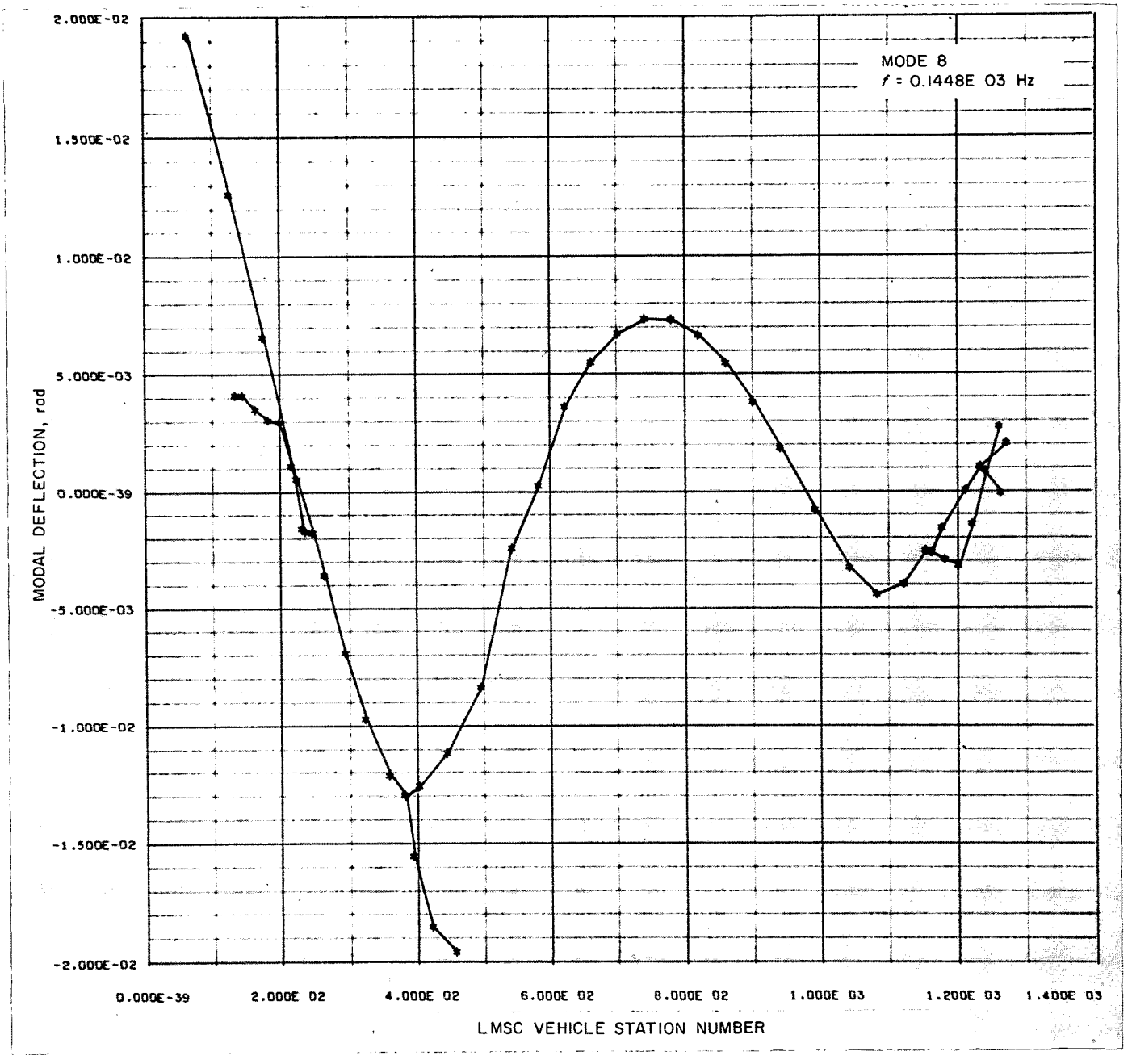
MODE 8
f = 0.1448E 03 Hz
2.000E-02
1.500E-02
1.000E-02
5.000E-03
0.000E-39
-5.000E-03
-1.000E-02
-1.500E-02
-2.000E-02
MODAL DEFLECTION, rad
0.000E-39
2.000E 02
4.000E 02
6.000E 02
8.000E 02
1.000E 03
1.200E 03
1.400E 03
LMSC VEHICLE STATION NUMBER

Fig. B-1 (contd)

PRECEDING PAGE BLANK NOT FILMED.

Appendix C

Numerical Values for *Atlas/Centaur/Surveyor* Mathematical Model

Table C-1. Joint coordinates for *Atlas/Centaur/Surveyor*[a]

JOINT NO.	GD/C STATION, INCHES
1	-0.3500E 02
2	0.0000E 00
3	0.3500E 02
4	0.7000E 02
5	0.1050E 03
6	0.1400E 03
7	0.1750E 03
8	0.2100E 03
9	0.2220E 03
10	0.2450E 03
11	0.2800E 03
12	0.3150E 03
13	0.3500E 03
14	0.2100E 03
15	0.1900E 03
16	0.1560E 03
17	0.1000E 03
18	0.1000E 03
19	0.1000E 03
20	0.1000E 03
21	0.1000E 03
22	0.1000E 03
23	0.1000E 03
24	0.1000E 03
25	0.1000E 03
26	0.1700E 03
27	0.3850E 03
28	0.4120E 03
29	0.4550E 03
30	0.4900E 03
31	0.5250E 03
32	0.5600E 03
33	0.5950E 03
34	0.6300E 03
35	0.6650E 03
36	0.7000E 03
37	0.7350E 03
38	0.7700E 03
39	0.8050E 03
40	0.8400E 03
41	0.8750E 03
42	0.9100E 03
43	0.9450E 03
44	0.9800E 03
45	0.1015E 04
46	0.1050E 04
47	0.1085E 04
48	0.1120E 04
49	0.1133E 04
50	0.1155E 04
51	0.1190E 04
52	0.1212E 04
53	0.1250E 04
54	0.1140E 04
55	0.1160E 04
56	0.1180E 04
57	0.1200E 04
58	0.1220E 04
59	0.1240E 04
60	0.5500E 03
61	0.4200E 03
62	0.4400E 03
63	0.4600E 03
64	0.4845E 03
65	0.1242E 04
66	0.1242E 04

[a]Described by Fig. 18.

Table C-2. Joint inertias for *Atlas/Centaur/Surveyor*

JOINT NO.	INERTIA, POUND INCHES SQUARED
1	0.97282E 04
2	0.34744E 05
3	0.95429E 05
4	0.38867E 06
5	0.46973E 06
6	0.10664E 07
7	0.15213E 07
8	0.10919E 07
9	0.86905E 06
10	0.79215E 06
11	0.11354E 07
12	0.17756E 07
13	0.88712E 06
14	0.43590E 06
15	0.75420E 06
16	0.89240E 06
17	0.11689E 03
18	0.62322E 03
19	0.35008E 04
20	0.80699E 04
21	0.35611E 03
22	0.81760E 02
23	0.53802E 03
24	0.12998E 03
25	0.44670E 02
26	0.11424E 07
27	0.14569E 07
28	0.30338E 07
29	0.47205E 06
30	0.23464E 07
31	0.43360E 06
32	0.52160E 06
33	0.23440E 06
34	0.45030E 06
35	0.11490E 06
36	0.26170E 06
37	0.39140E 06
38	0.30760E 06
39	0.54570E 06
40	0.32200E 06
41	0.63600E 06
42	0.65040E 06
43	0.17358E 07
44	0.17335E 07
45	0.24534E 07
46	0.24052E 07
47	0.19077E 07
48	0.23618E 07
49	0.57880E 06
50	0.28337E 07
51	0.45125E 07
52	0.79192E 07
53	0.52203E 07
54	0.56210E 06
55	0.45210E 06
56	0.55450E 06
57	0.23390E 06
58	0.26870E 06
59	0.44800E 06
60	0.35350E 06
61	0.25430E 06
62	0.75190E 06
63	0.75540E 06
64	0.31190E 06
65	0.40890E 07
66	0.30510E 07

Table C-3. Spring constants for *Atlas/Centaur/Surveyor*

JOINT A	JOINT B	K, IN-LB/RADIAN
1	2	0.12000E 09
2	3	0.28560E 09
3	4	0.66360E 09
4	5	0.13720E 10
5	6	0.24000E 10
6	7	0.34570E 10
7	8	0.35280E 10
8	9	0.10270E 11
9	10	0.10130E 11
10	11	0.66600E 10
11	12	0.66600E 10
12	13	0.66600E 10
9	14	0.11820E 11
14	15	0.50040E 10
15	26	0.30000E 10
26	16	0.93800E 09
16	17	0.85180E 03
16	18	0.18000E 05
16	19	0.19900E 06
16	20	0.10600E 07
16	21	0.54700E 05
16	22	0.19300E 05
16	23	0.14735E 06
16	24	0.43712E 05
16	25	0.16413E 05
13	27	0.66600E 10
27	28	0.86400E 10
28	29	0.76800E 10
29	30	0.94320E 10
30	31	0.94320E 10
31	32	0.94320E 10
32	33	0.71400E 10
33	34	0.59760E 10
34	35	0.59760E 10
35	36	0.64080E 10
36	37	0.73680E 10
37	38	0.78600E 10
38	39	0.80600E 10
39	40	0.80600E 10
40	41	0.85200E 10
41	42	0.89500E 10
42	43	0.10030E 11
43	44	0.10610E 11
44	45	0.11090E 11
45	46	0.11420E 11
46	47	0.11890E 11
47	48	0.12370E 11
48	49	0.30240E 11
49	50	0.31320E 11
50	51	0.24000E 11
51	52	0.41400E 11
52	53	0.22500E 11
49	54	0.60000E 11
54	55	0.14020E 11
55	56	0.70100E 10
56	57	0.14040E 10
57	58	0.14040E 10
58	59	0.14040E 10
28	61	0.31680E 11
61	62	0.84960E 10
62	63	0.12960E 10
32	60	0.18000E 11
63	64	0.45940E 07
52	65	0.59760E 08
52	66	0.89980E 09

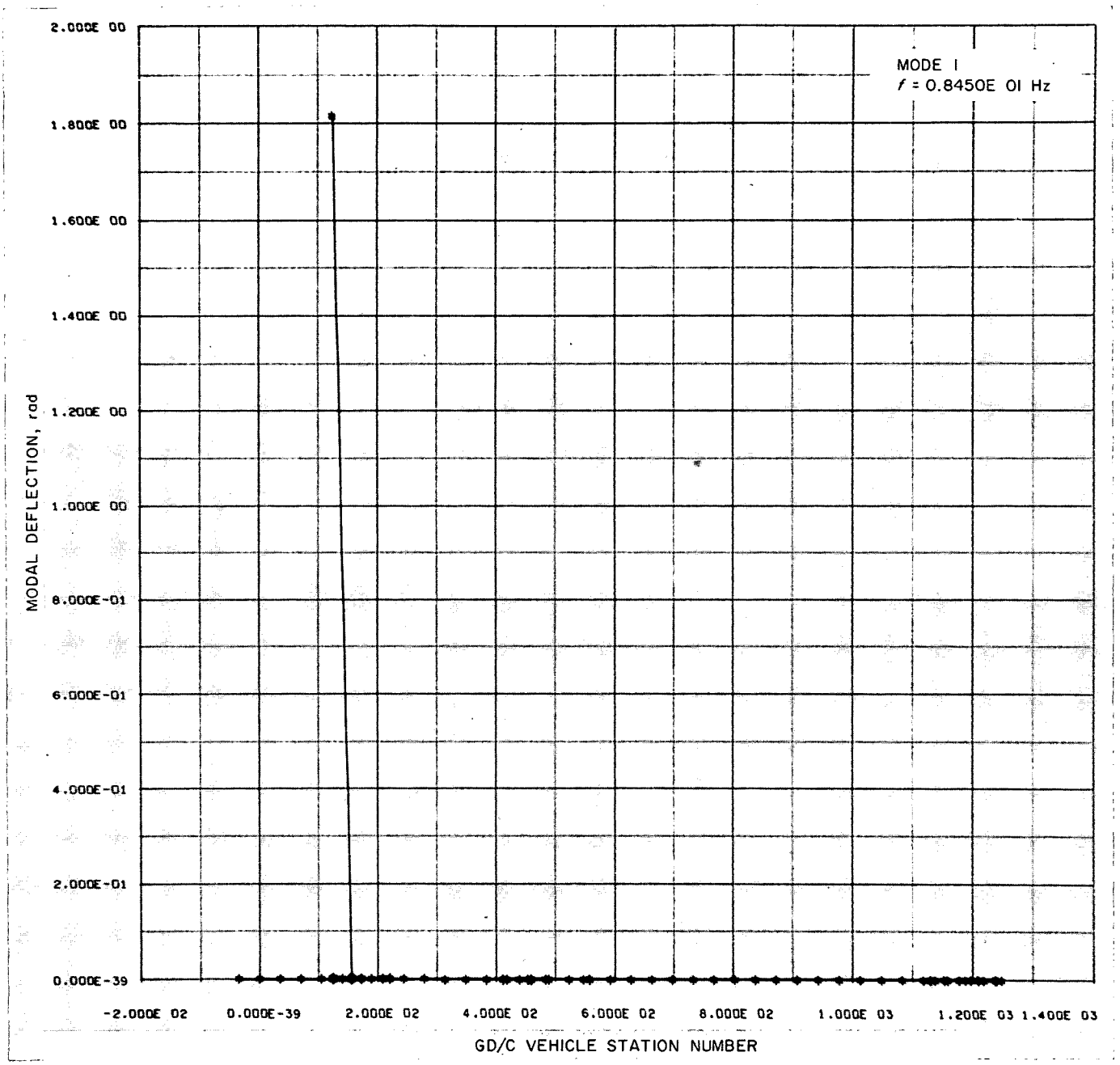

Fig. D-1. *Atlas/Centaur/Surveyor* torsion mode shapes

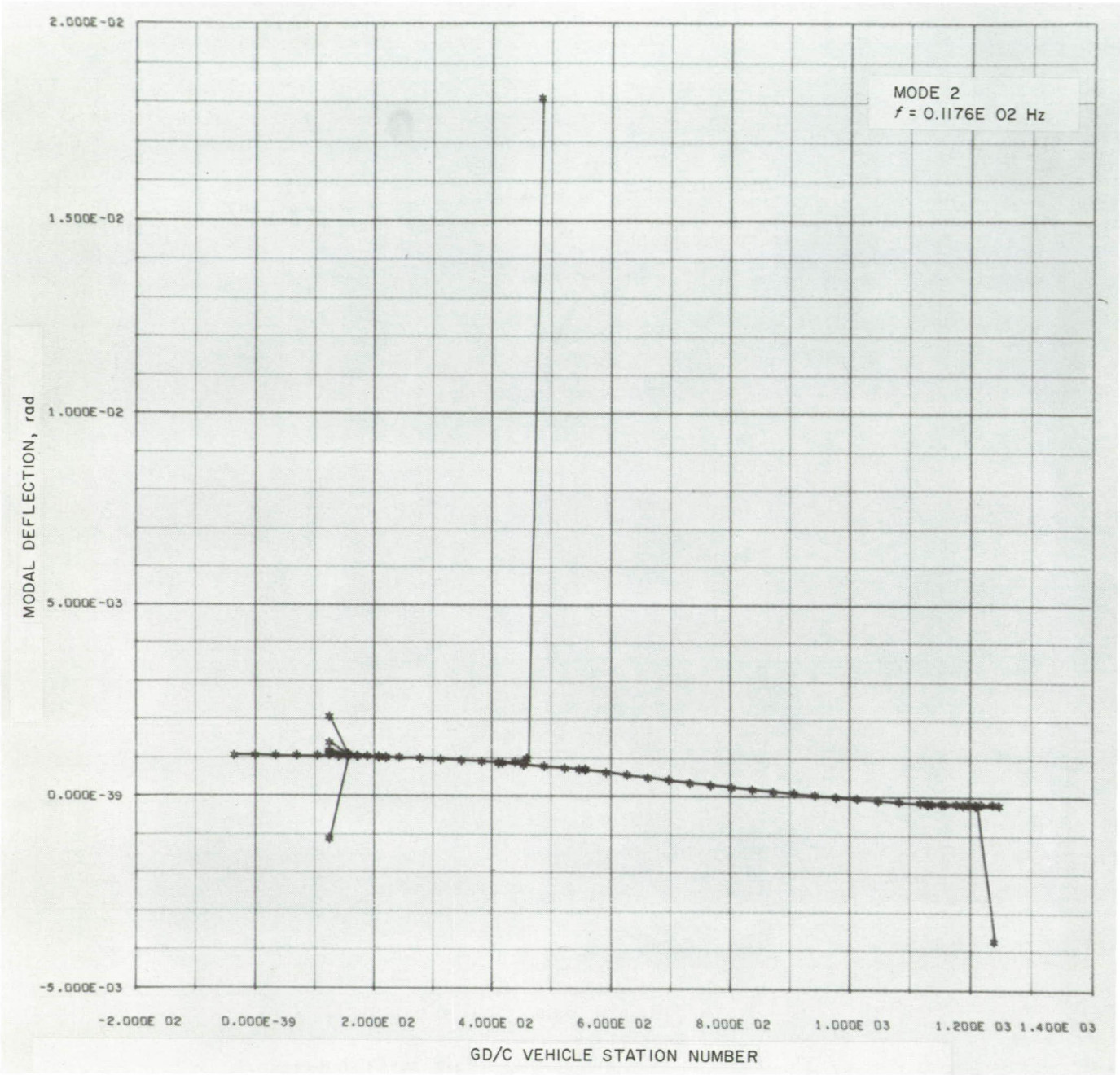
MODE 2
f = 0.1176E 02 Hz
2.000E-02
1.500E-02
1.000E-02
5.000E-03
0.000E-39
-5.000E-03
MODAL DEFLECTION, rad
-2.000E 02
0.000E-39
2.000E 02
4.000E 02
6.000E 02
8.000E 02
1.000E 03
1.200E 03
1.400E 03
GD/C VEHICLE STATION NUMBER

Fig. D-1 (contd)

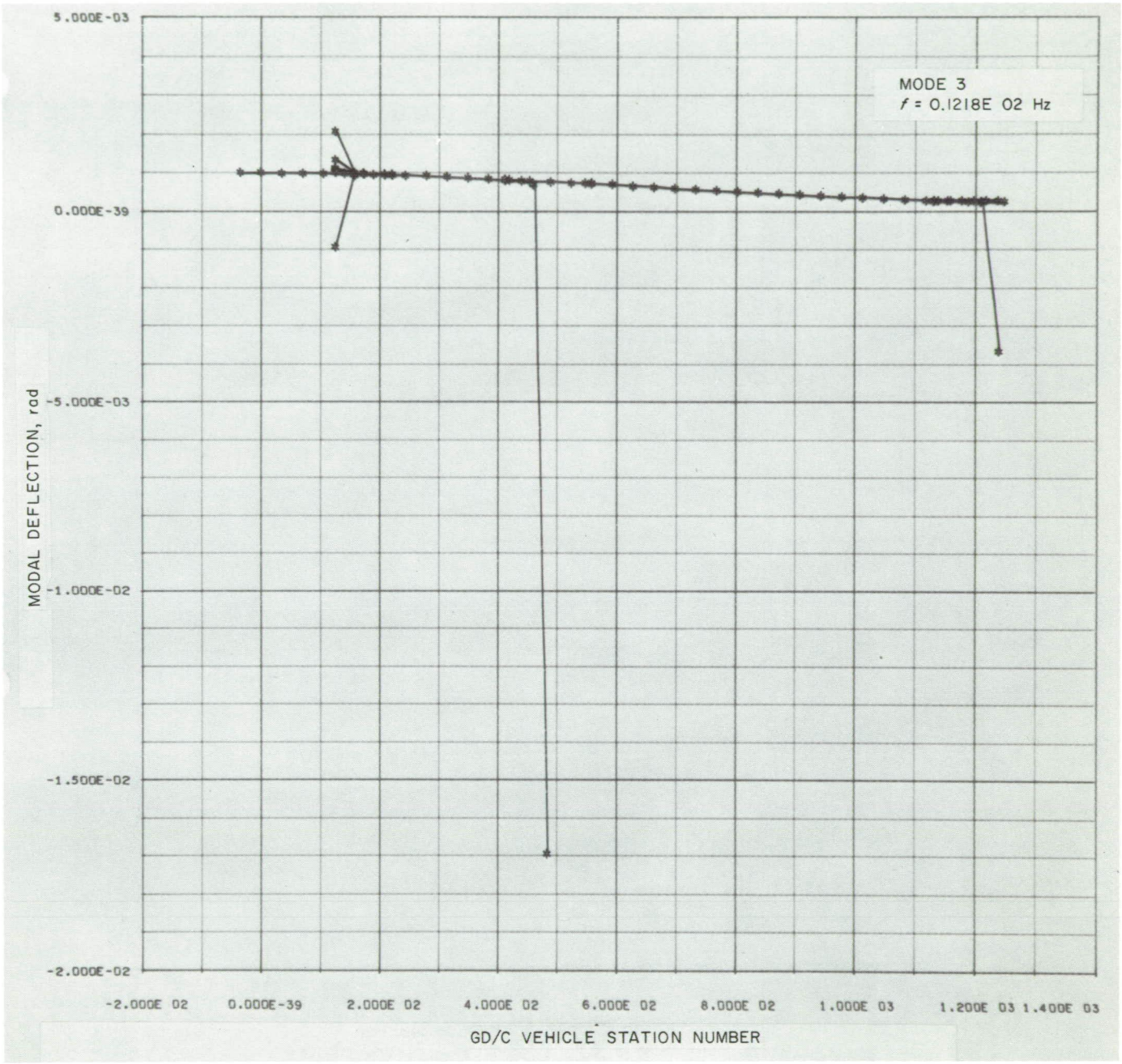
MODE 3
f = 0.1218E 02 Hz
5.000E-03
0.000E-39
-5.000E-03
-1.000E-02
-1.500E-02
-2.000E-02
MODAL DEFLECTION, rad
-2.000E 02
0.000E-39
2.000E 02
4.000E 02
6.000E 02
8.000E 02
1.000E 03
1.200E 03
1.400E 03
GD/C VEHICLE STATION NUMBER

Fig. D-1 (contd)

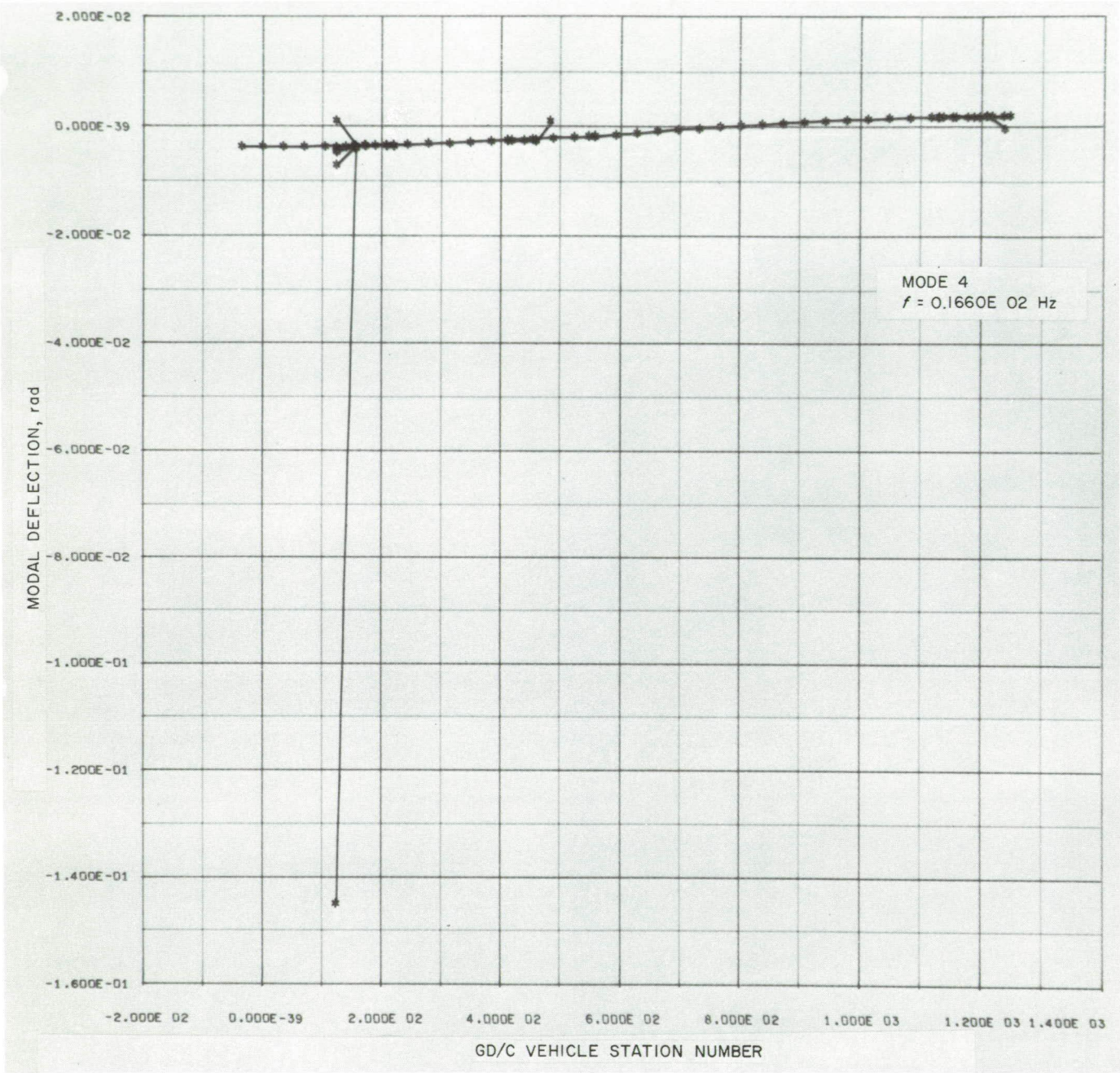
2.000E-02
0.000E-39
-2.000E-02
-4.000E-02
-6.000E-02
-8.000E-02
-1.000E-01
-1.200E-01
-1.400E-01
-1.600E-01
MODAL DEFLECTION, rad
MODE 4
f = 0.1660E 02 Hz
-2.000E 02
0.000E-39
2.000E 02
4.000E 02
6.000E 02
8.000E 02
1.000E 03
1.200E 03
1.400E 03
GD/C VEHICLE STATION NUMBER

Fig. D-1 (contd)

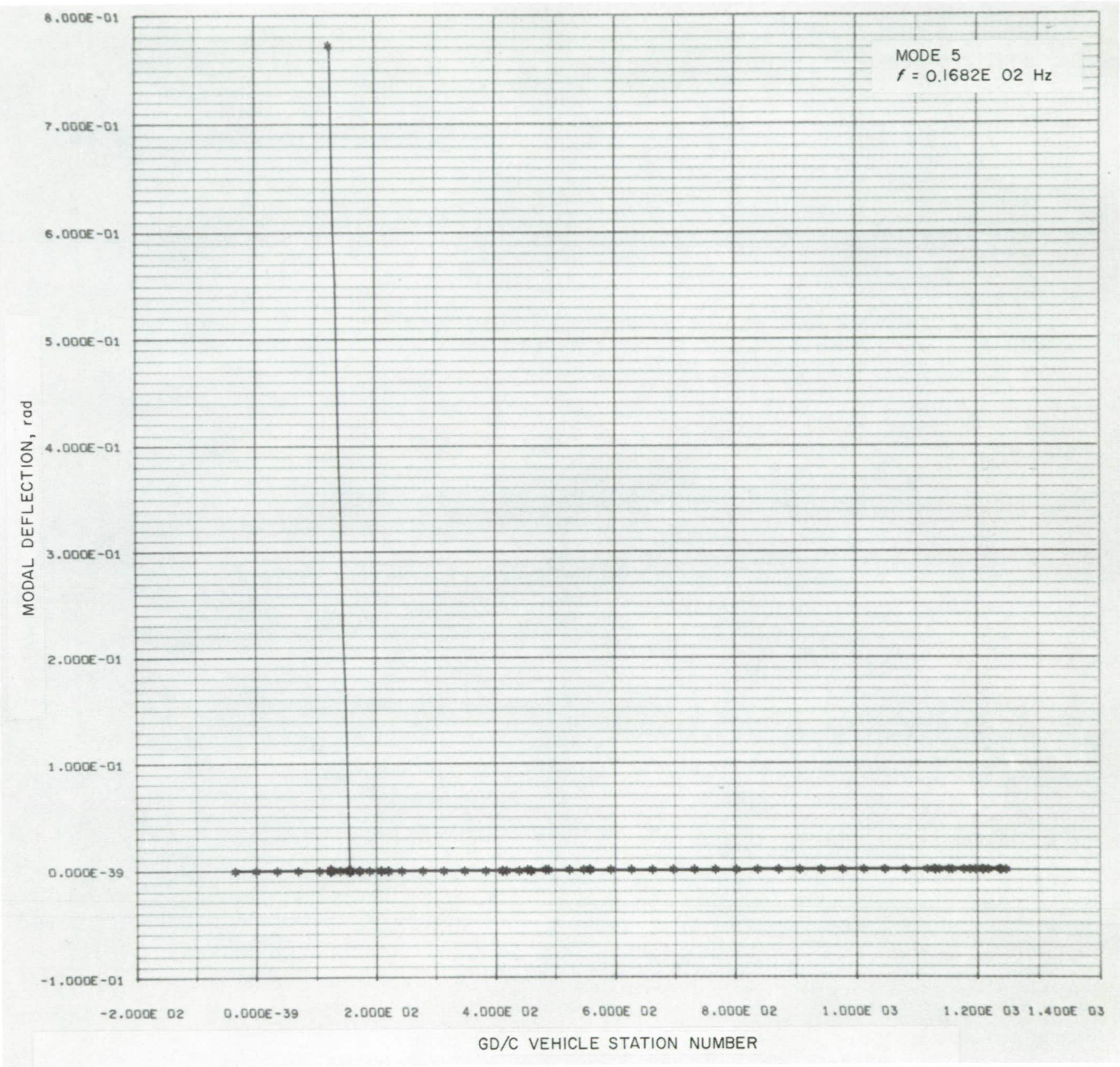
MODE 5
f = 0.1682E 02 Hz
8.000E-01
7.000E-01
6.000E-01
5.000E-01
4.000E-01
3.000E-01
2.000E-01
1.000E-01
0.000E-39
-1.000E-01
MODAL DEFLECTION, rad
-2.000E 02
0.000E-39
2.000E 02
4.000E 02
6.000E 02
8.000E 02
1.000E 03
1.200E 03
1.400E 03
GD/C VEHICLE STATION NUMBER

Fig. D-1 (contd)

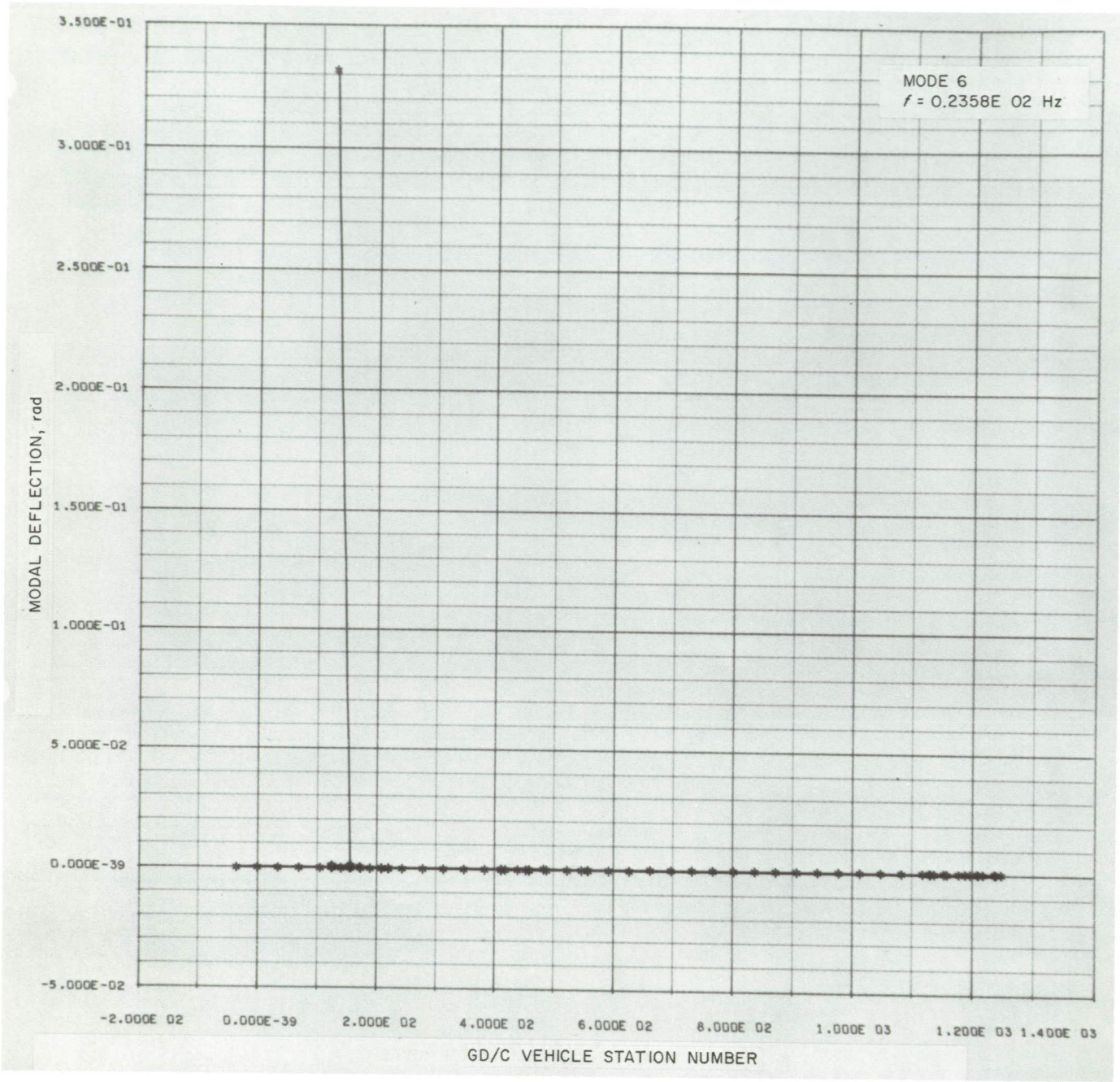
MODE 6
f = 0.2358E 02 Hz
3.500E-01
3.000E-01
2.500E-01
2.000E-01
1.500E-01
1.000E-01
5.000E-02
0.000E-39
-5.000E-02
MODAL DEFLECTION, rad
-2.000E 02
0.000E-39
2.000E 02
4.000E 02
6.000E 02
8.000E 02
1.000E 03
1.200E 03
1.400E 03
GD/C VEHICLE STATION NUMBER

Fig. D-1 (contd)

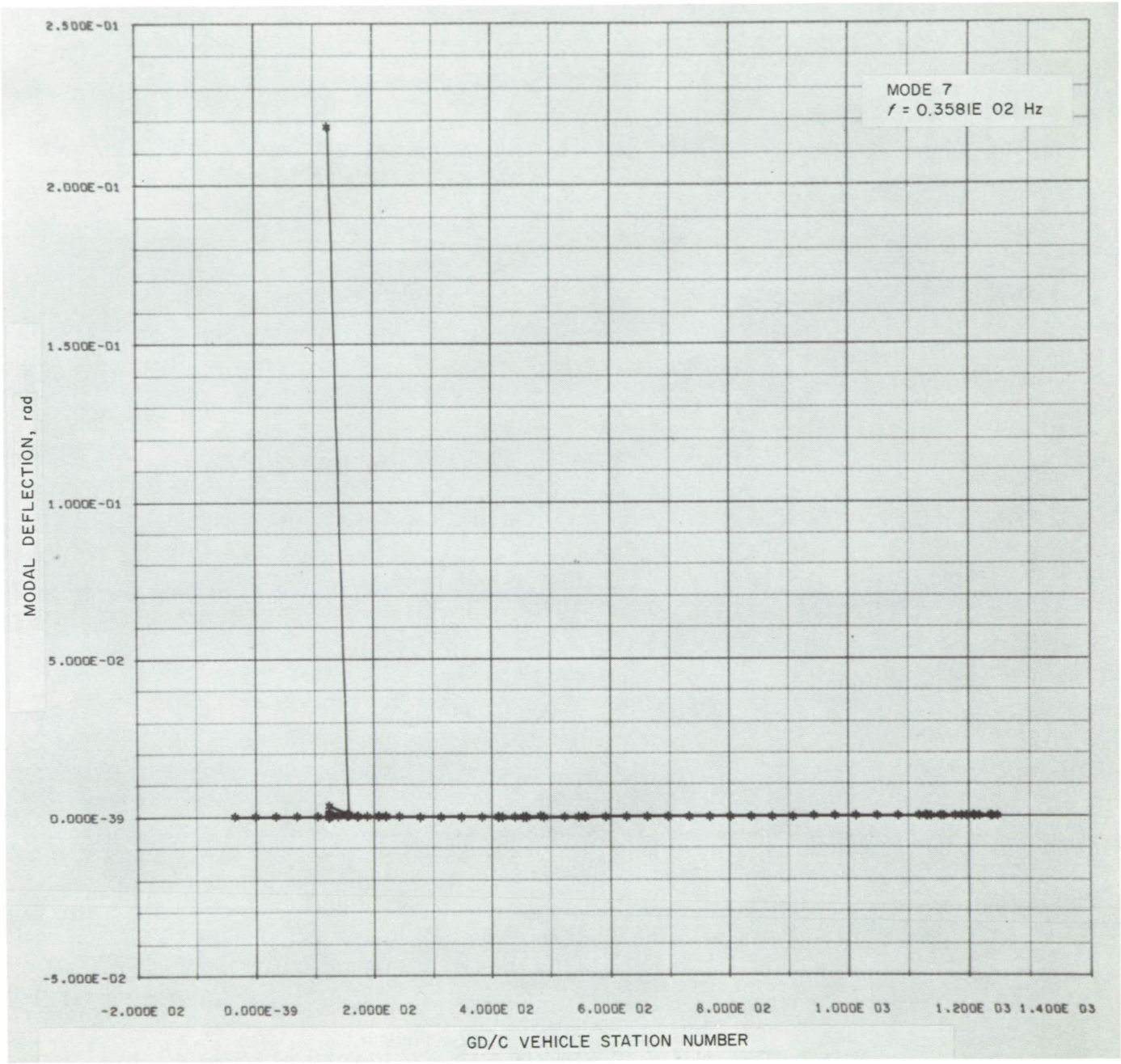
MODE 7
f = 0.3581E 02 Hz
2.500E-01
2.000E-01
1.500E-01
1.000E-01
5.000E-02
0.000E-39
-5.000E-02
MODAL DEFLECTION, rad
-2.000E 02
0.000E-39
2.000E 02
4.000E 02
6.000E 02
8.000E 02
1.000E 03
1.200E 03
1.400E 03
GD/C VEHICLE STATION NUMBER

Fig. D-1 (contd)

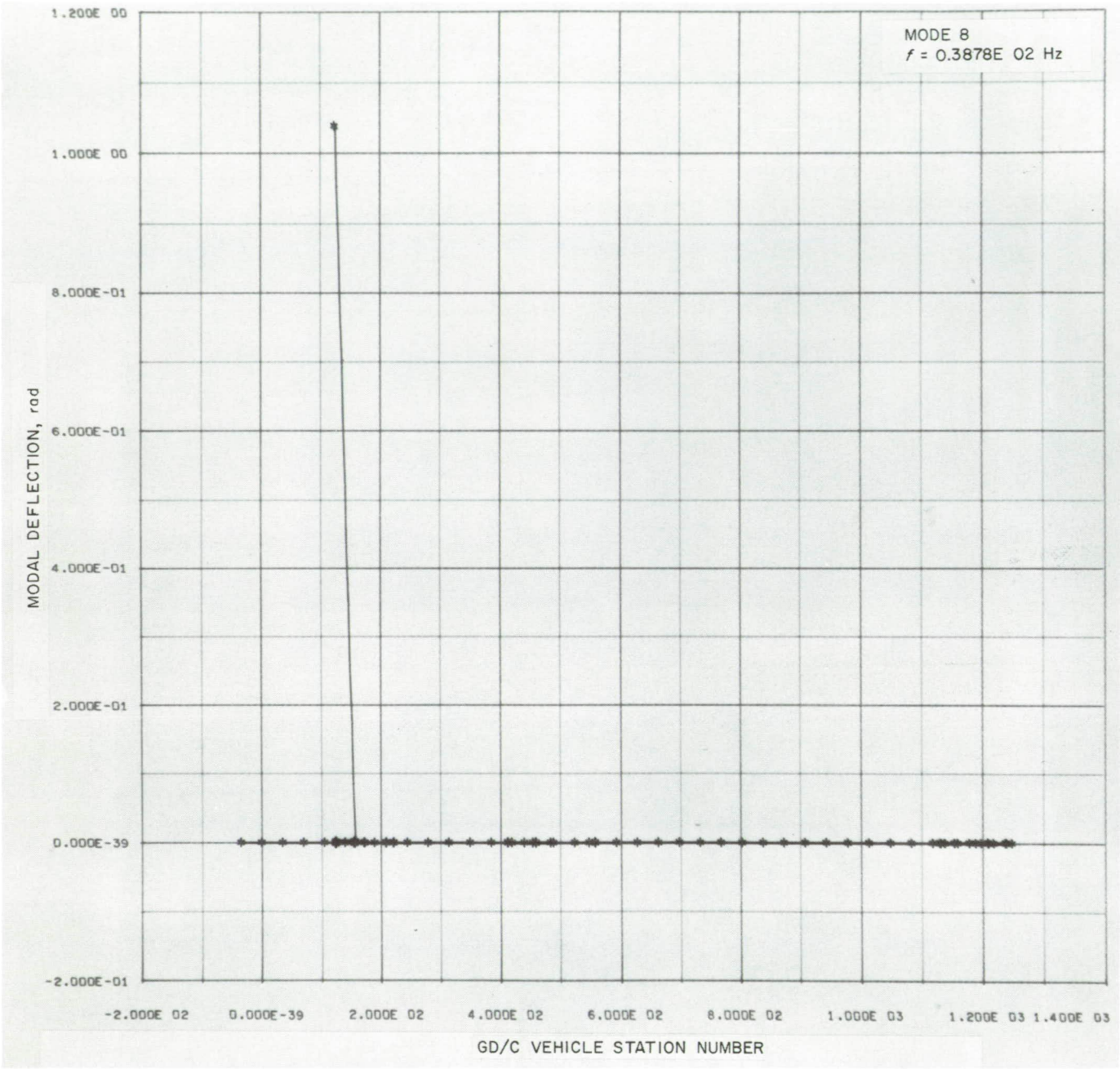
MODE 8
f = 0.3878E 02 Hz
1.200E 00
1.000E 00
8.000E-01
6.000E-01
4.000E-01
2.000E-01
0.000E-39
-2.000E-01
MODAL DEFLECTION, rad
-2.000E 02
0.000E-39
2.000E 02
4.000E 02
6.000E 02
8.000E 02
1.000E 03
1.200E 03
1.400E 03
GD/C VEHICLE STATION NUMBER

Fig. D-1 (contd)

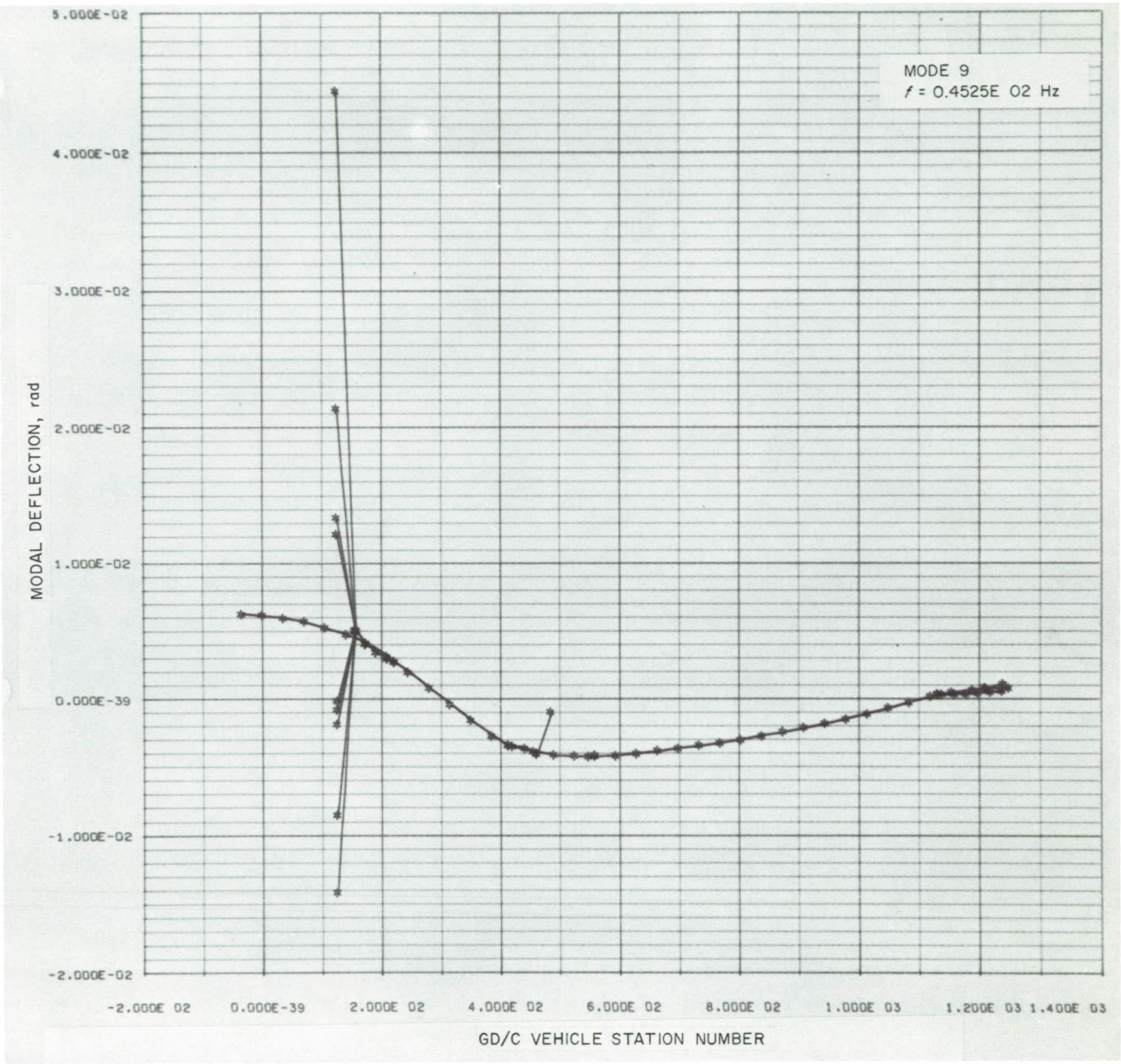
MODE 9
f = 0.4525E 02 Hz
5.000E-02
4.000E-02
3.000E-02
2.000E-02
1.000E-02
0.000E-39
-1.000E-02
-2.000E-02
MODAL DEFLECTION, rad
-2.000E 02
0.000E-39
2.000E 02
4.000E 02
6.000E 02
8.000E 02
1.000E 03
1.200E 03
1.400E 03
GD/C VEHICLE STATION NUMBER

Fig. D-1 (contd)

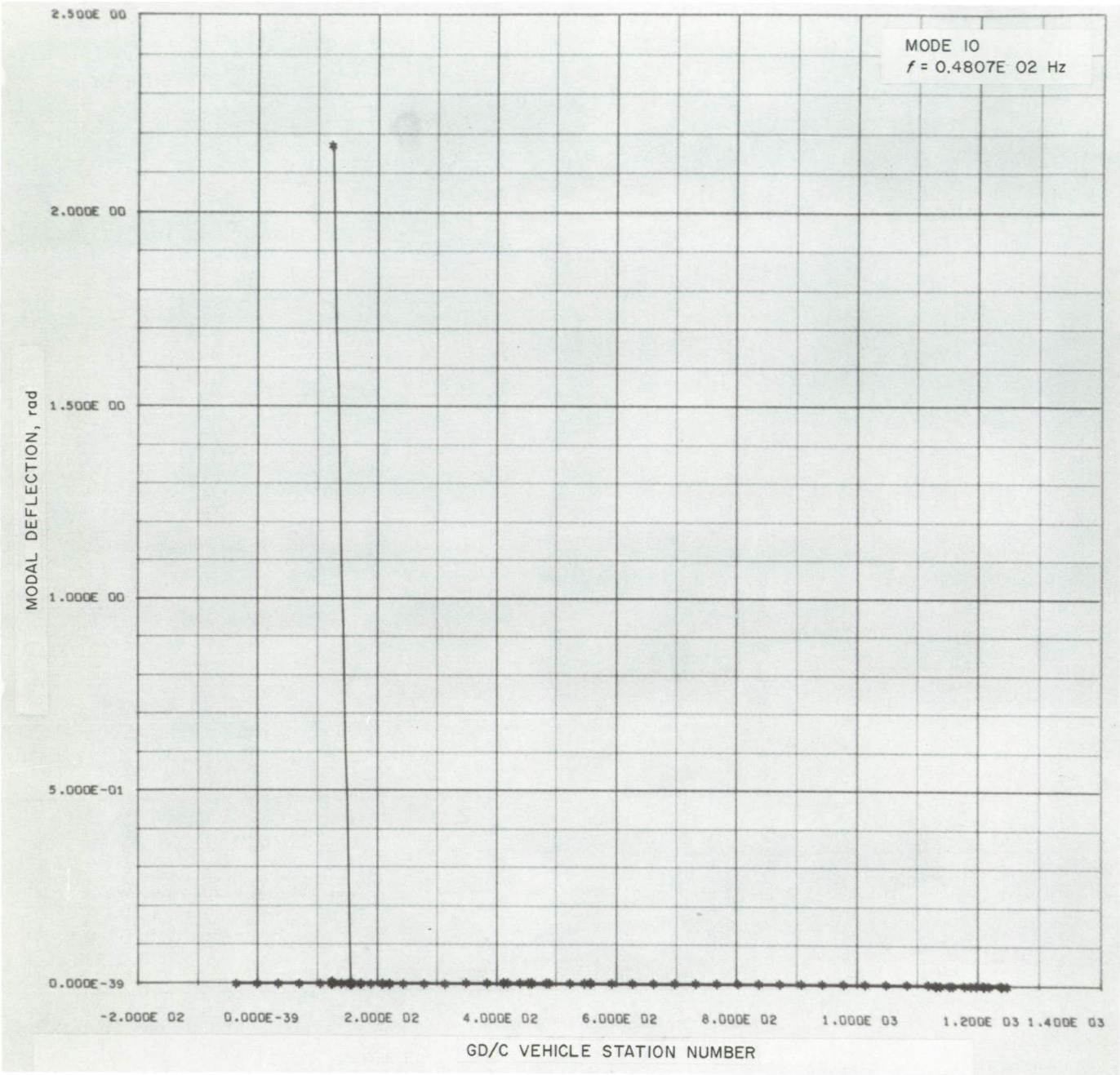
MODE 10
f = 0.4807E 02 Hz
2.500E 00
2.000E 00
1.500E 00
1.000E 00
5.000E-01
0.000E-39
MODAL DEFLECTION, rad
-2.000E 02
0.000E-39
2.000E 02
4.000E 02
6.000E 02
8.000E 02
1.000E 03
1.200E 03
1.400E 03
GD/C VEHICLE STATION NUMBER

Fig. D-1 (contd)

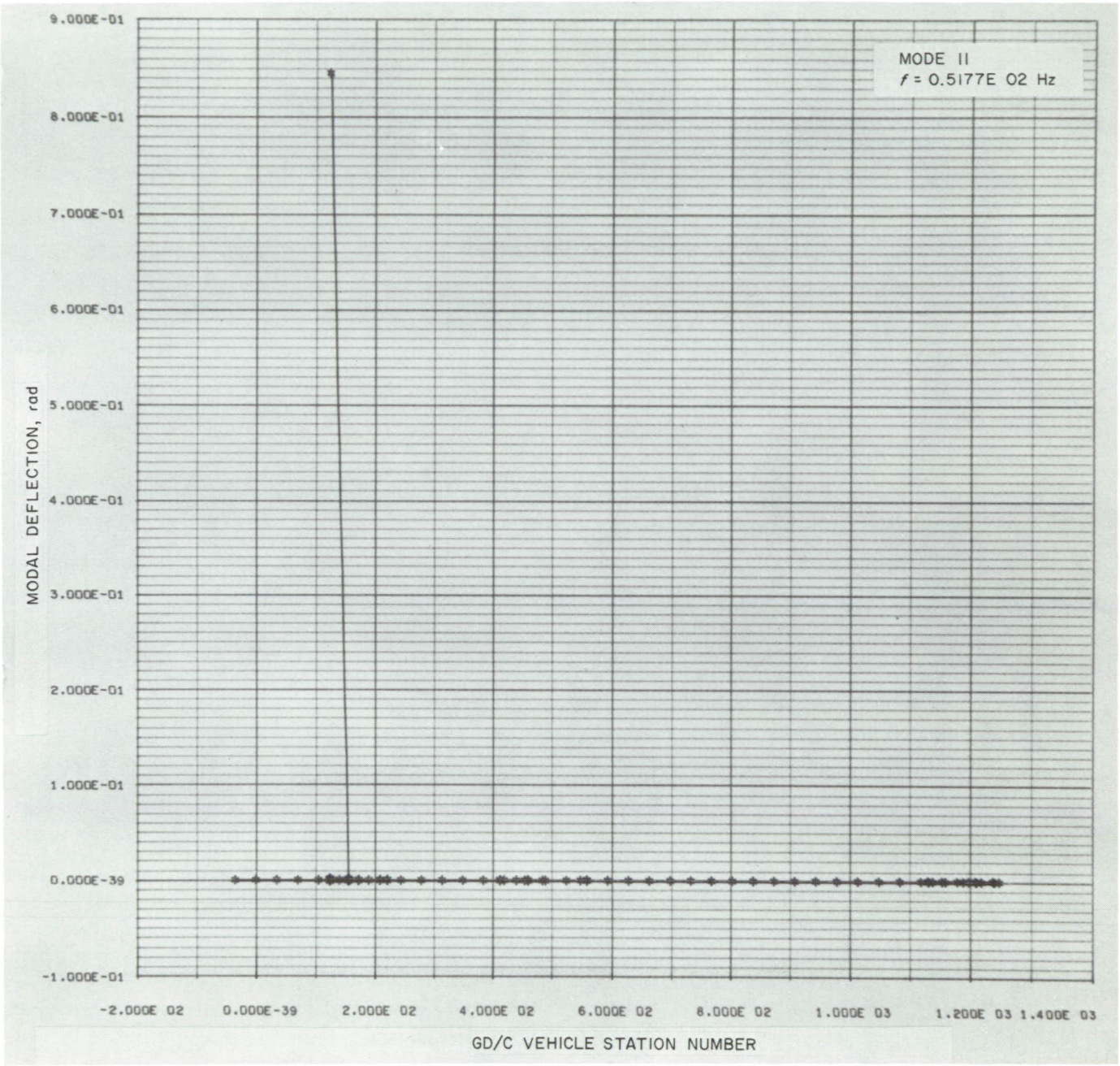
MODE 11
f = 0.5177E 02 Hz
9.000E-01
8.000E-01
7.000E-01
6.000E-01
5.000E-01
4.000E-01
3.000E-01
2.000E-01
1.000E-01
0.000E-39
-1.000E-01
MODAL DEFLECTION, rad
-2.000E 02
0.000E-39
2.000E 02
4.000E 02
6.000E 02
8.000E 02
1.000E 03
1.200E 03
1.400E 03
GD/C VEHICLE STATION NUMBER

Fig. D-1 (contd)

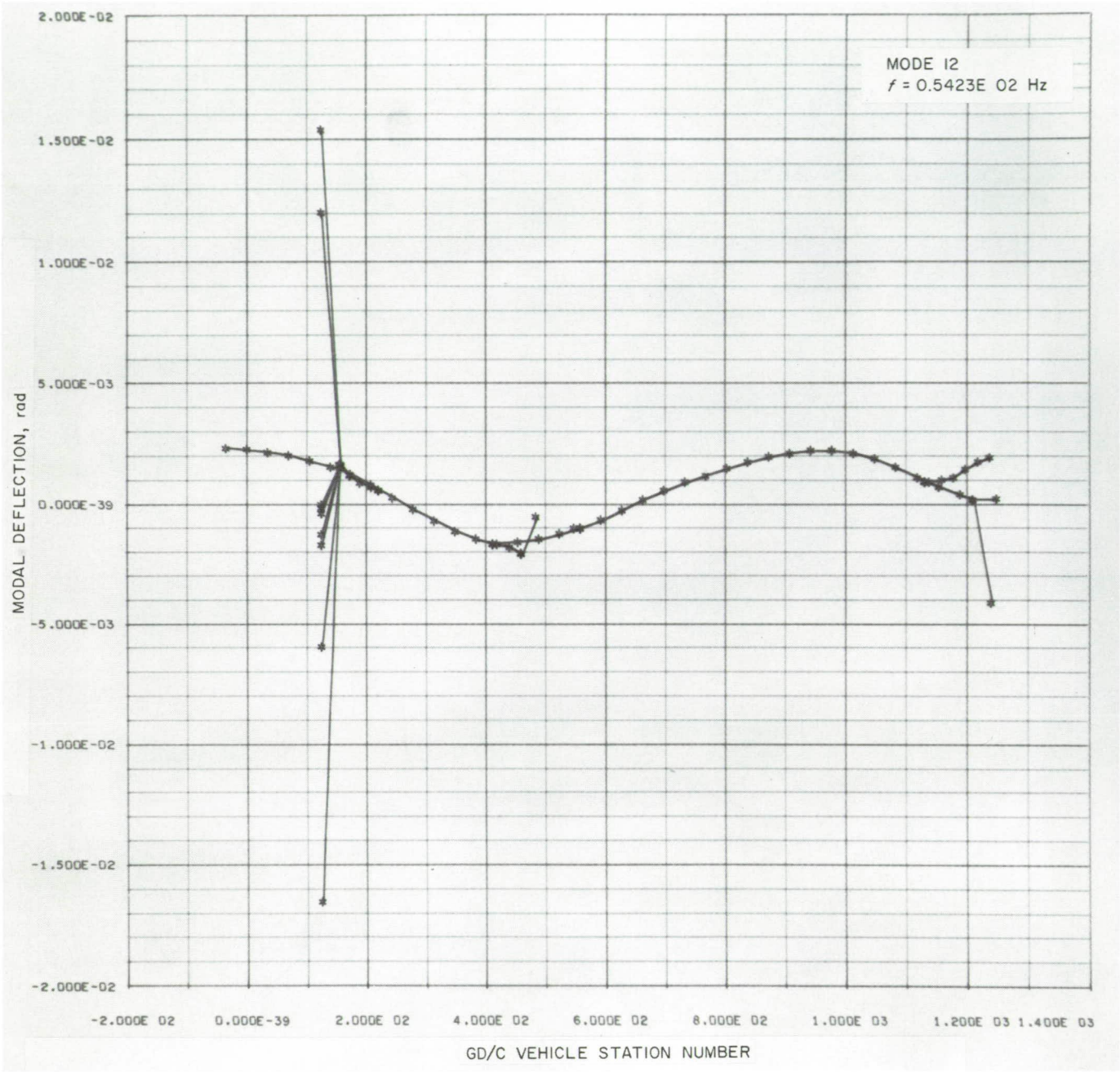
MODE 12
f = 0.5423E 02 Hz
2.000E-02
1.500E-02
1.000E-02
5.000E-03
0.000E-39
-5.000E-03
-1.000E-02
-1.500E-02
-2.000E-02
MODAL DEFLECTION, rad
-2.000E 02
0.000E-39
2.000E 02
4.000E 02
6.000E 02
8.000E 02
1.000E 03
1.200E 03
1.400E 03
GD/C VEHICLE STATION NUMBER

Fig. D-1 (contd)

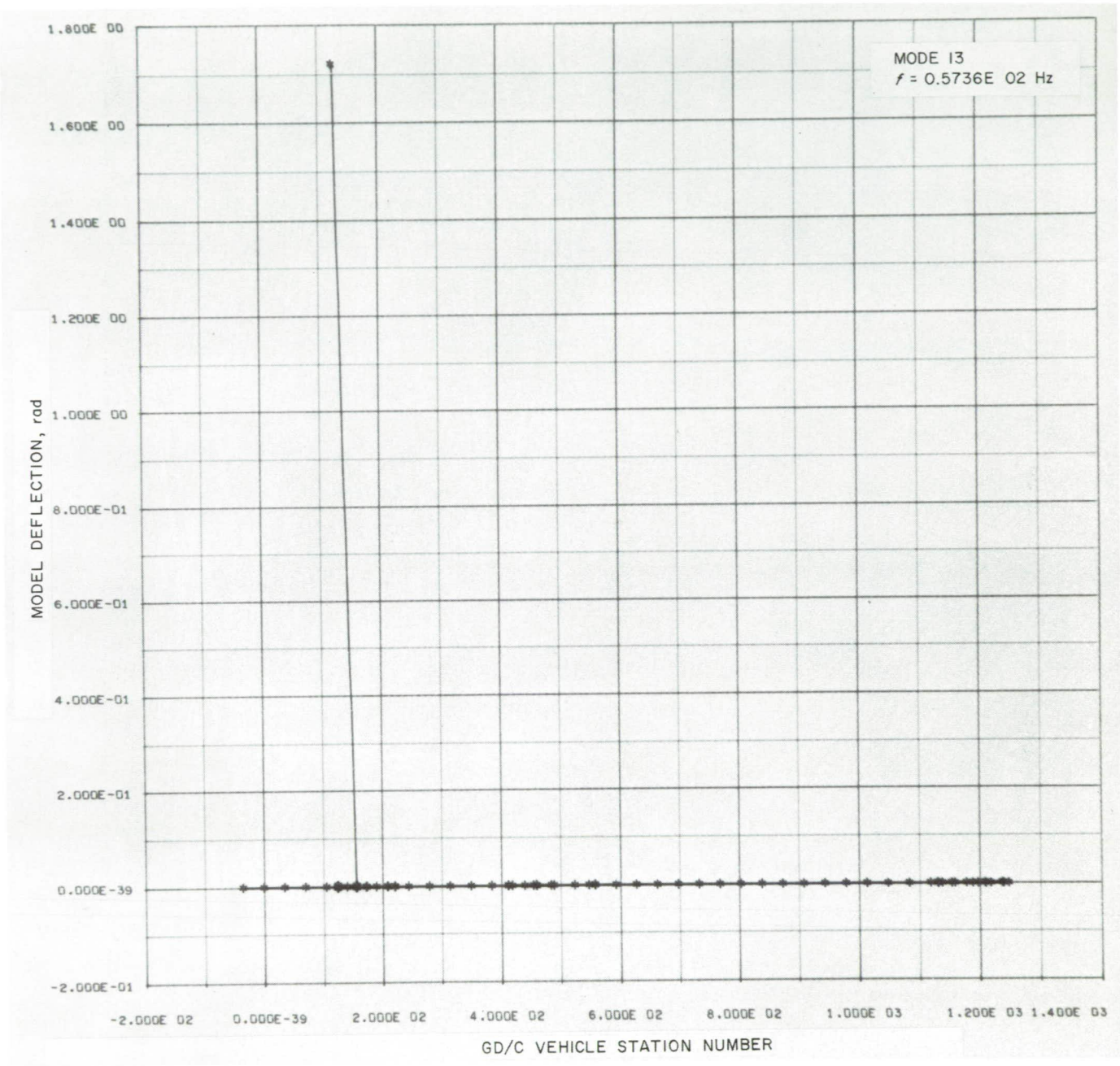
MODE 13
f = 0.5736E 02 Hz
1.800E 00
1.600E 00
1.400E 00
1.200E 00
1.000E 00
8.000E-01
6.000E-01
4.000E-01
2.000E-01
0.000E-39
-2.000E-01
MODEL DEFLECTION, rad
-2.000E 02
0.000E-39
2.000E 02
4.000E 02
6.000E 02
8.000E 02
1.000E 03
1.200E 03
1.400E 03
GD/C VEHICLE STATION NUMBER

Fig. D-1 (contd)

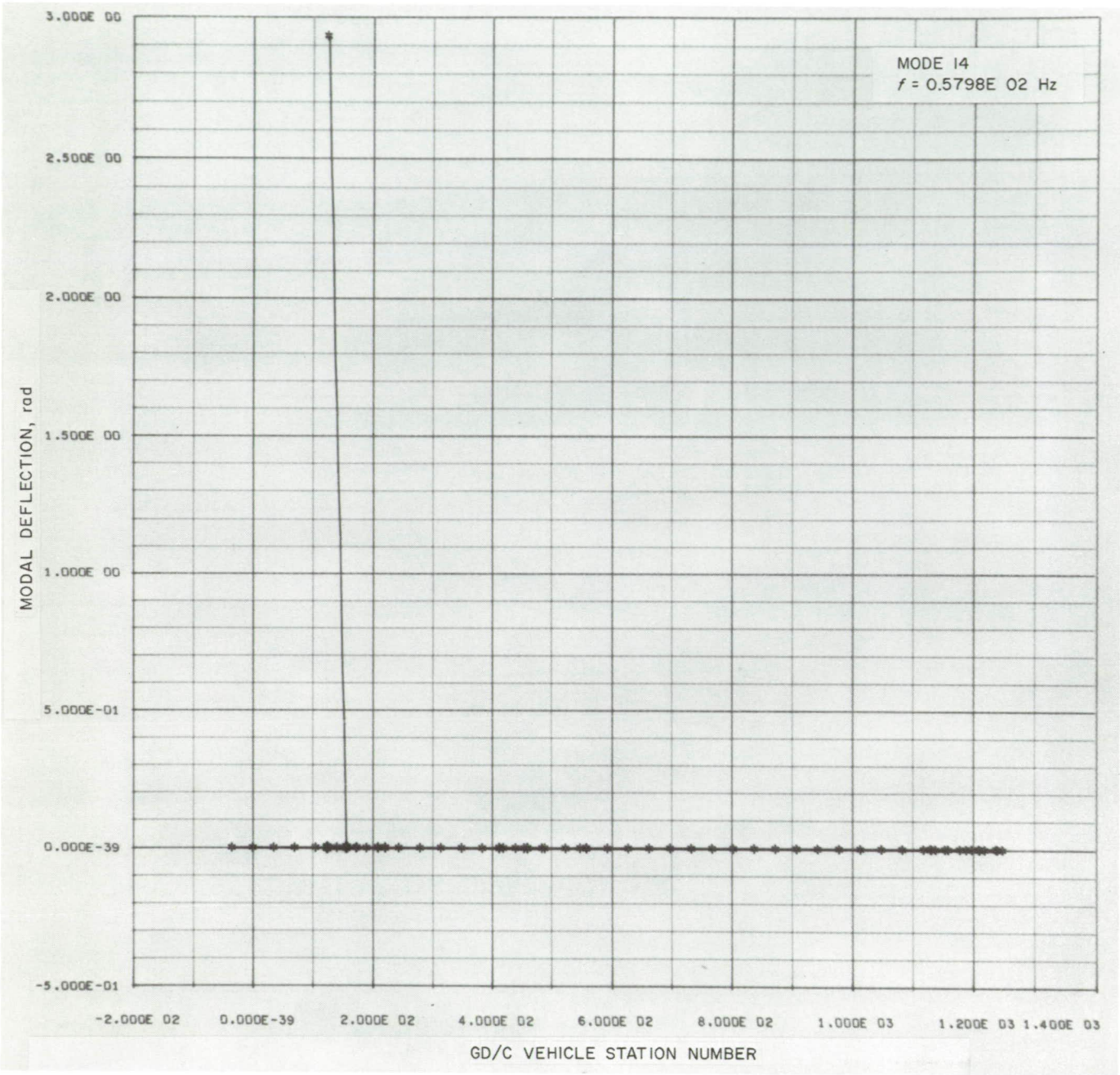
MODE 14
f = 0.5798E 02 Hz
3.000E 00
2.500E 00
2.000E 00
1.500E 00
1.000E 00
5.000E-01
0.000E-39
-5.000E-01
MODAL DEFLECTION, rad
-2.000E 02
0.000E-39
2.000E 02
4.000E 02
6.000E 02
8.000E 02
1.000E 03
1.200E 03
1.400E 03
GD/C VEHICLE STATION NUMBER

Fig. D-1 (contd)

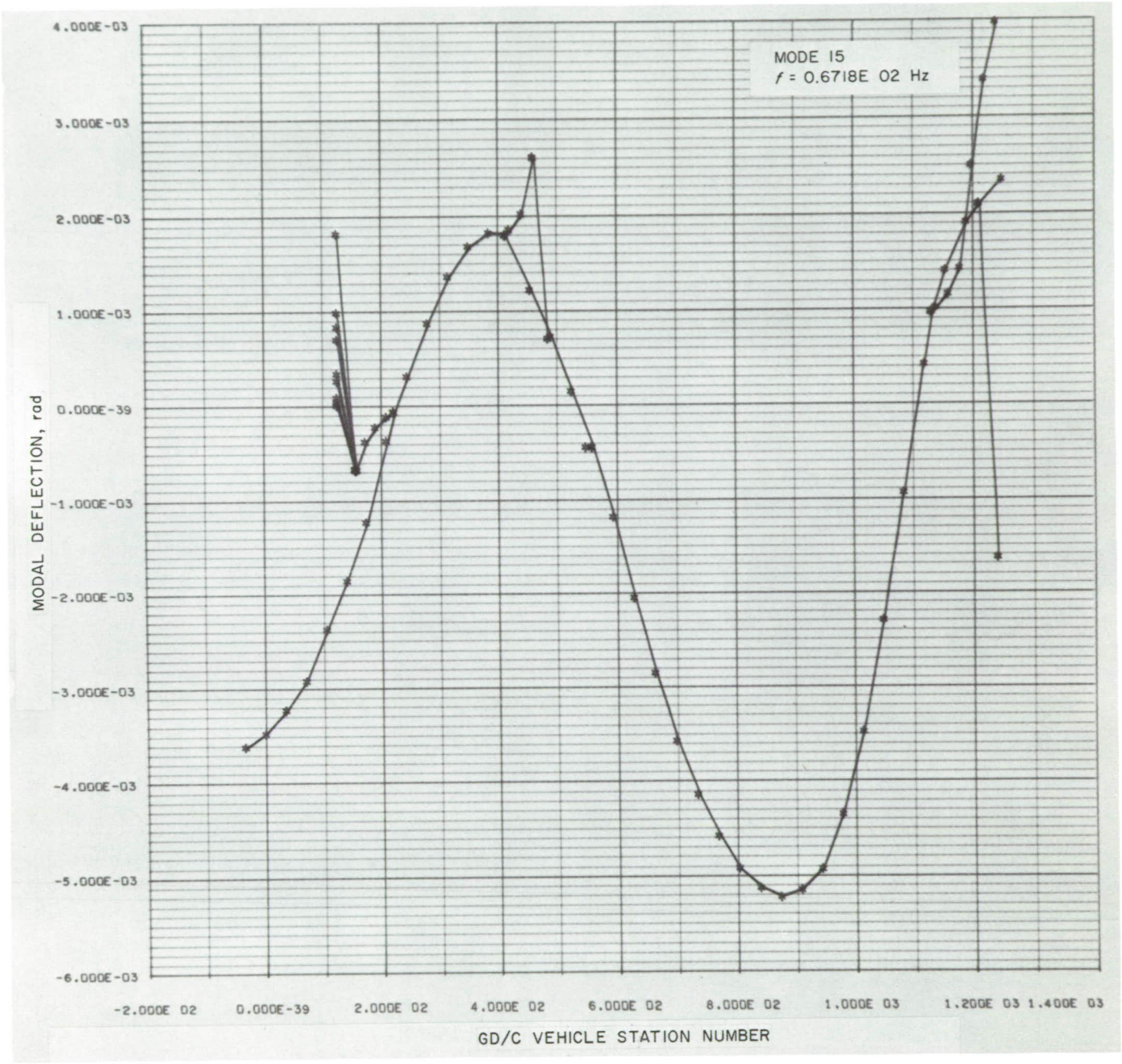
MODE 15
f = 0.6718E 02 Hz
4.000E-03
3.000E-03
2.000E-03
1.000E-03
0.000E-39
-1.000E-03
-2.000E-03
-3.000E-03
-4.000E-03
-5.000E-03
-6.000E-03
MODAL DEFLECTION, rad
-2.000E 02
0.000E-39
2.000E 02
4.000E 02
6.000E 02
8.000E 02
1.000E 03
1.200E 03
1.400E 03
GD/C VEHICLE STATION NUMBER

Fig. D-1 (contd)

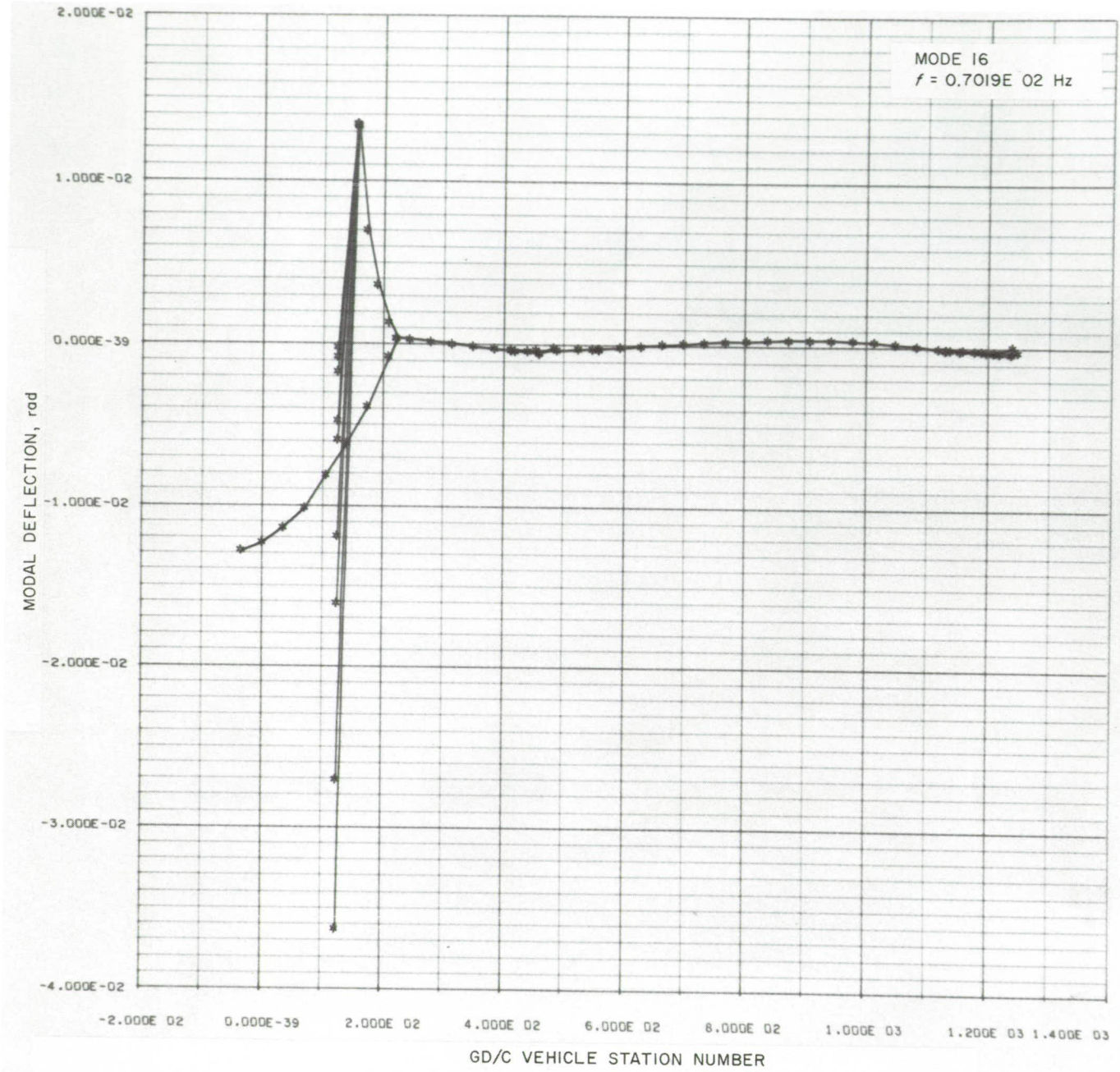
MODE 16
f = 0.7019E 02 Hz
2.000E-02
1.000E-02
0.000E-39
-1.000E-02
-2.000E-02
-3.000E-02
-4.000E-02
MODAL DEFLECTION, rad
-2.000E 02
0.000E-39
2.000E 02
4.000E 02
6.000E 02
8.000E 02
1.000E 03
1.200E 03
1.400E 03
GD/C VEHICLE STATION NUMBER

Fig. D-1 (contd)

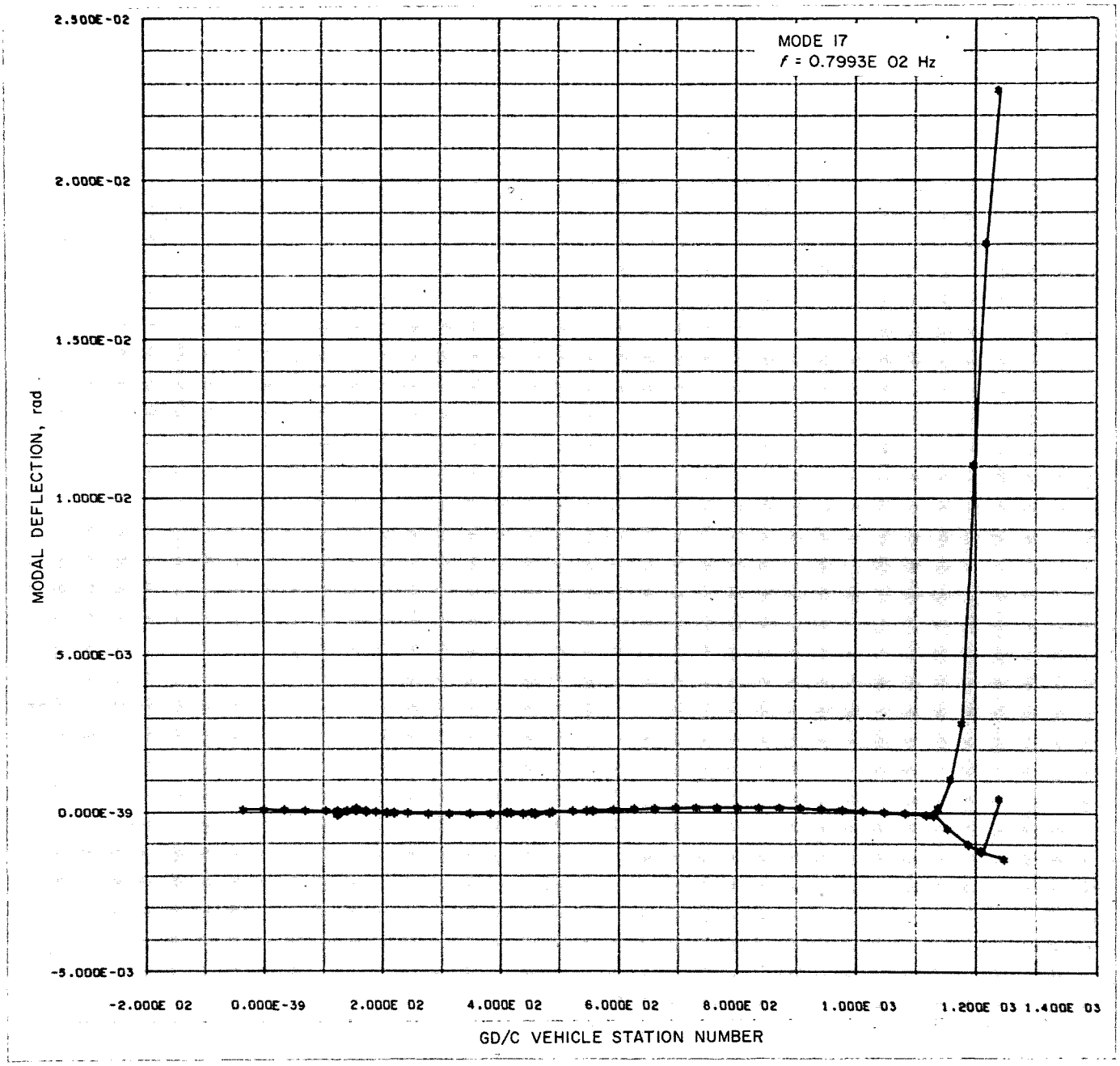
MODE 17
f = 0.7993E 02 Hz
2.500E-02
2.000E-02
1.500E-02
1.000E-02
5.000E-03
0.000E-39
-5.000E-03
MODAL DEFLECTION, rad
-2.000E 02
0.000E-39
2.000E 02
4.000E 02
6.000E 02
8.000E 02
1.000E 03
1.200E 03
1.400E 03
GD/C VEHICLE STATION NUMBER

Fig. D-1 (contd)

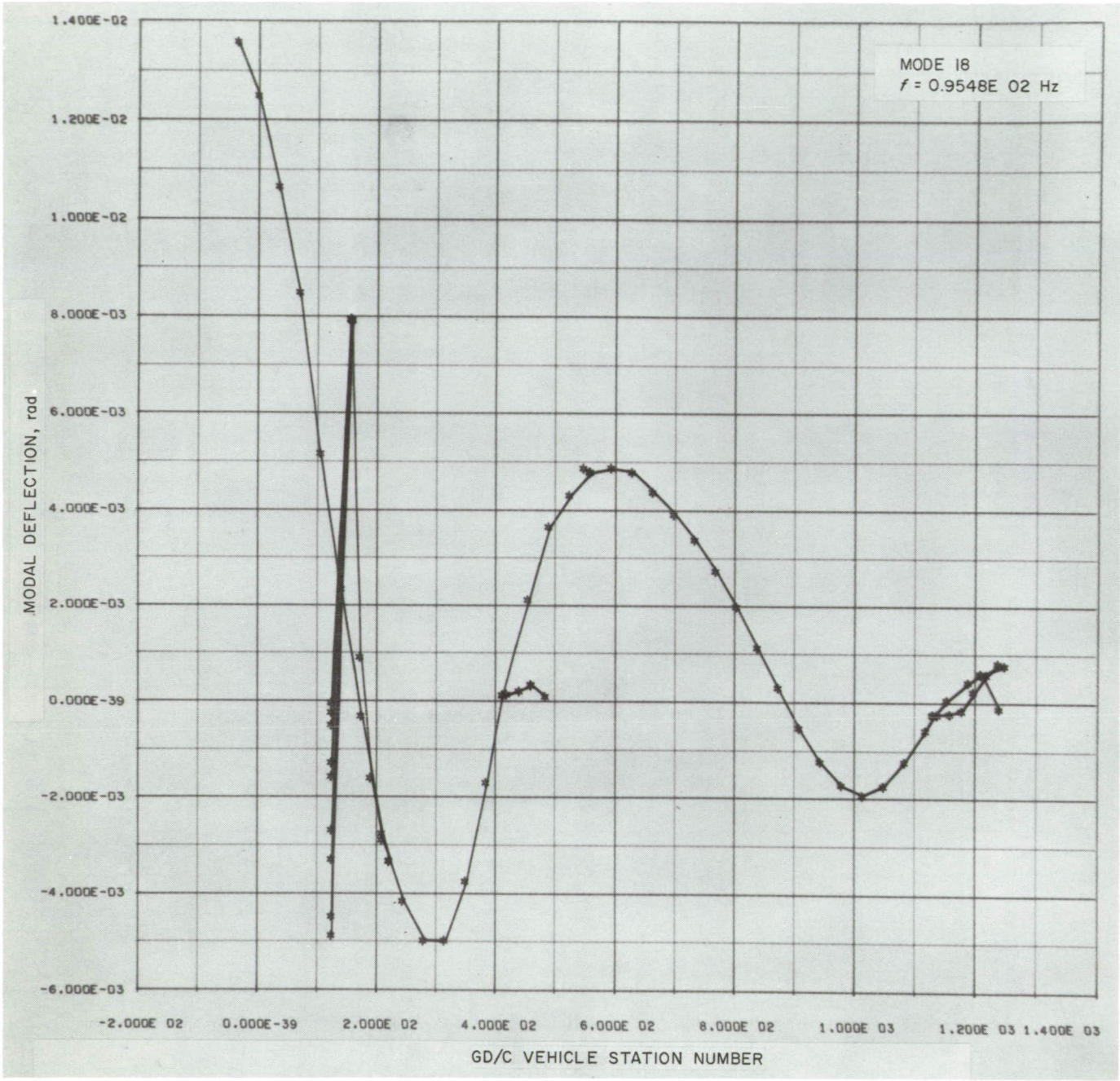
MODE 18
f = 0.9548E 02 Hz
1.400E-02
1.200E-02
1.000E-02
8.000E-03
6.000E-03
4.000E-03
2.000E-03
0.000E-39
-2.000E-03
-4.000E-03
-6.000E-03
MODAL DEFLECTION, rad
-2.000E 02
0.000E-39
2.000E 02
4.000E 02
6.000E 02
8.000E 02
1.000E 03
1.200E 03
1.400E 03
GD/C VEHICLE STATION NUMBER

Fig. D-1 (contd)

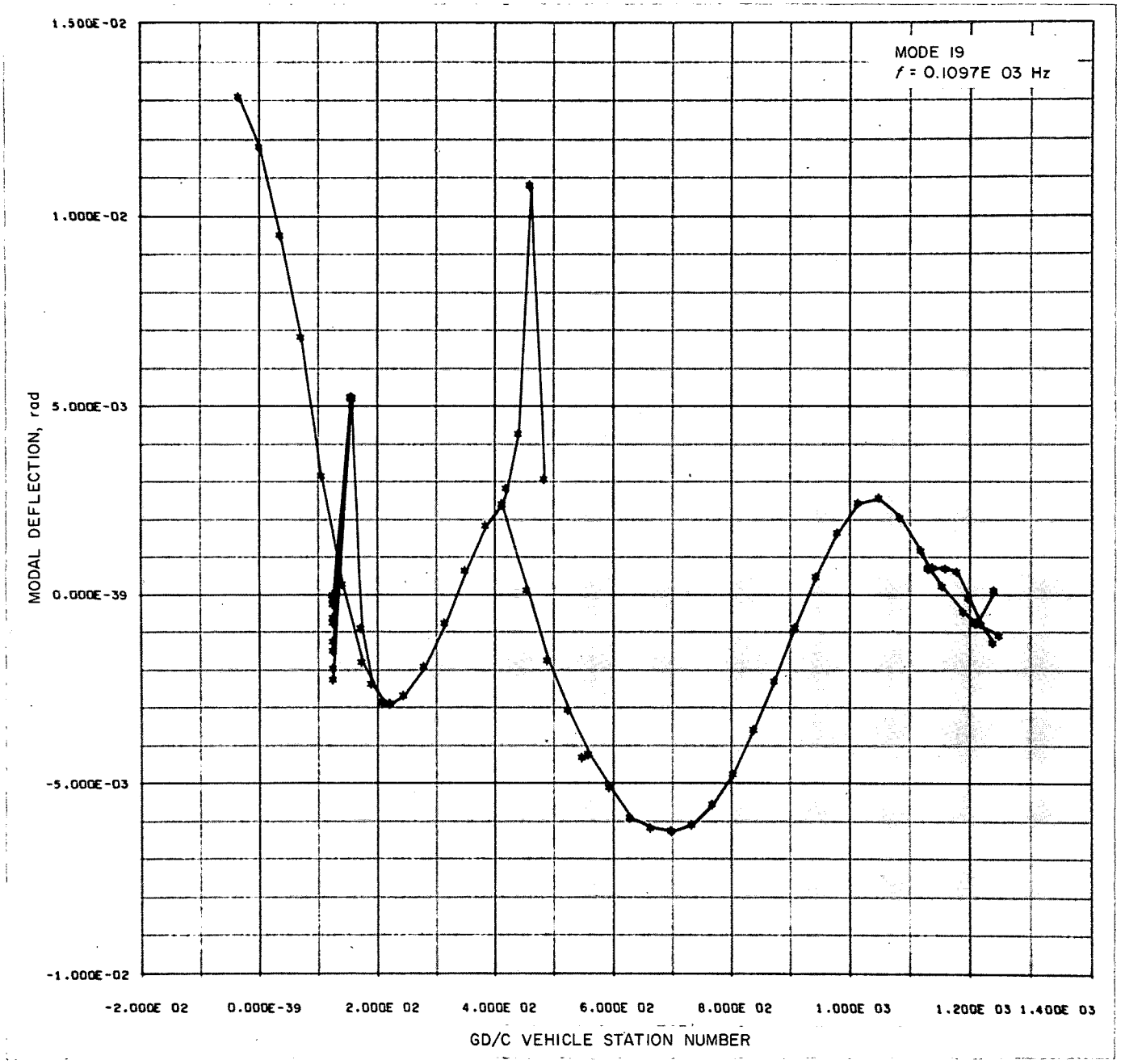
MODE 19
f = 0.1097E 03 Hz
1.500E-02
1.000E-02
5.000E-03
0.000E-39
-5.000E-03
-1.000E-02
MODAL DEFLECTION, rad
-2.000E 02
0.000E-39
2.000E 02
4.000E 02
6.000E 02
8.000E 02
1.000E 03
1.200E 03
1.400E 03
GD/C VEHICLE STATION NUMBER

Fig. D-1 (contd)

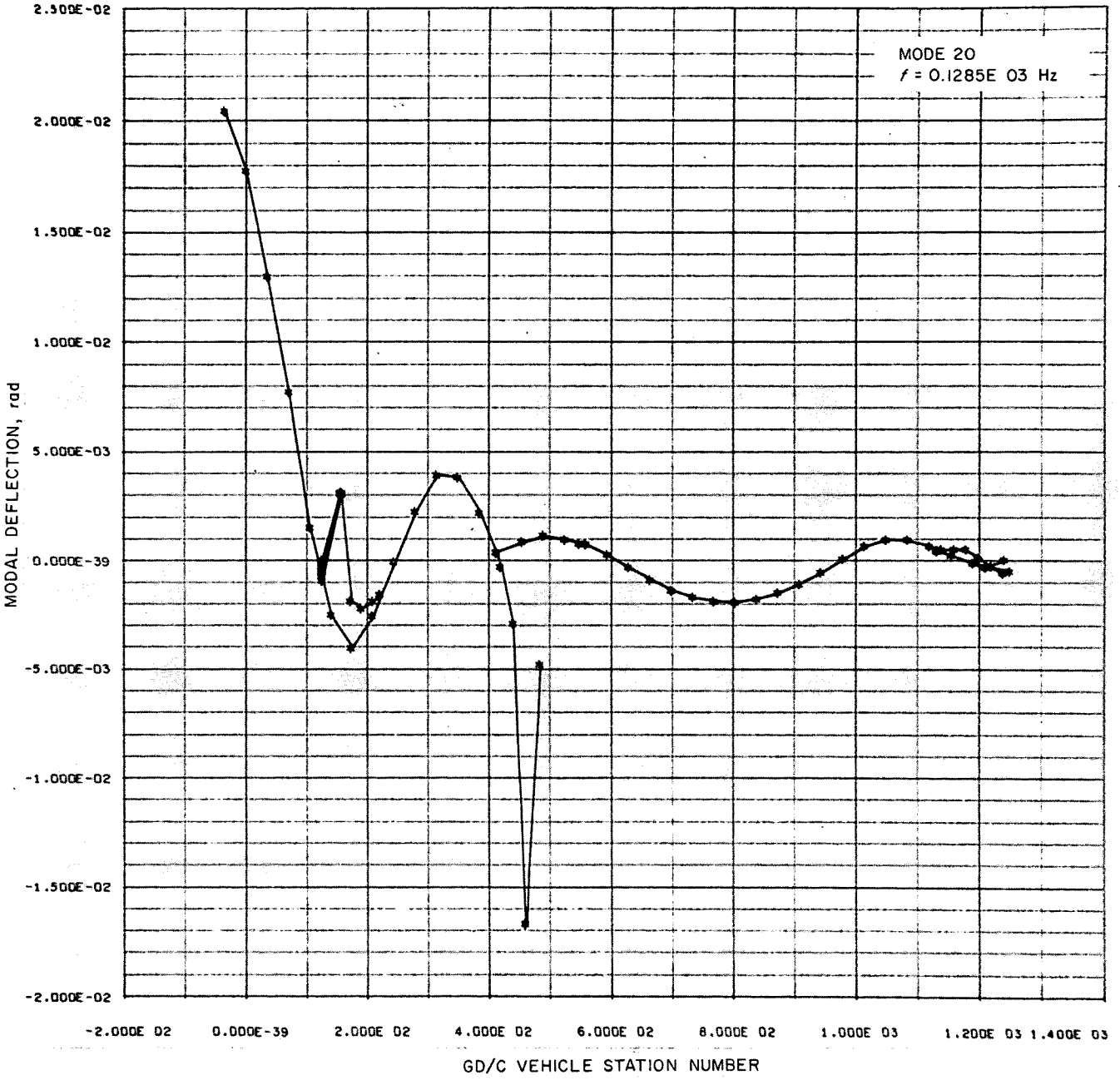
MODE 20
f = 0.1285E 03 Hz
2.500E-02
2.000E-02
1.500E-02
1.000E-02
5.000E-03
0.000E-39
-5.000E-03
-1.000E-02
-1.500E-02
-2.000E-02
MODAL DEFLECTION, rad
-2.000E 02
0.000E-39
2.000E 02
4.000E 02
6.000E 02
8.000E 02
1.000E 03
1.200E 03
1.400E 03
GD/C VEHICLE STATION NUMBER

Fig. D-1 (contd)

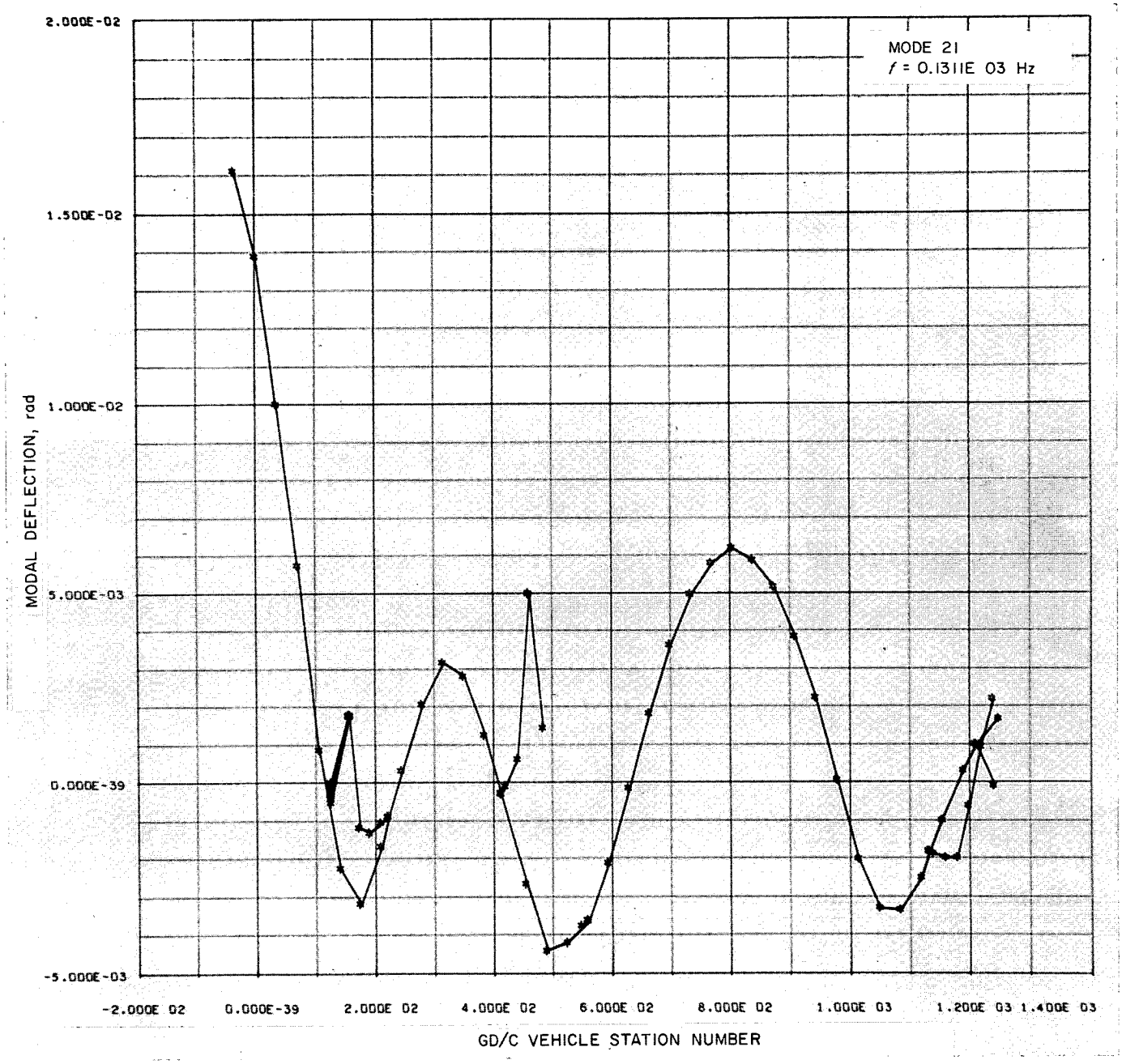
MODE 21
f = 0.1311E 03 Hz
2.000E-02
1.500E-02
1.000E-02
5.000E-03
0.000E-39
-5.000E-03
MODAL DEFLECTION, rad
-2.000E 02
0.000E-39
2.000E 02
4.000E 02
6.000E 02
8.000E 02
1.000E 03
1.200E 03
1.400E 03
GD/C VEHICLE STATION NUMBER

Fig. D-1 (contd)

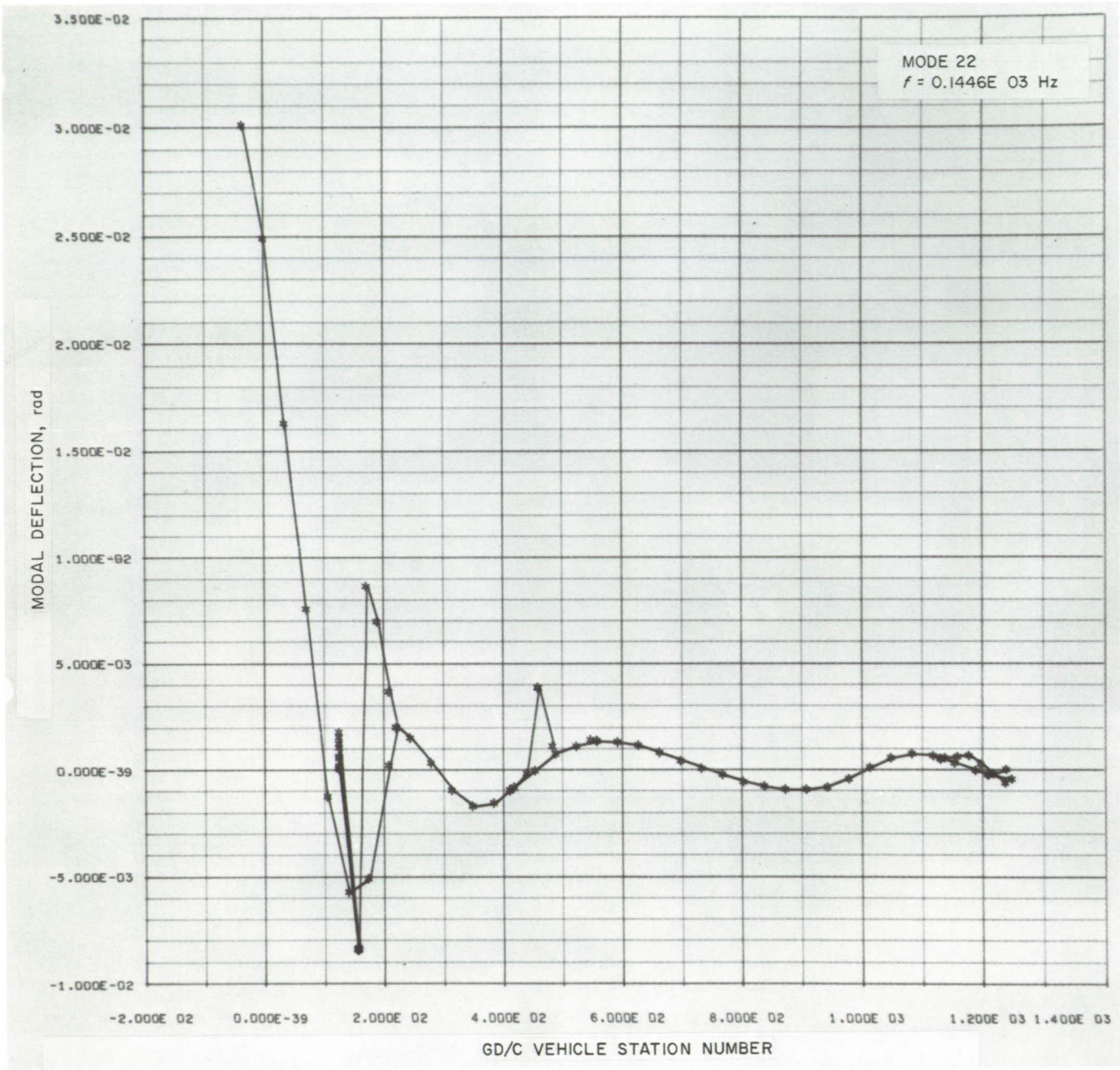
MODE 22
f = 0.1446E 03 Hz
3.500E-02
3.000E-02
2.500E-02
2.000E-02
1.500E-02
1.000E-02
5.000E-03
0.000E-39
-5.000E-03
-1.000E-02
MODAL DEFLECTION, rad
-2.000E 02
0.000E-39
2.000E 02
4.000E 02
6.000E 02
8.000E 02
1.000E 03
1.200E 03
1.400E 03
GD/C VEHICLE STATION NUMBER

Fig. D-1 (contd)

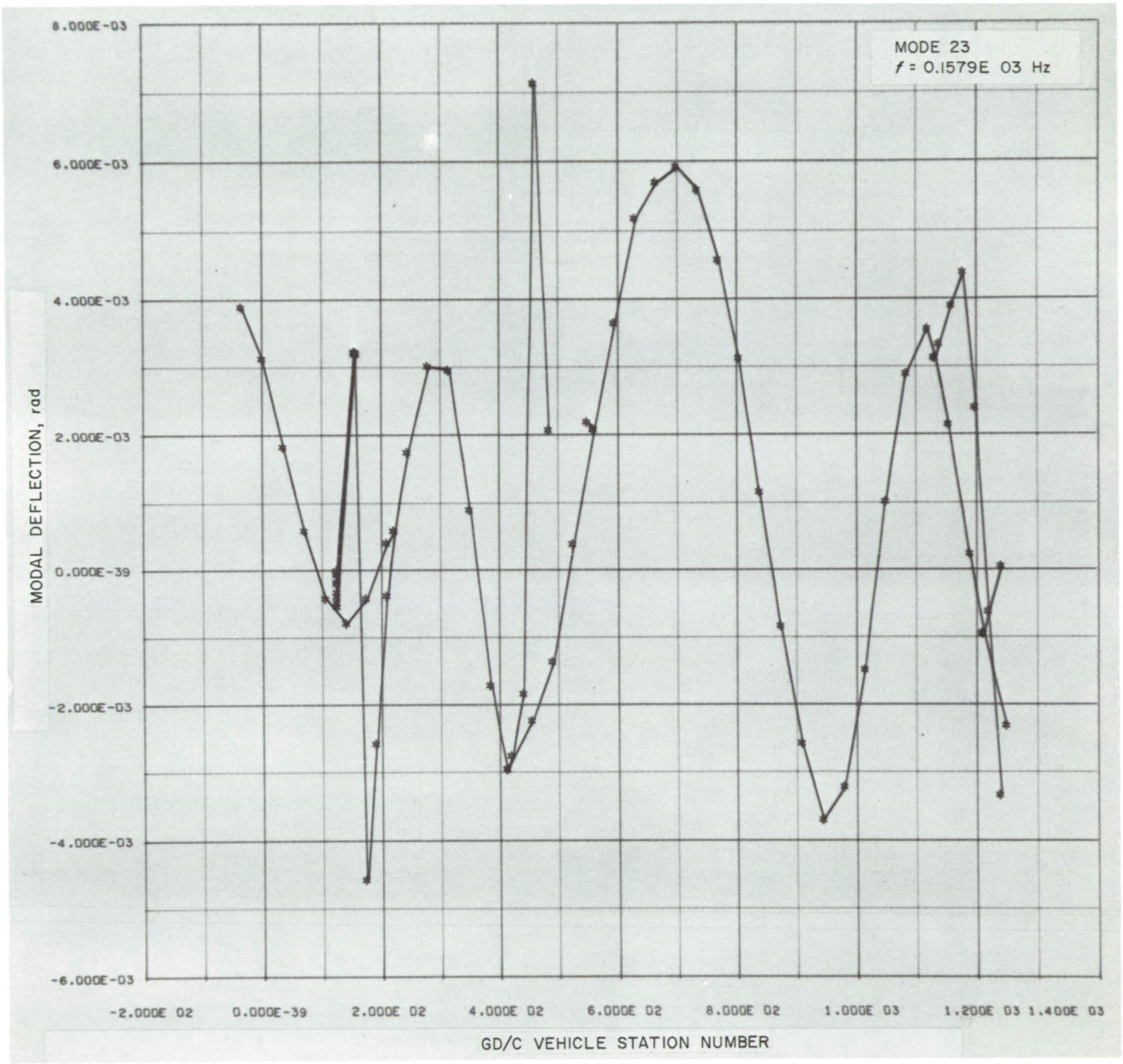
MODE 23
f = 0.1579E 03 Hz
8.000E-03
6.000E-03
4.000E-03
2.000E-03
0.000E-39
-2.000E-03
-4.000E-03
-6.000E-03
MODAL DEFLECTION, rad
-2.000E 02
0.000E-39
2.000E 02
4.000E 02
6.000E 02
8.000E 02
1.000E 03
1.200E 03
1.400E 03
GD/C VEHICLE STATION NUMBER

Fig. D-1 (contd)